FOG

Freiberg Online Geoscience

FOG is an electronic journal registered under **ISSN 1434-7512**

2019, VOL 56

Dead Sea and Ein Fehkha spring region, 2017

Cornelia Maria Wilske

Identification of water origin and water-rock interaction in a complex multi-aquifer system in the Dead Sea Rift by applying chemistry and isotopes

142 pages, 50 figures, 8 tables, 149 references

Foreword

This study was set up at the Helmholtz Centre for Environmental Research GmbH – UFZ (Department Catchment Hydrology in Halle) and contributes to the water resources research around the Dead Sea of accomplished projects: IWRM SMART II (Integrated Water Management, Sustainable Management of Available Water Resources with Innovative Technologies, 2010-2014, *C. Siebert* [27.06.2018]) and DESERVE (DEad SEa Research Venue, 2012 - 2017, *KIT* [2018]). The main goal of SMART II consisting of an international research consortium of Palestinian, Israeli, Jordanian and German scientists, deals with the dramatic water situation in the Jordan valley and adjacent countries and focuses on development of transferrable methods for sustainable water management in semi-arid water regions. DESERVE is a cooperation of KIT (Karlsruhe Institute of Technology), GFZ (German research centre for geosciences) and UFZ including partners from Israel (Hebrew University Jerusalem, The Institute of Earth Sciences (IES); Tel Aviv University (TAU), TAU Weather Research Center (TAU WeRC)) and Jordan (Al Balqa Applied University (BAU), Alhuson University College, Jordan) and Palestine. This project focus on environmental risks, water availability, and climate change under the unique conditions of the Dead Sea region and combines atmospheric, hydrological, and lithospheric research to understand processes and develop prediction models, remediation strategies, and risk assessments [*KIT*, 2018].

Contents

Figures

Tables

Abbreviations

AMS ..... accelerator mass spectrometry
AMSL ..... above mean sea level
BAU ..... Al Balqa Applied University
BMBF ..... Federal Ministry of Education and Research
BMSL ..... below mean sea level
CA ..... Cellulose acetate
Dept. ..... Department
DESERVE ..... DEad SEa Research Venue
DIC ..... Dissolved inorganic carbon
EC ..... electrical conductivity
EH ..... redox potential
EMA ..... Eastern Mountain Aquifer
EMWL ..... Eastern Mediterranean Meteoric Water Line
Eq. ..... equation
Fm. ..... Formation
GF/F ..... Glasfaser (glass fibre)/ Filter
GFZ ..... Helmholtz Centre Potsdam, German research centre for geosciences
GSI ..... Geological Survey of Israel
GWML ..... Global Meteoric Water Line
HDPE ..... High Density Polyethylene
HIS ..... Israel Hydrological Survey
HZDR ..... Helmholtz Zentrum Dresden Rossendorf
IAEA ..... International atomic energy agency
IC ..... ion chromatography
ICP ..... Inductively coupled plasma
IES ..... The Institute of Earth Sciences, Hebrew University Jerusalem
IWRM ..... Integrated Water Management
LMWL ..... Local Meteoric Water Line
LOD ..... limit of detection

Mekorot ..... Israel's National Water Company

MoST ..... Ministry of Science and Technology Israel

MS ..... mass spectrometry

MSL ..... mean sea level

$K_D^{Sr\text{-}Ca}$ ..... distribution coefficient of Sr and Ca in carbonate rock

KIT ..... Karlsruhe Institute of Technology, Germany

OES ..... optical emission spectrometry

PWA ..... Palestine Water Authority

REE+Y ..... Rare earth elements including Yttrium (Y)

SMART ..... Sustainable Management of Available Water Resources with Innovative Technologies

SPE ..... solid phase extraction

T ..... Temperature [°C]

TDE or TDS ..... total dissolved solids in [meq/l] or [mg/l]

TAU ..... Tel Aviv University

TAU WeRC ..... TAU Weather Research Center

TU ..... Technical University

UC ..... Upper Cenomanian

UFZ ..... Helmholtz Centre for Environmental Research GmbH

WMO ..... World Meteorological Organization

yr ..... year

YSEP ..... Young scientist exchange program

Acknowledgments

In the framework of the presented comprehensive research the following persons and institutions are acknowledged: I am very grateful to BMBF for funding this PhD thesis in the frame of the above-mentioned projects. For supporting participation in the Young scientist exchange program (YSEP), which includes two research stays at Tel Aviv University (in 2014) and The Hebrew University and Geological Survey of Israel in Jerusalem (in 2017), I thank BMBF and Ministry of Science and Technology Israel (MoST). I am very thankful to TU Bergakademie of Freiberg for supporting my research with a funding in the frame of "Maßnahme im Rahmen der Förderung der Gleichstellung" in 2015. For acceptance of my research project, supervision, supporting convenient ways to lab facilities and for scientific discussions and hints, I thank Prof. Dr. Broder Merkel from the TU Bergakademie Freiberg. For supervision, encouraging support in practical, theoretical and scientific tasks, long fruitful discussions about the interpretation of data in context of research questions, open ears and open doors, support of my research education, I thank my UFZ supervisor Dr. Christian Siebert. I thank Dr. Tino Rödiger for supervision and supporting my thesis - thank you for the scientific dialogue about the groundwater flow characteristics in the investigation area and the strong support during field campaigns. A special thank goes to Prof. Dr. Amitai Katz who stepped in as an official reviewer without hesitation.

For their warm welcome, contributing expertise to my research and time for discussions during my research stays, I deeply thank Prof. Dr. Amitai Katz again, as well as Prof. Dr. Abraham Starinski from the Hebrew University and Dr. Yoseph Yechieli and Dr. Naama Avrahamov from Geological Survey Israel as well as Dr. Nimrod Inbar and Dr. Annat Yellin – Dror from Tel Aviv University.

I thank Dr. Saed Khayat (Birzeits University, Palestine), Prof. Amer Marei (Al-Quds – University, Palestine) and Mohammad Hadidoun (Palestine Water Authority, PWA), who supported strongly my sampling campaigns and supported with contributing knowledge. For convenient sampling campaigns, I thank PWA (for support and access to wells) including Dr. Subhi Samhan and Dr. Deep Alhafour. I thank Mekorot (Israel's National Water Company - Tel Aviv), Dr. Yoseph Guttman, and Israel Nature Authority, Eldad, for providing and supporting access to sampling wells and springs. I also thank Prof. John Laronne and Noa Hillel from the Ben Gurion University (Beer Sheva), who both also supported with a warm and friendly place to sleep if necessary). For providing data from wells and water chemistry, I thank Israel Hydrological survey (HIS) and Geological Survey of Israel (GSI).

I thank the UFZ work group Dr. Stephan Weise, Dr. Kay Knöller, Dr. Stefan Geyer, Petra Blümel, Martina Neubert, Sandra Zucker-Gerstner, Silke Köhler, Daniela Reichert (Dept. Catchment Hydrology, UFZ) and Dr. Sibylle Mothes, Dr. Hans -Joachim Stärk, Dr. Monika Möder, Michaela Wunderlich, Ines Volkmann, Gabrielle Strenge (Analytical Department, UFZ) as well as Dr. Wolf von Tümpling, Christina Hoffmeister (Dept. River ecology, central Laboratory for water analytics & chemometrics, UFZ) for supporting my research, which includes mainly preparation and analyses of my samples and discussions of data or financial organisation.I had a great and educational time in the labs of TU Bergakademie Freiberg for $^{87}Sr/^{86}Sr$ analyses and Helmholtz Zentrum Dresden Rossendorf (HZDR) for ^{36}Cl analyses.

I am very glad and thankful for your strong support Prof. Marion Tichomirowa (TU Bergakademie Freiberg) and Dr. Silke Merchel, Dr. Georg Rugel, Dr. Stefan Pavetich and René Ziegenrücker (all from HZDR).

Dr. Axel Suckow, thank you for providing your lumped parameter software (Lumpy) and for your passions to explain me the secrets behind the dating models and groundwater dating.

I thank Daniela Budach and Dr. Thomas Degen for providing scientific discussions about the geological development and setting.

Thank you very much Dr. Agnes Sachse, Dr. Ulf Mallast and Christiane Meier for sharing your experiences in the area, contributing expertise from your fields of research and for always kind support. I thank Lena Roos cordially for her very kind help at all times.

For their belief in my power and their support, thoughts and understanding I thank warmly my mother and my family. You are the best.

Abstract

The present study deals with a hydrochemical investigation of the aquifer system on the western side of the Dead Sea to support future sustainable water management strategies. The investigation area extends from the mountainous area around Jerusalem and Ramallah to the lower Jordan Valley and the Dead Sea coast covering climate conditions of Mediterranean to semi-arid combined with a strong decrease of precipitation towards the Jordan Valley. The aquifer system is characterized by two main Cretaceous partly karstified limestone aquifers (Upper Cenomanian and the Albian layers). Above the Upper Cenomanian aquifer is a perched aquifer in the Turonian. The Cretaceous aquifers crop out in the recharge area along the mountainous ridge around Jerusalem and dip towards the lower Jordan Valley. The main Dead Sea transform fault cut the Cretaceous aquifers, which therefore emerge into the fault graben (Jordan Valley) with its Quaternary sedimentary fillings and along the Dead Sea coast. The main freshwater springs, called Ein Feshkha, are located at the north-western coast of the Dead Sea. To examine the groundwater resources of the Cretaceous aquifer, particularly groundwater origins, mixing processes, identification of water-rock interaction, dating of groundwater age ranges in the aquifers and identification of spring water origins at the Dead Sea coast and separation of Quaternary groundwater patterns, a combination of tracer is applied on water and rock samples. By application of the major and trace elements, the groundwater evolvement from recharge to discharge area can be traced. Upper Cenomanian aquifer and Albian aquifer are differentiable by $^{87}Sr/^{86}Sr$ ratio showing that water-rock interaction in the lower aquifer (Albian) or longer flow path lead to lower isotope ratios in the groundwater approaching rock ratio. By rare earth elements including yttrium (REE+Y), Turonian layers and its bearing groundwater are clearly differentiable from Upper Cenomanian and Albian aquifer and therefore further input from this upper part can be traced backwards to its origin. The stable isotope $\delta^{34}S$ is applied to distinguish between different sulphate sources contributing to the groundwater system. Similar to $^{87}Sr/^{86}Sr$, the two main Cretaceous aquifers can be separated by $\delta^{34}S$ based on intensity of mixing of rain water with rock. According to the $\delta^{34}S$ patterns, the two main springs of Ein Feshkha can be attributed to the main aquifers. Based on the karst conditions in the aquifer, groundwater age ranges are considered in short time frames. A combination of anthropogenic gases like CFC`s and SF_6 as wells as atom bomb related tracers like tritium and ^{36}Cl span a dating frame for the groundwater of the last 50-60 years. Via a lumped parameter model, age frames of wells of the Upper Cenomanian aquifer, which are situated close to the recharge area are estimated between 10-30 years mean residence time. The lower aquifer (Albian) contains a very low amount of tracer and indicates therefore groundwater fractions recharged before 1950. The multi-tracer method presented here for determining groundwater characteristics such as groundwater origin and development within aquifer systems is also applicable in other data-poor areas with complex hydrogeology (karst or fracture) under anthropogenic influence.

Zusammenfassung

Die vorliegende Studie befasst sich mit einer hydrochemischen Untersuchung des Aquifersystems auf der Westseite des Toten Meeres, um zukünftige nachhaltige Wassermanagementstrategien zu unterstützen. Das Untersuchungsgebiet erstreckt sich von Jerusalem und Ramallah bis zum unteren Jordantal zur Küste des Toten Meeres und deckt die klimatischen Bedingungen von mediterranen bis zu Halbtrockengebieten ab, kombiniert mit einem starken Rückgang der Niederschläge im Jordantal. Das Aquifersystem ist durch zwei kretazische, teilweise verkarstete Kalksteinaquifere (Schichten des oberen Cenomans und Albiums) charakterisiert. Oberhalb des oberen Aquifers liegt ein schwebender Aquifer im Turon. Die Kreideaquifere entspringen im Neubildungsgebiet entlang des Gebirgskamms um Jerusalem und sind in Richtung des unteren Jordantals geneigt. Durch die Hauptstörung des Jordan Grabens sind die Kreideaquifer angeschnitten und entlasten sich in den quartären Sedimentfüllungen im anschliessenden Jordantal und an der Küste des Toten Meeres. Die wichtigsten Süßwasserquellen, Ein Feshkha, liegen an der nordwestlichen Küste des Toten Meeres. Für die Untersuchungen der Grundwasserressourcen der kreidezeitlichen Grundwasserleiter, insbesondere Grundwasserherkunft, Mischprozesse, Identifizierung von Wasser-Gesteins- Wechselwirkungen, Datierung von Grundwasseraltersbereichen, Identifizierung der Herkunft des Quellen an der Küste des Toten Meeres und Abtrennung quartärer Grundwassermuster, wird eine Tracerkombination auf Wasser- und Gesteinsproben angewendet. Mithilfe der Haupt- und Spurenelemente kann die Grundwasserentwicklung vom Neubildungs- bis zur Abflussgebiet verfolgt werden. Oberer Aquifer und unterer Aquifer sind durch $^{87}Sr/^{86}Sr$ - Verhältnisse unterscheidbar. Durch sie kann gezeigt werden, dass Wasser-Gesteins-Interaktionen im unteren Aquifer (Albium) bzw. längere Fließwege zu niedrigeren Isotopenverhältnissen, d.h. ähnlich den von Gesteinsmustern, führen. Mit Hlife der seltenen Erdelemente inklusive von Yttrium (REE + Y) sind die turonischen Schichten des Turons und das hier befindliche Grundwasser deutlich vom oberen Aquifer und unteren Aquifer unterscheidbar, daher kann der weitere Input von diesem bis zu seinem Ursprung zurückverfolgt werden. Zur Unterscheidung von verschiedenen Sulfatquellen wird $\delta^{34}S$ verwendet: Ähnlich zum $^{87}Sr/^{86}Sr$ können die beiden Hauptaquifere durch $\delta^{34}S$ unterschieden werden, basierend auf dem Mischungsverhältnis von Regenwasser mit Gestein. Damit lässt sich auch der Wasserursprung der Quellen in Ein- Feshkha, d.h. für zwei Hauptquellen, aufklären. Basierend auf den Karstbedingungen der Grundwasserleiter werden Grundwasseraltersbereiche von kurzen Zeiträumen betrachtet. Mithilfe einer Kombination von anthropogenen Gasen in der Atmosphäre wie CFCs und SF_6 sowie atombombenbezogene Tracer wie Tritium und ^{36}Cl können Grundwässer im Rahmen der letzten 50-60 Jahre datiert werden. Über Lumped - Parameter Modelle konnten Grundwasseraltersbereiche von Brunnen des oberen Aquifers auf 10-30 Jahre mittlere Verweildauer abgeschätzt werden. Im unteren Aquifer sind die Tracerkonzentrationen sehr gering und weisen daher auf Grundwasserneubildung vor 1950 hin. Die hier vorgestellte Multitracer-Methodik zur Bestimmung von Grundwassercharakteristika wie Grundwasserherkunft und -entwicklung innerhalb von Aquifersystemen ist auch in anderen datenarmen Gebieten mit komplexer Hydrogeologie (Karst oder Störungen) unter anthropogenem Einfluss anwendbar.

1 Introduction

Water is the most important substance for life on earth. The survival of all organisms and for the human being is based on the global water resources. Depending on the different climate regions and the environmental and geological conditions, the available global freshwater is stored in glaciers (68.7%), surface water bodies like lakes and rivers etc. (1.2%) or in the subsurface (30.1%) [*Shiklomanov*, 1993]. Growing population on earth and therefore increasing industry and artificial irrigation has an effect on water quantity and quality. Environmental awareness and strong effort is needed to keep the freshwater resources health-friendly and free from anthropogenic contamination. In water scarce areas like semi- arid to arid regions, the freshwater resources are mainly accumulated in the subsurface. Groundwater resources in such dry regions can be stressed by low groundwater recharge rates and increasing water extraction for water supply. In dry regions, there is also a higher risk of groundwater vulnerability due to low vegetation cover and soil layer, which can hinder fast input of contamination in the subsurface via e.g. absorption processes. Such conditions occur also in the Dead Sea region and its adjoining aquifer systems.

This thesis comprises detailed analyses of the western Dead Sea aquifer system and the Lower Jordan Valley in Israel and the Palestine territories. Already in the last decades, national and international research teams have focused on the development of freshwater water resources and its extreme environmental conditions of the adjacent high saline lake Dead Sea, the deepest location on earth (~-430m BMSL in 2014). Here, the groundwater situation is continuously influenced by strong anthropogenic impact of increasing water extractions and the fatal decrease of the Dead Sea level (~1m/year after *Gertman and Hecht* [2002]).

Past hydrological studies and recent reports provide information about the western Dead Sea subsurface catchment, which extends from the mountain area around Jerusalem and Ramallah dip sharply towards the Dead Sea including its chemical varying spring outlets along the main graben fault/ Dead Sea coastline. Many of them have focused on main aquifer composition from the Cretaceous layers to the Quaternary deposits in the Lower Jordan Valley, while others investigated the origins of brine in the subsurface contributing the freshwater resources or occur in the spring waters. In addition, the specific composition and dynamics of the springs of the northern coast to the south are explored as well as groundwater dynamics and flow conditions in the fresh water aquifers.

On the base of the hydrogeological dynamics of the whole Dead sea aquifer system and its impressive development within one decade, the present research focuses on the characterization of the main western Cretaceous aquifers and interaction according to the seasonal precipitation input.

Knowledge about the Cretaceous aquifers and its groundwater interaction via faults and karst windows as well as its connection to the spring system would support the plans of new boreholes in suitable areas, where sustainable water supply and water in drinking quality are retained. Information about the water-bearing layers and its depth would give the basis for drilling cost-efficiently. The proposed hidden connection between groundwater resources of the graben flank and the graben fill are highly important for the management of the resources. Groundwater of the

Quaternary deposits (graben fill) is mainly used for agricultural irrigation due to salinization in the aquifer. In this context, it is necessary to understand where the water inside Quaternary deposits originates, recharges and discharges for future water supply plans in the densely populated area of the Lower Jordan Valley (e.g. Jericho). The outflow of the aquifer system - springs in Ein Feshkha form an ecosystem in the arid environment at the northwestern coast of the Dead Sea. Beside its attractiveness as local recreation area for tourists, the region provides a unique biodiversity including endemic fish species due to specific spring water composition. To preserve this uniqueness in the region, further experience of the behaviour and the dynamics of the aquifer system are necessary.

1.1 Objective

In arid regions, like the Dead Sea region, detailed hydrogeochemical investigations are needed to quantify and qualify the water resources for a sustainable management and information of isotopic signatures geochemical patterns bear additional hints to characterize the origin and evolvement of the water. Already many studies in the past provide well- reasoned knowledge about western Dead Sea aquifer system. On behalf of this information, a strong hydrochemical tracer combination was applied to handle following research aspects:

- Hydrochemical differentiation of the two main Cretaceous aquifers
- Figure of groundwater origin
- Chemical groundwater evolvement within the Cretaceous aquifer
- Decode chemical groundwater patterns according to aquifer composition and anthropogenic input
- Differentiation of saline sources and resulting patterns in the Quaternary section
- Separating spring chemistry related to aquifer origin, particularly for the main fresh water spring at the north western Dead Sea coast - Ein Feshkha
- Estimation of young groundwater infiltration times and mean residence times in the last decades

That means, the objectives of this study can be further specified in gaining detailed knowledge and understanding about the groundwater resources in the two main Cretaceous aquifers as part of the mobile Dead Sea water system. Playing an important role, the discharge area particularly the northwestern spring system is investigated in regard to groundwater origins and admixture sources.

The focus is to define the groundwater of Ein Feshkha and their individual components by application of geochemical tracers, which are characteristic for the respective aquifers (major and trace elements, $^{86}Sr/^{87}Sr$, $^{36}Cl/Cl$, $\delta^{34}S$, $\delta^{13}C$, REE+Y). The resulted conceptual model of groundwater origin, water/rock-interactions and groundwater dating can improve existing comprehensive numerical groundwater flow models.

1.2 Structure of the thesis

The present research study comprises a detailed hydrochemical investigation of the water resources of the western Dead Sea catchment. The combined tracer application focus on three main fields of investigation (Cretaceous aquifers, saline patterns of Quaternary section and age dating estimations of groundwater), which provides the bases for the structure of this thesis:

- Chapter 1 introduces to the topic of water shortage and its influence on the Dead Sea region as well as the relevance and motivation of this study.
- The study area is characterized in chapter 2 with special focus on the geological and hydrogeological background.
- In Chapter 3 the methodical tools are presented including all applied tracers and model application.
- Chapter 4 contains result and discussion. It is subdivided into three parts:

In the first part are presented and discussed aspects of the major ions (particularly Ca, Mg, Sr), stable isotopes ($\delta^{2}H_{H2O}$, $\delta^{18}O_{H2O}$, $^{87}Sr/^{86}Sr$, $\delta^{13}C_{DIC}$) and REE+Y, which are applied to examine the groundwater evolvement and groundwater origins in the Cretaceous aquifers. The second part contains results and discussion of trace element patterns by applied statistics and $\delta^{34}S_{Sulphate}$, $\delta^{18}O_{Sulphate}$ to identify input to the Cretaceous groundwater from saline sources of the Lower Jordan Valley and to uncover origins of the major springs (NW coast of the Dead Sea). In the third part results of dating tracers (Tritium, CFC`s, SF_6 and $^{36}Cl/Cl$ and anthropogenic trace substances) are presented and discussed for determination of age range of groundwater in the last 50 years.

- Chapter 5 provides the conclusions of all discussed results and presents and outlook for further studies or water management strategies.

2 The Dead Sea basin and its adjacent western aquifer system

2.1 Geography

The investigation area, the western Dead Sea groundwater catchment is part of Israel and the Palestinian territories. From west to east, the region covers the Jerusalem/Ramallah mountain ridge (up to 1200 AMSL), which is connected to a dry hilly area (transition zone) and the flat plain of the Lower Jordan Valley including the Dead Sea. From the morphologic point, the area is special due to the sharp decline in a distance of ~25km, from ~1200 AMSL in the mountains to ~-430 AMSL at the Dead Sea surface. Additionally, valley cuttings so called wadis shape further the landscape from west to east. The northern end is located in the Ein Samia region and the southern end lies in the area of the Herodion and Bani Naim well fields and includes the whole catchment of the Ein Feshkha springs, a spring area in the northwestern coast of the Dead Sea (Figure 2).

2.2 Climate

The area is influenced by the Mediterranean Sea, where precipitation mainly originates from. The catchment can be separated into four climatic zones in which the mountains comprise a dry humid mesothermal zone with precipitation rates of 700 – 1000 mm/y during the winter season. Connected to the east, the transition zone consists of a semi-arid mesothermal climate in the eastern slopes and arid mesothermal conditions with precipitation rates of 100- 400 mm/y during winter season in the western slopes [*Thornthwaite and Mather*, 1955; *Toll*, 2008]. Towards the Lower Jordan Valley and the Dead Sea, precipitation rates decrease below 100 mm/y and are influenced by arid climate [*Thornthwaite and Mather*, 1955; *Toll*, 2008].

2.3 Vegetation and land use

Vegetation cover is mainly characterized by climatic parameters: In the mountains, park forest is the predominant vegetation form. A community of Ceratonia and Pistacia lentiscus are drought and heat resistant plants growing at elevations of 0-300 AMSL [*Danin*, 1988]. In the connected slopes occur steppe to desert vegetation [*Danin*, 1988]. Along the dry Dead Sea coast and in the Lower Jordan Valley occur desert savannoid vegetation with punctual swamps and reed thickets [*Danin*, 1988]. Settlements and urbanization are mainly located in the mountains, e.g. in Jerusalem, Ramallah, Hebron etc. and Lower Jordan Valley (e.g. Jericho). Low density population extends along the western slopes. Strong agriculture activities are located around Jericho, partly at the wadi outlets of e.g. Wadi Og (date plantations) or discharging valley of Wadi Nueima (citric fruits or banana plantations) as well as around the settled areas in the central mountains.

2.4 Geology / Hydrogeology

The investigation area is part of a tectonic setting involving the connection of the African- Arabian plate, the Eastern Mediterranean sub-plate (part of the Arabian plate) and Anatolian plate (Figure 1). Here, the Arava-Dead Sea-Jordan Rift separates the Arabian sub –plate from the African plate, while Cyprian Arc (and the Peri-Arabian ophioliths) bounds African and Anatolian plate [*Flexer et al.*, 2005]. The geological development of the Eastern Mediterranean and Levant crosses tectonic steps with periods of subsidence and uplift and lateral facies changes [*Flexer et al.*, 2005]:

In the Late Precambrian, during the Pan-African orogeny, an agglomeration of plutonic igneous rock, extrusive ingenious rocks as well as ophiolites, metasediments took place e.g. in the Arabian-Nubian Massif, Tauriden (Menderes) and Eastern Mediterranean (Eratothenes), which is followed by a stepwise and regional peneplanisation. Paleozoic deposits were eroded due to post Permian uplifts resulting into residuals of Ordovician- Devonian and earliest Triassic.

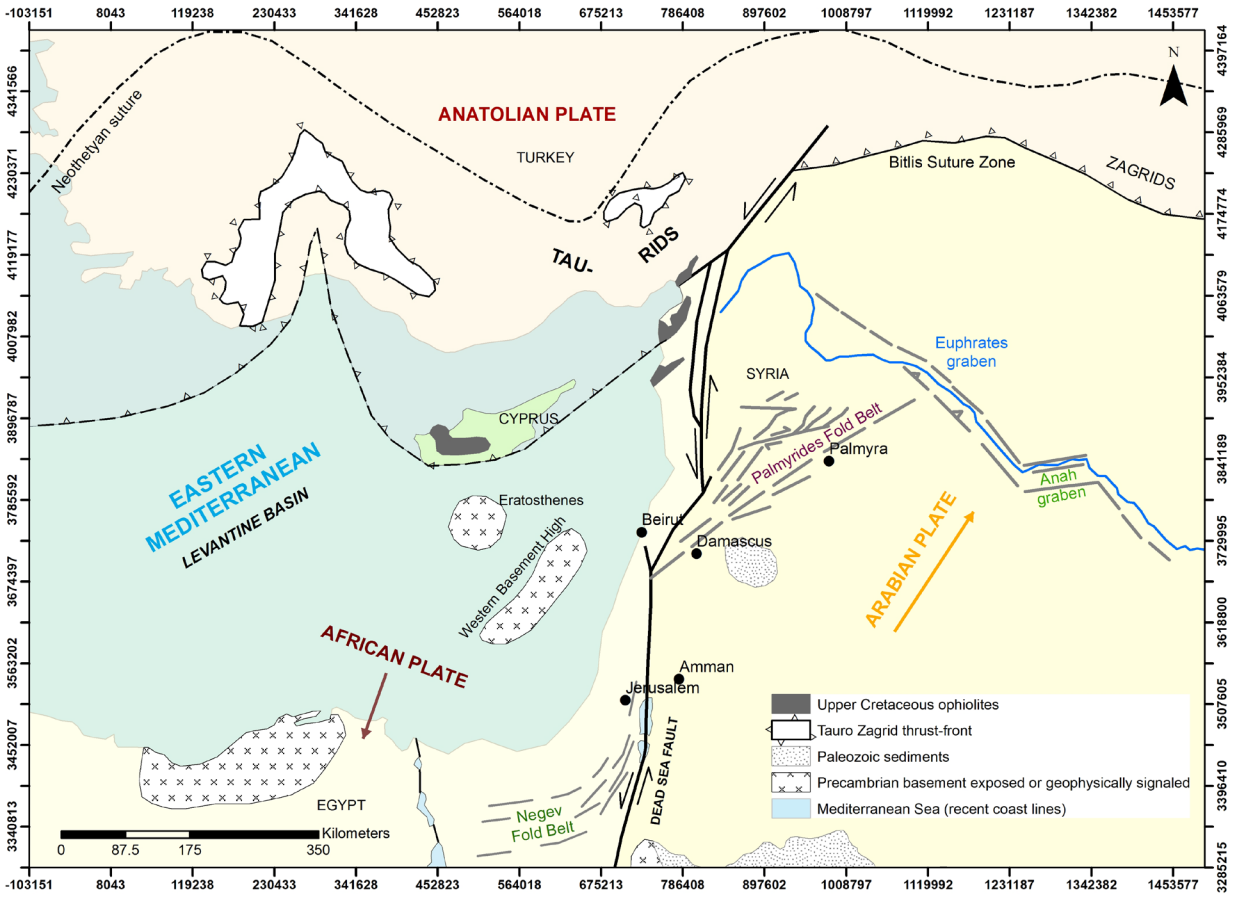

Figure 1 Regional plate tectonic pattern showing main Levant features like Dead Sea transform and Gondwanian elements (modified after *Flexer et al.* [2005] and *Hirsch et al.* [1995]), Projection UTM, WGS 1984

The opening of the Neotethys across Gondwana in the Early Triassic was followed by cyclic sedimentary deposition of the Ramon Group (Olenekian-Rhaetian), Arad Group (Pliensbachian-Tithonian), the Galilee Group (Berriasia-Aptian) and the Judea Group (Albian- Coniacian) in the Mesozoic (230-80 Ma) until the middle Cretaceous, which were partly disturbed by intra cratonic rifting, uplifts, volcanic activities and/or eustatic sea level changes.

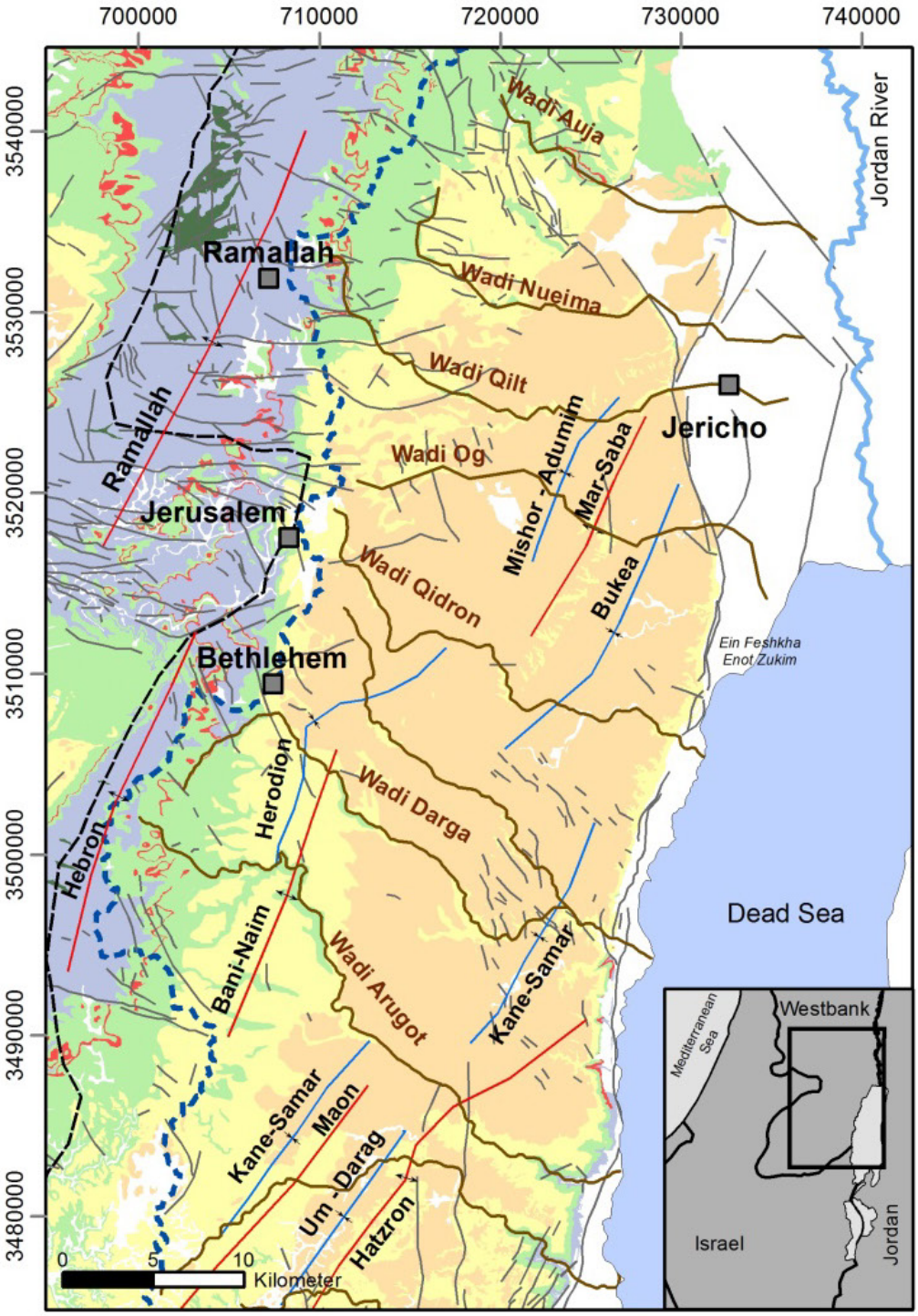

Figure 2 Geological map 1:200.000 (Projection UTM Zone 36 N, WGS 1984) with structural elements, fold structures after *Begin* [1974], *Mor and Burg* [2000], *Raz* [1986], *Roth* [1973], *Shachnai* [2000], *Sneh and Avni* [2011]; *Sneh and Roth* [2012], * after *Gräbe et al.* [2013]

A phase of collision followed, which resulted in an inversion of Early Mesozoic faults like the deformation of the Negev-Palmyrid belts and asymmetrical folding of the S-shaped Syria arc. This folding covered the northern Sinai to Palmyrids and were formed asymmetric in the Negev and Jerusalem mountain area (Figure 1). During the Senonian-Paleocene to Eocene, carbonatic and siliceous sedimentation of the Mount Scopus took place according to forming of the Syria arc. A drop of sea level effected regional regression, emergence and erosion during the mid-Oligocene possibly caused by tectonic rebounds. Starting in the late- Oligocene, Gondwana was divided into African and Arabian plate by opening the Red Sea.

The progressive collision with the Neo-Thetyan Anatolian plate generated development of the Jordan Rift - a sinistral strike slip fault, which opened a chain of rhomb-shaped grabens along the Jordan-Gulf of Aqaba-Line. Via transgression the rift was filled with sea water penetrating from the Mediterranean Sea into the rift [*Rosenthal et al.*, 2009]. Precipitation of evaporates and development to hypersaline conditions happened for Sdom Sea (post-Messinian). During Pleistocene the freshwater Samra Lake (790-1250 ka) was formed by fluvio-lacustrine conditions [*Zak*, 1967]. Progressing salinization of the Samra Lake as a result of evaporate dissolution from Sdom Sea result in to transition to the Lisan Lake (11- 70 ka). The latest remnant of ongoing salinization and evaporation can be found in the recent Dead Sea [*Horowitz*, 2001; *Rosenthal et al.*, 2009; *Zak*, 1967].

Regarding the recent local geological situation, the investigated aquifers are part of the eastern arm of a morphologic and geological fold structure (Eastern Mountain Aquifer – EMA, Figure 3). The top of this Ramallah-Jerusalem-Hebron mountain ridge is shifted to east in comparison to the geological fold top (Figure 2). This causes a shifted surface and subsurface water divide (see Figure 2). The top of the geological fold is eroded and along the mountain ridge the lower and upper Cretaceous layers until Aptian are exposed. This mountainous zone builds the recharge area. Towards east, the Cretaceous layers lie almost parallel to the declining morphological surface (~5° layer dip) controlling a general groundwater flow from west to east.

Smooth anticlinal- and syncline fold structures [*Flexer and Honigstein*, 1984] characterize Cretaceous layers in the transition zone. Theses anticline- syncline structures can influence the groundwater flow or causes preferential flow paths, particularly also by declination of the structures, e.g. “Mishor-Adumim, Marsaba and Bukea”-fold structure is declined to graben fault/ Jericho. The Cretaceous layers are cut by the N-S Dead Sea transform fault and form of a sharp escarpment at the Jordan-Dead Sea rift valley. The valley is filled heterogeneously with sediments from both sites of the rift and forms the deposits of the temporary flooding like e.g. Lake Lisan during the Quaternary. Along the graben fault and in the Quaternary sediments the groundwater of the Cretaceous layers emerges, particularly along Dead Sea coast. Here the Ein Feshkha spring region is the main freshwater/ brackish water spring outflow at north western coast of the Dead Sea. There are springs, which emerge into the Dead Sea during the whole year (e.g. “Enot Zukim”) and also some seasonal springs emerging only in the summer season (e.g. “Summer spring”).

There are some local characteristics like wadi structures incised in the Cretaceous aquifers, which can be discussed partly as a result of erosion and/or reasoned by faults. Along the wadi valleys, springs emerges from the Turonian layers like in the Wadi Qilt or from the upper Cenomanian layers like in the Wadi Arugot (see Figure 2). The composition of the lithostratigraphy from Quaternary to lower Cretaceous is summarized in the following table and chapter part and table 1.

Table 1 Stratigraphic table including aquifer characterization [*Rofe and Raffety*, 1963]

Age	Epoch	Group	Formation (Israeli terminology)		Formation (Palestinian terminology)
Quaternary	Holocene/ Pleistocene	Dead Sea Group	Alluvium		Lisan
			Lisan		
	Pliocene		Samra		
Cretaceous	Senonian	Mt Scopus Group	Hatrurim	Gahreb	Abu Dis
			Mishash		
			Menuah		
	Turonian	Upper Judea Group (UJGA)	Nezer	Bi'na	Jerusalem
			Shivta		
			Derorim		
	Upper Cenomanian		Weradim		Upper Bet - Lehem
			Kefar Sha'ul		Lower Bet - Lehem
			Amminadav		Hebron
	Lower Cenomanian		Moza	Ein Yorqe'am	Yatta
			Beit Meir		
	Albian	Lower Judea Group (LJGA)	Kesalon		Upper Beit Kahlil
			Soreq		
			Giv'at Ye'arim		Lower Beit Kahlil
			Kefira		
	Aptian	Kurnub Group	Qatana		Kobar
			Ein Qinya		

Aquifer characteristics

Aquifer
Aquitarde
Aquiclude

Holocene/ Pliocene – Lisan

The Lisan Fm. is distributed along wadi outlets and in the Jordan Valley and its highest deposition areas are at 180 m below MSL [*Begin*, 1974]. Laminated aragonite-chalk, gypsum and clay are the composition of Lisan with a few sandstone and pebble beds [*Begin*, 1974]. Fossil traces of hypersaline to fresh-water facies and sediment structures as ripple marks, slumps were mapped by *Begin* [1974]. The average thickness is 35 m in the Jericho map [*Begin*, 1974].

Pliocene - Samra Formation

Layers of the Samra Fm. are deposited along the western part of the Jordan Valley, at the basis along the marly cliffs of the Jordan River and partly on top of the desert slopes of the transition zone. Main components are conglomerates, sandstones and silt, so there is a differentiation into two units of silt or coarse clastic possible [*Begin*, 1974]. Within the silt layers, an occurrence of mainly brown calcareous silt and beds of unconsolidated pebbles in interposition with Lisan Fm. is

common [*Begin*, 1974]. The coarse clastic deposits are composed mostly of hard conglomerates or consolidated pebble beds and partly calcarenite and beds of silt [*Begin*, 1974].

Senonian - Ghareb Formation & Hatrurim Formation

The Ghareb Fm. consists of yellow chalk and partly limonite and bitumen. In the Jericho area, it is exposed with an average thickness of 35 m [*Begin*, 1974] and overlies the Mishash Fm. [*Rosenfeld and Hirsch*, 2005]. In the area of the Marsaba syncline, the Gahreb Fm. is associated with the Hatrurim Fm. caused by contact metamorphism [*Rosenfeld and Hirsch*, 2005]. In comparison to sedimentary deposition of the Ghareb Fm., the Hatrurim Fm. is composed of an unstructured accumulation of dense crystallized calcium – silicates, irregular crossed by calcite veins with high temperature minerals.

Senonian – Mishash Formation/ Abu Dis Formation

In the north of the investigation area (Ein Samian, Wadi Auja), the Mishash Fm. /Abu Dis is subdivided into an upper and lower part and in the southern area it is undifferentiated. The lower part contains white chalk interbedded of thin chert. At the basis occurs a chert/flint and chalk complex of 3- 10 m thickness, so called “double chert” [*Begin*, 1974]. The chert is identifiable by its brown colour and dark brown patina [*Begin*, 1974]. In the upper part of the Mishash Fm. the chert components increase in size and reach a thickness of 2 m forming a cliff. The chalk, which follows above the massive chert, is intra-formational folded and characterised by thin chert beds, brittle phosphoritic chalk, accessory siliceous phosphorite and siliceous limey concretions (up to 1m) [*Begin*, 1974].

Senonian – Menuah Formation/ Abu Dis Formation

The Menuah Fm. /Abu Dis Fm. contains chalk and limey chalk with fossiliferous and bituminous characteristics [*Begin*, 1974]. The lower part shows mostly grey, hard chalk, which changes into white, brittle chalk in the upper part. The formation is exposed along the Marsaba anticline (Figure 2) and ranges in thickness of 25- 40 m in the north [*Begin*, 1974], [*Shachnai*, 2000] to 70 m [*Hirsch*, 1983] to the south of the investigation area.

Turonian – Bi’na Formation/Jerusalem Formation

The Bi’na Formation/Jerusalem Formation consists of fine limestones and dolomites. It is characterised by layers up to 1m and vertical fissure. The deposition of the limestone is poorly fossiliferous, mostly homogenous as it is observed in the outcrops of the Wadi Qilt area. Here, the contact to the overlying layers of Menuah Fm. is defined by a transition to chalk [*Roth*, 1973]. To the north the Bi’na Formation is separately mapped in the Formations Nezer, Shivta and Derorim [*Begin*, 1974], particularly in the Wadi Auja and in the Ein Samia. Total thickness of Bi’na formation is observed constantly up to 100 m [*Hirsch*, 1983].

Upper Cenomanian – Weradim Formation/ Upper Bet- Lehem Formation

The Weradim Fm./Upper Bet – Lehem contains types of well-bedded and massive dolomite including lenses of crystalline limestone [*Rosenfeld and Hirsch*, 2005]. It crops out in the mountain region with a thickness of 30 m [*Shachnai*, 2000] increasing to 50-150 m towards south [*Hirsch*, 1983].

Upper Cenomanian – Kefar Shaul Formation/ Lower Bet – Lehem Formation

The Kefar Shaul Fm./ Lower Bet – Lehem is described as a layer with rich megafauna implying Middle Cennomanian age. The formation is built of an argillaceous, fossiliferous limestone including a marl with an upper part of laminated, fossiliferous limestone [*Rosenfeld and Hirsch*, 2005]. In the mountains, the layers are exposed with a thickness of up to 180 m [*Shachnai*, 2000] and wedges out to up to 15 m [*Hirsch*, 1983]. A sharp contrast to the underlying Ammindav Fm. and overlying Weradim Fm. caused by a facies change is visible [*Rosenfeld and Hirsch*, 2005].

Lower Cenomanian – Aminadav Formation/ Hebron Formation

The Aminadav Fm./Hebron Fm. is mainly dolomite, which changes to limestone in the upper part [*Rosenfeld and Hirsch*, 2005]. Accessory, quartzolite (silicified inclusion) is embedded [*Rosenfeld and Hirsch*, 2005]. In the north of Jerusalem, the Aminadav Fm. /Hebron Fm. is exposed with a thickness of 160 m [*Shachnai*, 2000] and varies towards the south between 40-90 m [*Hirsch*, 1983].

Lower Cenomanian – Moza Formation, Beit Me'ir Formation,
Ein Yorqe'am Formation/ Yatta Formation

In Jerusalem, the Moza Fm. is exposed as a marly layer with a thickness of 10-15 m [*Sneh and Avni*, 2011]. In the Jericho region, the Moza Fm. is considered as part of the Ein Yorqe'am Fm. The Ein Yorqe'am Fm. is also exposed e.g. in Wadi Auja and is here subdivided into two parts, where the Beit Meir Fm. is situated in between [*Hirsch*, 1983]. The upper part of the Ein Yorqe'am Fm. consists of mainly three types of layers [*Hirsch*, 1983]:

- Yellow to white chalk including parts of marl and limestone, which are correlated with the Moza Fm. in the Jerusalem area.
- Limestone, which shows bedding of grey, hard biomicritic layers and accessory chert nodules.
- Directly on top of the Beit Me'ir Fm., the Ein Yorqe'am Fm. is a soft, fossiliferous limestone or chalk.

The Beit Me'ir Fm. also called Beit Me'ir tongues comprises a soft, yellow to grey dolomicrite, which is generally well-bedded, partly laminated, with accessory chert nodules [*Begin*, 1974]. Thickness varies with up to 50 m [*Begin*, 1974]. Moza, Beit Me'ir and Ein Yorqe'am formations act as aquiclude between Albian and Upper Cenomanian.

Albian – Kesalon Formation/ Upper Beit Kahlil Formation

The Kesalon Fm. /Upper Beit Kahlil Fm. contains well - bedded limestone, which are partly biomicrite and partly dolomitic biomicrites and show a cliff-forming ostreid bank on the top [*Hirsch*, 1983]. It is up to 20 m thick [*Hirsch*, 1983].

Albian – Soreq Formation/ Upper Beit Kahlil Formation

The Soreq Fm. (lower part of the Upper Beit Kahlil) is characterised by argillaceous dolomite [*Rosenfeld and Hirsch*, 2005]. This layer is 60 - 130 m thick (*Hirsch* [1983], *Shachnai* [2000]) and contains marl and the bedding of the soft dolomite is regular and definite [*Rosenfeld and Hirsch*, 2005].

Albian – Givat Yearim Formation/ Lower Beit Kahlil Formation

The Givat Yearim Fm./Lower Beit Kahlil is dominated by dolomite beds, which are characterised by finely crystalline dolomite with appearance of coarse crystalline dolomite [*Rosenfeld and Hirsch*, 2005]. Secondly, platy quartzolite layers including fossils like rudists or bivalves are embedded in the upper part [*Rosenfeld and Hirsch*, 2005]. The formation varies in thickness from 40 to 70 m (*Hirsch* [1983], *Shachnai* [2000]) and is exposed along the anticline axis in the mountain region.

Albian – Kefira Formation/ Lower Beit Kahlil Formation

The Kefira Fm./Lower Beit Kahlil Fm. belongs to the lower part of the investigated aquifer (lower Judea group aquifer). It contains mainly well-bedded limestones [*Rosenfeld and Hirsch*, 2005] and the thickness ranges from 100 to 166 m (*Hirsch* [1983], *Shachnai* [2000]). Layers of limey dolomite alternate within the limestone and in the upper and lower parts there are interpositions of oolitic limestone [*Rosenfeld and Hirsch*, 2005]. The whole formation contains characteristic cavities [*Rosenfeld and Hirsch*, 2005].

3 Methodology

The western Dead Sea aquifer system was investigated on hydrochemical tracers in the groundwater and aquifer rocks. In this chapter, the sampling strategy and procedure as well as the analysis methods of each parameter group in the laboratories is described.

3.1 Sampling

Sampling time

Sampling was accomplished almost every three months within duration of two year. The sampling cycle started in June/July 2012.

Table 2 Overview of sampling cycle

Sampling	Season
June/July 2012	Summer
October/November 2012	End of summer/ Begin of winter
February 2013	Winter
May/June 2013	End of winter/ Begin of summer

The sampling times are correlated with summer season and winter season in the region. By referring on chapter 2.2 Climate and 2.3 Vegetation and land use, the summer season is characterized by low precipitation rates and high temperatures/ evaporation rates whereas the winter season is the main time for rain and groundwater recharge. In relation to this, effects on groundwater chemistry by anthropogenic substances of agriculture origin or urban source mobilized via rain water would be evaluable. In addition to the generated data in 2012 and 2013, the results include analyses from 2007-2011, which are provided in the frame of SMARTII by the UFZ work group (Dr. Christian Siebert, Dr. Stefan Geyer Dr. Tino Rödiger) for the same sampling locations/regions.

Sampling locations

The investigation area is affected by its geology and by anthropogenic factors such as settlements and infrastructure. These facts frame the basis for the selection of the sampling sites, which are related to the main groundwater aquifers (Upper Cenomanian aquifer (UC) and Albian aquifer) and aquifer outlets (springs) (Figure 3).

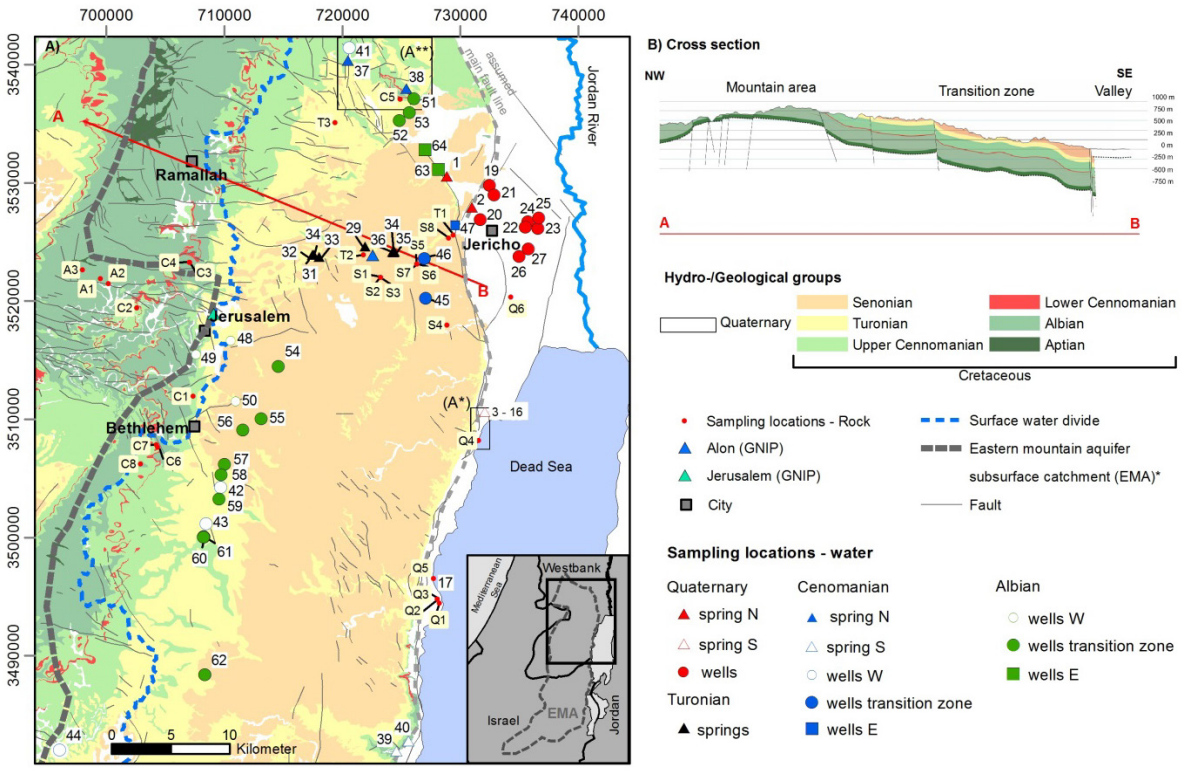

Figure 3 Hydro -/ Geological map of the Western Dead Sea catchment (Projection UTM Zone 36N, WGS 1984) including sampling locations, subset A* corresponds to Figure 5, subset A corresponds to Figure 4, geological map and cross section after (e.g. *Begin* [1975], *Mor and Burg* [2000], *Roth* [1973], *Sneh and Avni* [2011]), * after *Gräbe et al.* [2013]**

The sampling was focused on wells for water supply (serviced by Mekorot and PWA) of the Upper and Lower Cretaceous aquifers in the mountain area. In the Lower Jordan Valley/Jericho, groundwater samples of the Quaternary section were taken from private wells for agriculture use or water supply wells serviced by PWA (Table 3). In the area between the mountains and the graben fault are few wells available due to increasing depth to water table. Natural aquifer outlets of the Cretaceous layers were sampled in Wadi Qilt, Ein Samia, Ein Auja (Figure 4) and Ein Dyouk.

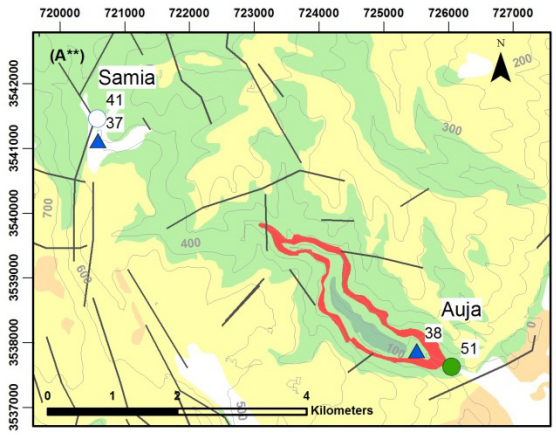

Figure 4 Geological situation of sampling locations surrounding Samia and Auja (subset A of Figure 3, including legend), morphologic contour lines (50 m SRTM)**

Table 3 Overview of sampling locations sorted after aquifer and region of sampling, numbering (No.) according to figure 3

No.	Station
Springs N	
1	Ein Dyouk
2	Ein Su ltan
Springs S	
3	Ein Feshkha creek
4	Ein Feshkha spring
5	Ein Feshkha - creek izik
6	Ein Feshkha Magnum
7	Ein Feshka -Ripple
8	Ein Feshkha - Summe r Spring
9	Ein Feshkha - Eselsquelle
10	Ein Feshkha - Red Stones
11	Ein Feshkha - Fig Spring
12	Ein Feshkha - Green Algea
13	Ein Feshkha - Stream
14	Ein Feshkha (untere r Ablauf)
15	Ein Feshkha - Big Swimming Pool
16	Ein Feshkha - Enot Zukim 1+2
Lower Jordan Valley - pore water	
17	Pore water 1 Darga
18	Pore water 4 Ein Feshkha
Wells	
19	Khader Humaidat
20	Abu Khalil
21	Saed Abu Ali well
22	Arab Project 19-14/67
23	Arab Project 19-14/66
24	Arab Project 19-14/70
25	Arab Project 19-14/72
26	Jericho well
27	19-13/24A
Dead Sea	
28	Dead Sea

No.	Station
Springs S	
29	Ein Fawwar
30	Ein Fara/ Ein Ferat 1a
31	Ein Ferat 1b
32	Ein Ferat 2
33	Ein Ferat 3
34	Ein Qilt
35	Ein Qilt upper
36	Ein Qilt lower

No.	Station
Springs N	
37	Ein Samia 1
38	Ein Auja
Springs S	
39	Arugot uppe rmos t
40	Ein Gedi
Wells W	
41	Ein Samia 2
42	Herodion 1
43	Beit Fajjar
44	Al Rehiyya
Wells - Transition zone	
45	Mitzpe Jericho 2
46	Mitzpe Jericho 5
Wells E	
47	Jericho 2

No.	Station
Wells - W	
48	Jerusalem 4
49	Je r u s a l e m 1
50	Je r u s a l e m 6
Wells - Transition zone	
51	Auja 2 well
52	Auja 3 well
53	Auja 4 well
54	Al Azaria 3
55	Al Azaria 1
56	Shdema 1
57	PWA 3
58	Herodion 2
59	Herodion 3
60	Herodion 4
61	Herodion 5
62	Bani Naim 3
Wells E	
63	Jericho 4
64	Jericho 5

The sampling site Ein Feshkha (Figure 5), most important aquifer outlet of the NW Dead Sea catchment, was investigated in every sampling campaign. The southern part of the nature reserve with the main spring outlet close to the entrance (Enot Zukim 1+2) and smaller springs emerging along NE-SW orientated sections were the major focus. In the northern part of the nature reserve, springs do not exist anymore since 2009 according to mapping activities of GSI in the last years. Due to limited access to the nature reserve at the beginning of the study, small springs were sampled only during later campaigns.

Rock samples were collected of the exposed lithology according to the important exposed aquifer formations in October 2012 (stratigraphy in Table 1, Figure 3). Pore water was derived from sediment samples, which were obtained close to the Dead Sea shore in a depth of 2.5 m from the Dead Sea Fm. at Ein Feshkha and Darga, respectively. Applying an adapted squeezer, the pore water was extracted on site and immediately filtered and stabilized for further analyses of cations, anions and strontium isotopes.

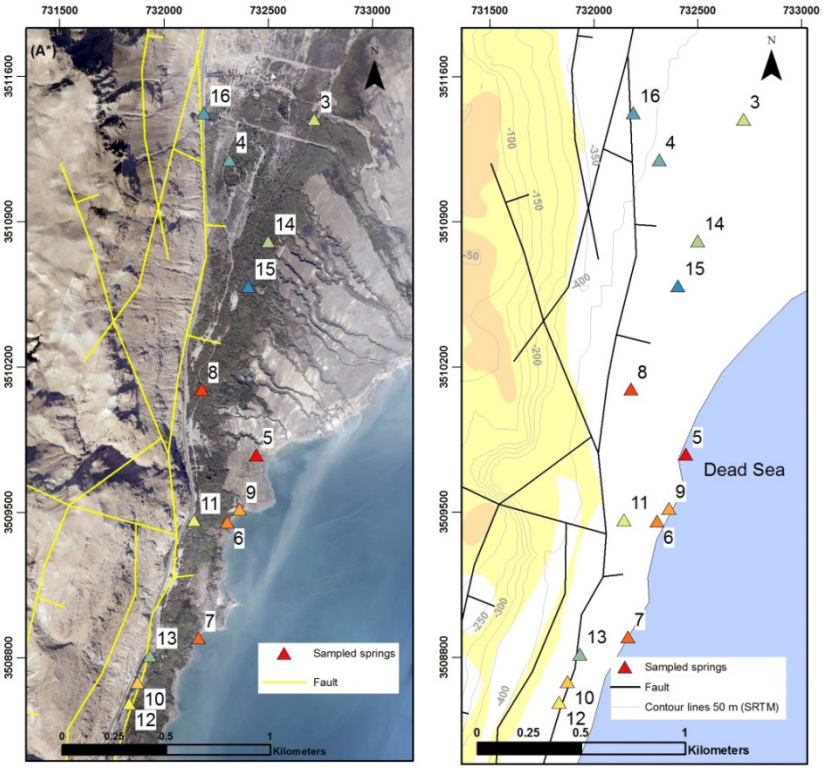

Figure 5 Sampling map of Ein Feshkha (subset A* of figure 3), left side: topographic map [*Mallast et al.*, 2013], right side: geological map; sampling points are located on deltaic platform of post - Lisan Alluvium (largely Holocene), geologic and fault distribution after (*Begin* [1974], *Lubberts and Ben-Avraham* [2002])

3.2 Sampling procedures and analytical methods

The following sub-chapter, the preparation and analyses methods for each parameter group are summarized. The detailed justifications and relevance for the research objectives are explained in chapter 4, 5 and 6.

3.2.1 Groundwater and rock analyses

Major ions and trace elements

For sampling of major ions and trace elements, clean HDPE-bottles of 30 - 60 ml volume were used. In the field, a syringe plus 0.45µm CA filter (Sartorius) was applied to provide filtrated sample for a cation sample and anions sample. Before filling the bottle completely, each bottle was rinsed three times with filtrated water. HNO_3, 20µl, is added via pipette to the cation sample for conservation (provide pH < 2). Bicarbonate is analysed by titration (digital HACH titrator, Germany) with H_2SO_4 until pH 4.3 on site. On site parameters (pH, T, EH, EC) were measured by using WTW 350i (WTW, Germany). The Analytical Department of the UFZ prepared and analysed the major ion samples. For Na, K, Ca, Mg, ICP-OES - Spectro Ciros CCD (Spectro Analytical Instruments, Germany) was used and Cs was analysed with ICP-MS - iCAP Q (Thermo Fisher Scientific, Germany). Cl, Br, sulphate and nitrate were measured with IC - Dionex ISC 2000 (Thermo Fisher Scientific, Germany).

At the UFZ Magdeburg, preparation and analyses of trace elements were conducted for Cd, Cr, Cu, Fe, Ni with an ICP-MS (Agilent 7500 c, USA) and for Ba, Sr, B, Li, Rb, Mn, U and As with an ICP-OES (Perkin Elmer 7300 DV, Germany). Trace elements were analysed on two types of samples:

- "diluted" content in the water (filtrated with 0.45µm CA filter (Sartorius) and acidified with 20µl HNO_3)
- "suspended"/ total content in the water (no filtration, acidified with 20µl HNO_3)

Analyses were given in mg/l and on the bases of the atomic masses of each parameter (Ca, Mg, Sr, Na, K, Cl, SO4, NO3 and HCO3) and ion charge; all concentrations were transferred to meq/l. The calculation of cation-anion balances was used to evaluate the quality of water analysis [*DIN38402-62*, 2014]:

$$\Delta_{meq/l} = \frac{(\Sigma_{meq+} - \Sigma_{meq-})}{(\Sigma_{meq+} + \Sigma_{meq-})} < 5\%$$

Equation 1

Ion balances of the generated data set show ion balances mainly < 5%. To obtain equalized ion balances of anions and cations for all water analyses, concentration of HCO_3 were calculated from the subtraction of major cations sum (Ca, Mg, Na, K) and major anion sum (Cl, SO_4, NO_3). Total dissolved content in the water samples were calculated in mg/l (TDS) and in meq/l (TDE). All results are presented in appendix A.1.

Rare earth elements and yttrium (REE+Y)

REE+Y were filtered into HDPE bottles using Sartobran 0.2 µm filter cartridges (Sartorius, Germany) coupled to a peristaltic pump. HDPE bottles were pre-cleaned by steam stripping with ultrapure 6N HCl (Merck, Germany). For REE-analyses, to a total of 4.5 L of sample was taken. Respective amounts of sub-boiled HCl were added on site to stabilize samples at pH of 2 and 1 ml of 100 ng/ml Tm-spiked solution were added for later recovery control of REE+Y in the pre-concentration treatment. The low concentrations of REE+Y require pre- concentration by the following method. The acidified samples (V=4.5 L; pH=2) were passed through a pre-conditioned

C18 Sep-Pak cartridge at a rate of 1 L/h. Cartridges were pre- conditioned in the laboratory, loading them with a liquid ion exchanger (2-Ethylhexyl phosphate, Merck Millipore). After washing REE+Y-loaded cartridges with 50 mL of 0.01 M sub-boiled HCl, REE+Y were eluted by 40 mL of 6 M sub-boiled HCl at a rate of 3 mL/min. The eluates were evaporated to incipient dryness and the residues dissolved in 2 mL of 5 M sub- boiled HNO_3 and spiked with an internal standard to be used to correct the internal drift of the response factors in the ICP-MS (Xseries II, Thermo Scientific, Germany) measurements at the FSU (Friedrich-Schiller-University) Jena, wherever necessary. The recovery of the Tm- spikes was better than 94%.

Rock samples were homogenized and grounded (<70µm) by the use of an achat mill (ball mill, Pulverisette 6“, Fritsch, Germany) and further prepared in two ways:

(i) Rock leaching for analyses of dissolvable REE+Y

Rock leaching experiments included different leaching steps (2,4,6,8 and 16h) of a rock sample (grounded and milled to <70µm) and a cation exchange resin in a water phase (procedure modified after *Möller and Giese* [1997]. In every leaching step a certain amount of rock powder was mixed with cation exchange resin (AG 50W-X8, Bio - Rad AG) and 30 ml ultrapure water in an ultrasonic bath. After the leaching reaction, the cation exchange resin was separated from the rock powder and eluted slowly (~45 min elution time) with 50ml M HNO_3 (ultrapure) to obtain REE+Y. Eluate was evaporated to 5ml and filled to 10 ml with ultrapure water. Measurements were accomplished with ICP-MS (La-ICP- MS “Element XR”, Thermo Scientific, Germany) at the Analytical department of UFZ Leipzig.

(ii) Total rock digestion

For total rock digestion (ii) grounded rock samples (<70µm) were treated with a mixture of HNO_3, HF and $HClO_4$ at FSU (Friedrich-Schiller-University) Jena. The extract was analysed with ICP-MS (XSeries II, Thermo Fisher Scientific) and ICP-OES (725 ES, Agilent).

C1 – standardization by the use of C1 chondrite composition [*Anders and Grevesse*, 1989] is applied to prepare comparable REE+Y patterns. Results of groundwater and rock samples (C1 normalized) are given in appendix A.6.

Stable isotopes – δ^2H and $\delta^{18}O$ of water

For sampling of the stable water isotopes, HDPE-bottle were used, and three times rinsed with filtrated (CA 0.45 µm filter + syringe, Sartorius) sampling water before filling the bottle. The water isotope ratios of $\delta^{18}O$ and δ^2H were analysed with a Picarro L 2121-I Isotopic Liquid Water Analyzer ($\delta^{18}O$ 2σ = 0.4‰ and δ^2H 2σ =1.5‰). Results are given in δ notation (δ^2H_{water}, $\delta^{18}O_{water}$) as parts per thousand (‰) deviations relative to the Vienna Standard Mean Ocean Water (VSMOW, from IAEA).

Stable isotopes - $\delta^{34}S$ & $\delta^{18}O$ of sulphate, $\delta^{13}C$ & $\delta^{18}O$ of carbonate

For analyses of stable isotopes of sulphate and carbonate, solid samples were precipitated from groundwater samples. A volume of 1.5l unfiltered groundwater was collected. On site, the chemicals sodium hydroxide (Merck) in pellets and barium chloride dihydrate (Merck) in solid

phase were added to induce the precipitation of sodium carbonate and barium sulphate according to the following chemical reactions (Eq.2 and Eq.3):

$$NaOH + HCO_3^- \rightarrow NaCO_3 \downarrow + H_2O$$

Equation 2

$$BaCl_2 * H_2O + SO_4^{2-} \rightarrow BaSO_4 \downarrow + 2Cl^- + 2H_2O$$

Equation 3

The 1.5 l bottles were stored for two days to collect the complete precipitate of the sample on the bottom of the bottle. For transportation to the laboratory, the precipitation was separated and filled into HDPE-bottle (60-30 ml). In the stable isotope laboratory of the Helmholtz environmental research centre in Halle, the precipitates were filtered (0.45µm cellulose-acetate filter, Sartorius), washed with distilled water and dried (65°C). After a second drying step to remove organic material (500°C, 2h), an Isotope ratio mass spectrometer (IRMS delta S Finnigan MAT) coupled with continuous flow combustion technique was used to determine the perspective isotope ratios. Analytical error (2σ) was ±0.3‰ for sulphur and ±0.6‰ for oxygen. Results are given in δ notation ($\delta^{34}S_{sulphate}$, $\delta^{18}O_{sulphate}$) as parts per thousand (‰) deviation relative to the Vienna Cañon Diablo troilite (VCDT) standard and Vienna Standard Mean Ocean Water (VSMOW, from IAEA). The IAEA-distributed reference material NBS 127 ($BaSO_4$) was used.

Rock samples (crushed, finely grounded, homogenized, 2g) for $\delta^{34}S_{sulphate}$ & $\delta^{18}O_{sulphate}$ were heated with 6 M HCl (50 ml) until boiling point to digest the rock matrix and for separation of the carbonate fractions. After cooling, separation of the indissoluble parts (sulphate free) was obtained via filtration and 50 ml distilled water was added. By adding 5ml BaCl2, bariumsulphate was precipitated (see Eq. 3), which was then dried and analysed. For analysis of $\delta^{13}C$ in the stable isotope laboratories of the Helmholtz centre for environmental research, the samples were dried, homogenized and added to phosphoric acid in closed, helium-cleaned vials to extract CO_2 for the measurement (IRMS - Delta V Plus in combination with Gasbench). Carbon isotopes were analysed in reference to VPDB (Vienna Pee Dee Belemnite) and oxygen isotopes are analysed in reference to VSMOW (Vienna Standard Mean Ocean Water). Rock samples for $\delta^{13}C$ were crushed, finely grounded, homogenized and further treated in the same way as precipitate from the water samples.

Stable isotopes – $^{87}Sr/^{86}Sr$

For $^{87}Sr/^{86}Sr$ water samples, HDPE bottles (cleaned with ultrapure vaporized 6 M HCl) were used. In the isotopic laboratory of the TU Bergakademie Freiberg, the samples were evaporated, and the residues dissolved in 3.5 M HNO_3 (ultrapure). By standard cation exchange, strontium was separated and the specific isotope ratios and analysed with a TIMS (Finnigan MAT 262) in reference to international standard material NBS-987 [*Tichomirowa et al.*, 2010]. $^{87}Sr/^{86}Sr$ measurements of ten scans were repeated up to 20 times to achieve acceptable error statistics (mean 2σ=0.00002). $^{87}Sr/^{86}Sr$ analysis of rock samples were conducted by dissociation of finely grounded rock material with ultrapure 2.5 M HCl to get readily dissolvable carbonate and sulphate contents for further separation of Sr by standard cation ion exchange (procedure like water samples).

3.2.2 Age tracer in groundwater

$^{36}Cl/Cl$

Samples for ^{36}Cl analyses were filled in pre-cleaned bottles (250 ml to 500 ml) and acidified with diluted HNO_3. Analyses of ^{36}Cl in groundwater were carried out in Helmholtz Centre Dresden Rossendorf at the accelerator mass spectrometry (AMS) facility DREsden AMS (DREAMS) [*Akhmadaliev et al.*, 2013]. The preparation steps consist of (i) precipitation of the chloride fraction via adding sliver nitrate solution and subsequent dissolution of the AgCl in NH_3; (ii) separation of chlorides from sulphates by precipitation of the sulphates using saturated barium nitrate solution; (iii) re – precipitation and conserving of AgCl with silver nitrate solution [*Merchel et al.*, 2011]. ^{36}Cl was measured with AMS relative to the stable Cl isotopes, ^{35}Cl and ^{37}Cl [*Pavetich et al.*, 2014; *Rugel et al.*, 2016] and is given as ratio $^{36}Cl/(^{37}Cl+^{35}Cl)$ (termed $^{36}Cl/Cl$ in the text).

Tritium

Tritium samples were collected in 500 ml bottles after flushing 3 times with sampled water. Tritium sample preparation and measurement were conducted by the isotope hydrology group of the Helmholtz centre of Environmental research. The preparation steps are described in *Trettin et al.* [2002] and consist of electrolytic enrichment of 400 ml water sample and measurement via liquid scintillation counting. With this method, a detection limit of 0.5 TU is achieved with a relative standard error of 10% for tritium concentrations (> 0.5 TU).

CFC`s and SF_6

Samples for CFC`s and SF_6 were taken in clean glass bottles saved in tins following the methodology provided by the laboratory of Dr. Oster (Wachenheim). After flushing 3 times the bottle and tin in a container of 10l with sampling water (Figure 6), the bottle and tin were closed under water to prevent atmospheric input [*Oster et al.*, 1996]. The gases CFC`s and SF_6 were analysed in the laboratory of Dr. Oster by gas chromatography after *Oster et al.* [1996] and *Bullister and Weiss* [1988].

Figure 6 Sampling of CFCs and SF_6 from well pump; left: well pump and 10l container for sampling, right: 10l container with glass bottle and tin connected with a tube to the pump during flushing with water

Organic trace substances

Organic trace elements (Naproxen, Acesulfame K, Simazine) were sampled in pre- cleaned 1l glas brown bottles with the use of a glass microfiber filter (0.7 µm, GF/F, Whatman). Organic trace substances were extracted by solid phase extraction (SPE) using a polar modified polystyrene-divinylbenzene copolymer sorbent (Chromabond Easy, Machery-Nagel). The frozen SPE cartridges were transported to the lab, Department of Analytical Chemistry of Helmholtz Centre for Environmental Research (UFZ). After elution of the organic trace compounds with methanol they were analysed with HPLC-MS-MS (Agilent 1260, Agilent Technologies, Germany coupled with and QTrap5500 mass spectrometer (AB Sciex, Germany)). Limits of Quantification (LOQ) were for Naproxen 5 ng/l, Acesulfame K 3 ng/l and Simazine 2 ng/l.

3.3 Statistical data evaluation method

Statistical analysis was applied to analyse the associated elements and specific patterns in groundwater in terms of identification of specific saline patterns originating in the Quaternary section as well as Cretaceous groundwater patterns and also detection of local anthropogenic inputs. The statistical evaluation was accomplished with the tool Statistica [*TIBCOSoftwareInc.*, Copyright 1984-2017]and includes the following steps:

Box-Whisker-Plot

Box-Whisker-Plots are a display format of the descriptive statistics, which includes calculated statistical information of the data. The calculated boxes show the median and 25% quartile and 75% quartile. Maximum and minimum is given by the whisker range of the box. Outliers are added with open dots. This type of plot gives the possibility to differentiate between trace element groups including between dissolved and suspended trace element concentrations. Form of the plot informs about normal distribution and potential skewness of the data set. Based on the different extension of box and whiskers, conclusion can be obtained about excess of the data.

Z-scores

Processing step of data for the multivariate statistical analysis was a transformation of each measurement value into a unit-less value. This so- called calculation of z-scores is an appropriate method to standardise data with comparable distributions. It bases on the following equation [*Lohninger*, 08.10.2012]:

$$z_i = \frac{x_i - \bar{x}}{s}$$

Equation 4

z_i represents the calculated z-score, $x_i$refers to original measurement value and the standardisation is calculated with mean $\bar{x}$ and standard deviation s. The applied statistic is related to the total data set including the groundwater data of the two main aquifers as well as the discharging spring in the complete area. To get insight, whether the distinct aquifer and spring

follows specific patterns the different groups were considered separately in the applied statistical analysis.

Cluster analysis

Cluster analysis is a method of the multivariate statistics and aims to find structures (clusters) in the data set [*Lohninger*, 08.10.2012]. By considering of the distance between observation (cases) in a multidimensional data phase, a cluster analyses can solve e.g. following aspects: amount of groups (cluster) in a dataset, which type of object belong to which cluster and how uniform is the cluster [*Lohninger*, 08.10.2012]. Results of a cluster analysis can be presented in hierarchical methods (e.g. dendrogram) and non-hierarchical methods (e.g. k-means clustering), or display methods (principal component analysis or non-linear projections) [*Lohninger*, 08.10.2012]. For hierarchical and non-hierarchical calculations, data are formed in matrix shape [*Schönwiese*, 2006]:

$\{acd\}$, with influences (coordinates, dimensions) c = 1,…, m and single data d, f = 1,.., n

Dendrograms are often applied to display relations between clusters [*Lohninger*, 08.10.2012]. A dendrogram shows multidimensional data space in a tree structure. Objects, which are close to each other in the multidimensional phase are connected by a horizontal line and result into a cluster forming a new object. Distances of specific cluster pairs are characterized by the level of each horizontal line.

There are different cluster algorithms to calculate distances between the clusters. Type of grouping was proposed by *Lance and Williams* [1967] in a recursions formula, cluster algorithm:

$$b'_{qi} = tb_{pi} + ub_{qi} + vb_{pq} + w\left|b_{pi} - b_{pq}\right|$$

t, u, v, w	system parameter
$b_{pi,}\, b_{qi}, b_{pq}$	distance between cluster (or objects)
b'_{qi}	new distance between new cluster q and the new objects i

Equation 5

By application of Ward`s method, homogeneous (as possible) clusters are aimed to find by every step of merging data with minimum of heterogeneity to one cluster (*Steinhausen and Langer* [1977] in *Schönwiese* [2006]), expressed with following supplemented equation from above:

$$b'_{qi} = \frac{(z_p + z_i)}{(z + z_i)b_{pi}} + \frac{(z_q + z_i)}{(z - z_i)b_{qi}} + \frac{(-z_i)}{(z - z_i)b_{pq}}$$

number of objects

z_p	number of objects in cluster p
z_q	number of objects in cluster q
z_i	number of objects in cluster i

Equation 6

To reach minimal heterogeneity, cluster/data of lowest relation to a defined heterogeneity degree were merged stepwise (*Steinhausen and Langer* [1977] in *Schönwiese* [2006]). Ward`s method uses squared Euclidian distances, which are appropriate for a two- dimensional case describing the distance between two specific data points based on the theorem of Pythagoras [*Schönwiese*, 2006]:

$$Euclidian\ distance = \sqrt{\Sigma_{i=1}^{m}\left(x_{cd} - x_{cf}\right)^2}$$

Equation 7

4 Results and discussion

4.1 Groundwater origin and evolution

High-quality groundwater resources are the backbone of water supply in semi-arid areas. Thus their yield and their hydrochemical evolution were studied intensely, particularly in respect to salinization, an abundant phenomenon in these regions (e.g. *Herczeg et al.* [2001], *Hogan et al.* [2007], *Lyons et al.* [1995], *Vengosh et al.* [1999]). Likewise, in multi- aquifer systems, the knowledge about origin and hydrochemical evolution of the individual involved water bodies is fundamental (e.g. *Coppola et al.* [2003], *Rao and Mamatha* [2004]). The aim becomes intricate, when such a system is fed by a common recharge area, composed of similar lithology, and intensely fractured and folded, as given for the Eastern Mountain Aquifer (EMA), shared by Israel and Palestine authorities (Figure 2). To overcome these difficulties and to evaluate aquifer-specific water/rock interactions, we conjointly investigated major element ratios, rare earth element (REE+Y) patterns and stable Sr- and C-isotopes in groundwater and aquifer rocks. To identify the origin and evolution of groundwater in complex aquifer systems, the application of major element ratios and REE+Y has been proofed to be a powerful tool (e.g. *Johannesson et al.* [1997], *Möller et al.* [2003]; *Möller et al.* [2007], *Christian Siebert et al.* [2014]). Further, to differentiates between groundwater according to their hosting aquifers of different ages and to reveal inter-aquifer mixing, $^{87}Sr/^{86}Sr$ signatures and $\delta^{13}C_{DIC}$ have been applied successfully in (e.g. *Wigley and Plummer* [1976], *A Starinsky et al.* [1980], *Stein et al.* [1997], *Dogramaci and Herczeg* [2002], *Négrel and Petelet-Giraud* [2005], *Amitai Katz and Starinsky* [2009], *Shand et al.* [2009], *Tichomirowa et al.* [2010], *Alemayehu et al.* [2011], *Starinsky and Katz* [2014]).

Stable isotopes in carbonate aquifer systems

Carbonate species in the investigation area refer on calcite/ aragonite, dolomite occurrences and mixed mineral species as high Mg-calcite and low Mg-calcite in sediment deposits of the Cretaceous. Deposition and formation of mineral paragenesis in the Cretaceous are related to the past seawater composition and CO_2 pressure in the atmosphere. Studies of carbonate cycles in Phanerozoic times from (e.g. *Steuber and Rauch* [2005], *Rauch* [2005], *Stanley and Hardie* [1998]) report correlations of Mg/Ca ratios and Sr/Ca ratios respectively with sea level. The Sr/Ca ratio of sea water is related to the Mg/Ca and both ratios show anticyclical patterns in Phanerozoic times [*Rauch*, 2005]. During the Cretaceous the global sea level reached a maximum and the Mg/Ca ratio is low and with an increasing trend by decreasing sea level to Tertiary. In carbonates, the minerals calcite, aragonite and dolomite provide the most important source of strontium in relation to Ca substitution in cation exchange processes. Strontium in seawater is precipitated as carbonate and is correlated with the calcite and aragonite precipitation [*Veizer et al.*, 1999]. Ancient seawater is also attributed by specific $^{87}Sr/^{86}Sr$ and $\delta^{13}C$ ratios through time [*Veizer et al.*, 1999] and the global Strontium signal of marine carbonate deposition during the Cretaceous ranges from 0.7072 to 0.708 (e.g. *Steuber and Veizer* [2002]; *Veizer* [1989]; *Veizer et al.* [1997]; *Veizer et al.* [1999]). The $\delta^{13}C$ ratios of marine carbonates in the Cretaceous are 6 to -2 ‰ VPDB [*Veizer et al.*, 1999]. Recent

atmosphere contains comparatively low values of -8 to -10 [*Hoefs*, 1987]. Dissolution processes of carbonate are a function of CO_2 pressure in the aquifer system and dependency of temperature. These system conditions cause incongruent or congruent dissolution of the carbonates and a fractionation of carbon isotope take place, especially between $CaCO_3$ and CO_2 [*Hoefs*, 1987].

4.1.1 Evaluation of meteoric water input

The $\delta^{18}O$ and $^{\delta}2H$ signatures of the groundwater vary between -5 ‰ and -6 ‰ and between 21‰ and -27‰ (Appendix A.2), respectively. Most of the samples extracted from the Cretaceous aquifers plot between the Global Meteoric Water Line (GMWL) (Figure 7 & Figure 8), which is defined through $\delta^2H=8x\delta^{18}O+10$ (e.g. *Dansgaard* [1964], *K. Rozanski et al.* [1993]) and the Local Meteoric Water Line (LMWL), which is calculated by isotope data from stations Jerusalem, and Alon [*IAEA/WMO*, 2017] and given by the equation $\delta^2H=6.4x\delta^{18}O+13.6$ ($R^2=0.8$). In comparison the sampled pore water range between -1 to 11 ‰ for δ^2H and between 4 to 7‰ for $\delta^{18}O$ pointing to the Dead Sea waters. It can be shown that the Ein Feshkha springs follow a trend starting from the fresh water towards the isotopic enriched waters of the pore water, which is result of mixing between brine and freshwater [*Zilberman et al.*, 2017]. Groundwater of the Cretaceous groundwater (including recharge area and transition zone) tends to an enrichment of $\delta^{18}O$ and δ^2H given by low shift of the values from the LWML indicating a fractionation process (Figure 7 & Figure 8).

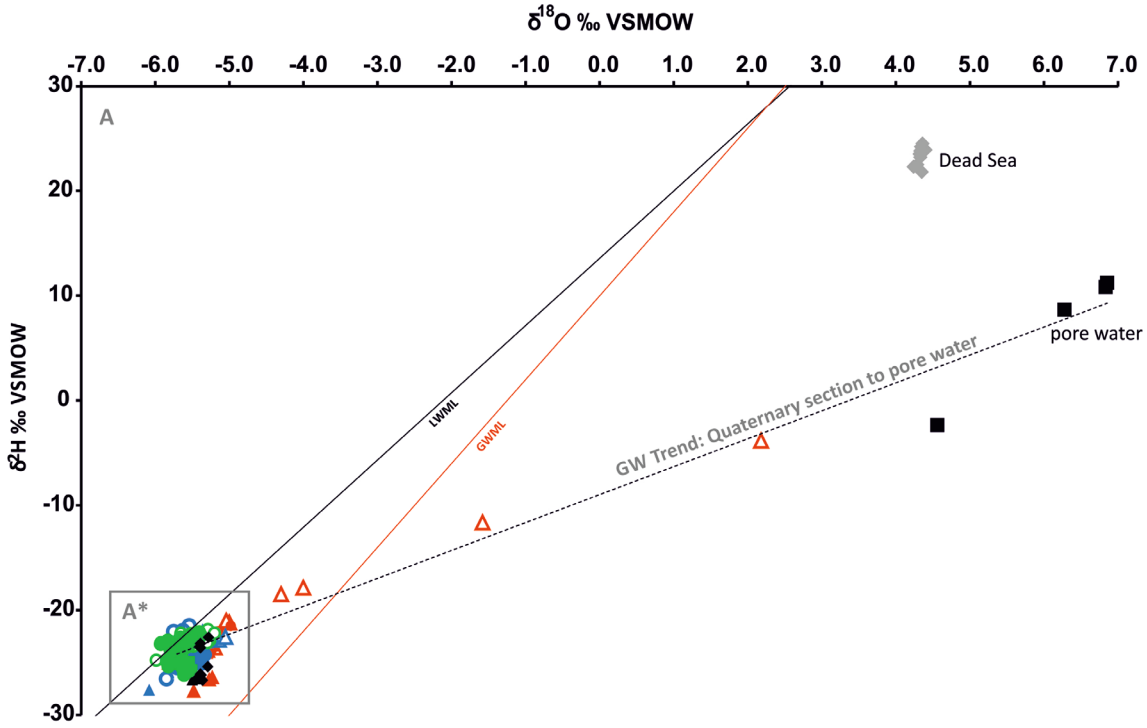

Figure 7 Stable water isotopes of the groundwater in Cretaceous and Quaternary aquifers; Groundwater (springs and pore water) in Quaternary sediments trend to heavier isotope ratios; legend and subset A* corresponds to Figure 8

The Eastern Mediterranean Meteoric Water Line (EMWL) $\delta^2H=8x\ \delta^{18}O+22$ [*Gat and Carmi*, 1970] exhibit a higher d-excess than the global meteoric water line [*Gat and Dansgaard*, 1972]. The shifting of the deuterium excess from 10 ‰ (GWML) to 22‰ (EMWL) refer to climatic conditions

controlling air humidity in this region [*Moser and Rauert*, 1980] due to the same slope of 8. In comparison to the EMWL and GWML, the slope of the LMWL is below 8 indicating evaporation during rainfall (*Dansgaard* [1964], *Friedman et al.* [1962]).

The- d-excess of the Groundwater samples is mainly below the EMWL with varying values between 14‰ and 23‰ (Appendix A.2, Figure 7 & Figure 8). Consequently, the fractionations of the fresh waters refer to evaporation of local rainwater (d-excess =13.6%) during infiltration and at the soil surface. Consequently, recent groundwater recharge (<4 years) can be identified. To the graben deposits the groundwater (including wells in the discharge area and Ein Feshkha springs) tends to enrichment in $\delta^{18}O$ and $^{\delta}2H$ validating admixture of pore water (Figure 7).

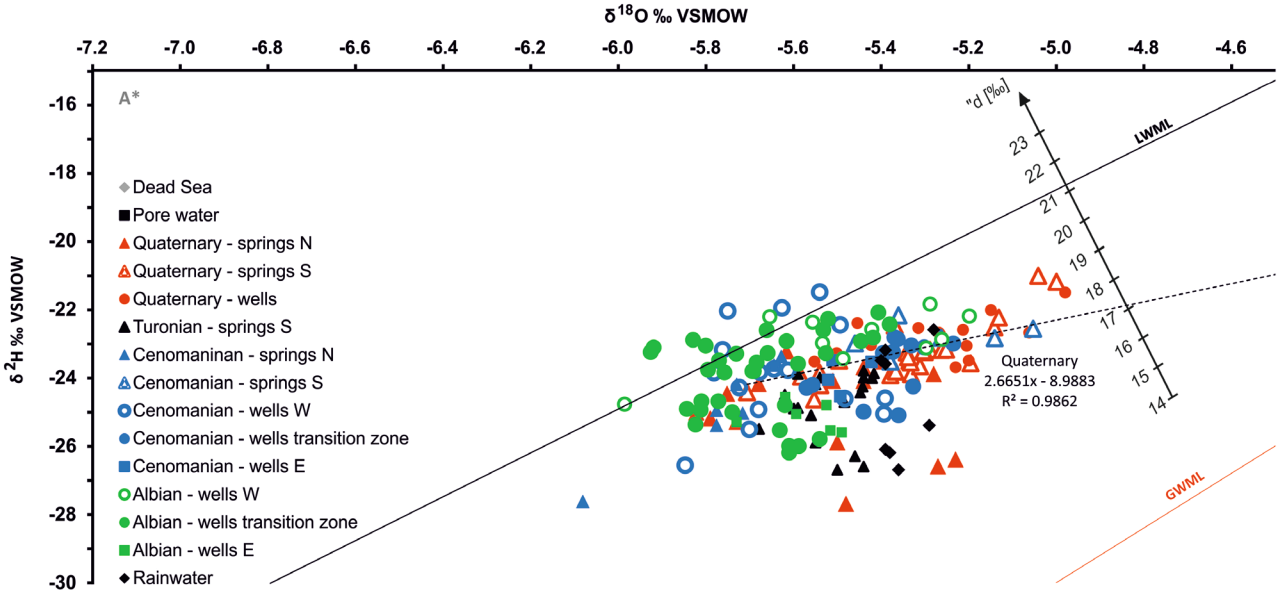

Figure 8 Stable isotopes of groundwater in Cretaceous aquifers (subset of Figure 7) related to LMWL –Local meteoric water line and GMWL – Global meteoric water line

4.1.2 Groundwater types and evolution

The sampled groundwater is characterised by a neutral pH of 6.8 to 7.7 (Appendix A.1), and their contents of total dissolved solids (TDS) vary significantly between 500 mg/l in Cretaceous aquifer to more than 6000 mg/l in Quaternary aquifers. A summary of major ions results including Sr, which contains maximum, minimum and mean is presented in Table 4. The Ein Feshkha spring waters are differentiable from the groundwater in the Quaternary aquifer and built a group with increasing sulphate, chloride and magnesium concentrations. Dead Sea pore water in Ein Feshkha is characterized by high chlorinity and elevated magnesium concentrations (Table 4). Molar Na/Cl values of 0.66-1. are common in marine carbonate aquifers hosting relictic seawater and halite (Na/Cl=0.68-1), resemble those of precipitation (Na/Cl=0.87, *B. Herut et al.* [1992]) or refer to ion exchange processes with clay minerals, resulting in Na/Cl ratio >1. Groundwater obtained from down-faulted blocks of Upper Cenomanian and Albian aquifer (Jericho 2, 4, 5 wells) close to the western main transform fault (Figure 9) become more saline, indicated by TDE of 22-37 and molar Na/Cl ratios of 0.46-0.7, indicating contribution of seawater brines (Na/Cl= 0.86, e.g. *Bruland* [1983] in *Hodge et al.* [1998]), which exist within the Graben.

Table 4 Maximum, minimum and mean of ion concentrations Ca, Mg, Sr, K, Na, HCO_3, SO_4 and Cl [meq/]

		meq/l Na^+	meq/l K^+	meq/l Mg^{2+}	meq/l Ca^{2+}	meq/l Sr^{2+}	meq/l Cl^-	meq/l $SO4^{2-}$	meq/l HCO^{3-}
Quaternary - pore water	Maximum	1758	195	3702	831	7.4	6721	7.1	2.5
	Minimum	1121	171	3246	695	6.3	6378	5.8	1.6
	Mean	1696	191	3329	722	6.5	6620	6.5	1.9
Quaternary - springs N	Maximum	1.6	0.13	2.7	4.96	0.0091	1.7	0.6	5.6
	Minimum	0.9	0.06	1.8	3.42	0.0028	1.0	0.4	3.1
	Mean	1.2	0.07	2.4	4.08	0.003	1.4	0.5	4.6
Quaternary - springs S	Maximum	23.3	1.44	19.0	11.08	0.05	47.3	1.3	6.2
(Enot Zukim)	Minimum	14.6	0.86	11.9	7.24	0.03	27.2	0.7	3.6
	Mean	19.0	1.09	14.8	9.83	0.04	37.0	1.0	4.9
Quaternary - springs S	Maximum	55.2	4.07	63.6	26.05	0.14	152.3	1.8	5.2
(Summer spring)	Minimum	41.6	2.92	42.0	18.01	0.11	114.7	1.2	4.4
	Mean	50.5	3.48	51.3	21.66	0.12	132.2	1.5	4.8
Quaternary - springs S	Maximum	55.2	4.19	63.6	26.05	0.15	152.3	4.0	6.5
(Ein Feshkha)	Minimum	14.6	0.86	11.9	7.24	0.03	27.2	0.7	3.6
	Mean	21.4	1.18	16.2	10.78	0.05	59.7	1.4	5.0
Quaternary - wells	Maximum	57.4	3.84	28.1	13.62	0.12	85.3	10.0	7.8
	Minimum	3.4	0.17	5.0	2.45	0.02	4.3	0.7	4.0
	Mean	19.8	1.93	14.2	9.33	0.04	40.1	4.4	5.8
Turonian - springs	Maximum	1.0	0.10	2.3	3.98	0.004	1.1	0.4	5.7
	Minimum	0.7	0.06	1.6	3.36	0.003	0.8	0.3	3.6
	Mean	0.8	0.08	2.0	3.54	0.003	0.9	0.3	4.5
Cenomanian - springs N	Maximum	1.8	0.28	2.1	5.04	0.005	1.9	0.5	5.5
	Minimum	0.8	0.03	1.3	3.1	0.003	0.8	0.2	3.4
	Mean	1.0	0.05	1.8	3.74	0.004	1.3	0.3	4.1
Cenomanian - springs S	Maximum	3.6	0.10	2.9	3.39	0.032	3.9	1.6	5.4
	Minimum	3.1	0.07	2.4	3.03	0.023	3.1	1.1	3.5
	Mean	3.2	0.08	2.8	3.11	0.025	3.5	1.2	4.4
Cenomanian - wells W	Maximum	1.1	0.06	2.7	3.75	0.007	1.3	0.3	6.4
	Minimum	0.7	0.02	1.7	2.78	0.004	0.7	0.1	2.4
	Mean	0.8	0.03	2.4	3.26	0.004	1.0	0.2	4.4
Cenomanian	Maximum	1.9	0.12	2.8	4.16	0.012	2.2	0.7	6.2
Wells transition zone	Minimum	1.6	0.07	2.3	2.61	0.007	1.9	0.5	3.3
	Mean	1.8	0.10	2.5	3.6	0.009	2.0	0.6	4.2
Cenomanian - wells E	Maximum	7.0	0.38	6.2	5.89	0.017	12.8	0.8	5.4
	Minimum	4.7	0.27	4.4	4.36	0.013	6.6	0.4	4.0
	Mean	5.7	0.32	5.2	4.96	0.016	9.8	0.6	4.6
Albian - wells W	Maximum	1.3	0.10	2.3	4.31	0.008	1.9	0.4	4.7
	Minimum	0.7	0.03	1.9	3.12	0.004	0.8	0.1	3.3
	Mean	1.2	0.04	2.2	3.47	0.005	1.4	0.3	4.0
Albian	Maximum	1.1	0.05	2.9	3.69	0.017	1.4	0.3	8.0
Wells transition zone	Minimum	0.6	0.03	2.0	2.5	0.006	0.6	0.1	3.7
	Mean	0.7	0.04	2.4	3.15	0.008	0.8	0.2	4.6
Albian - wells E	Maximum	4.3	0.24	4.4	4.56	0.014	8.0	0.6	4.4
	Minimum	3.1	0.13	3.9	3.79	0.011	5.7	0.3	3.7
	Mean	3.3	0.19	4.1	4.24	0.011	6.5	0.5	4.2

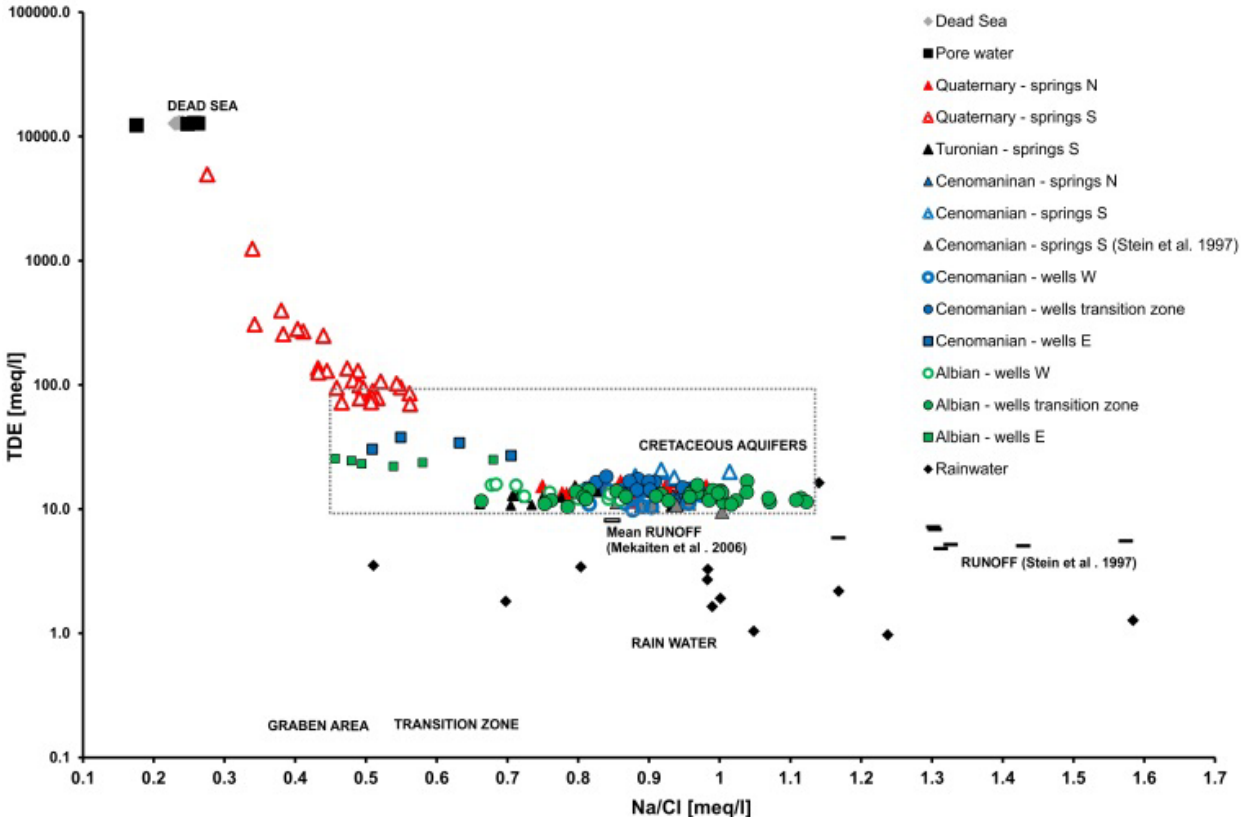

Figure 9 Total dissolved equivalents TDE vs. molar Na/Cl ratios to identify groundwater evolvement from rain and run off (*Mekaiten* [2006], *Stein et al.* [1997]) to Dead Sea, subset Cretaceous aquifer corresponds to figure 9

Finally, groundwater from wells within the Graben show highest salinities of TDE= 23-204 and Na/Cl of 0.42-1.01 (Figure 9), which is the result of mixing with the brines and dissolution of halite (Na/Cl=1). Groundwater in Ein Feshkha show widespread salinities (TDE=23.1-1,242) and Na/Cl of 0.34-0.56, which is related to the admixture of interstitial brine (Na/Cl=0.18-0.26), which soaks the dry-falling Dead Sea sediments.

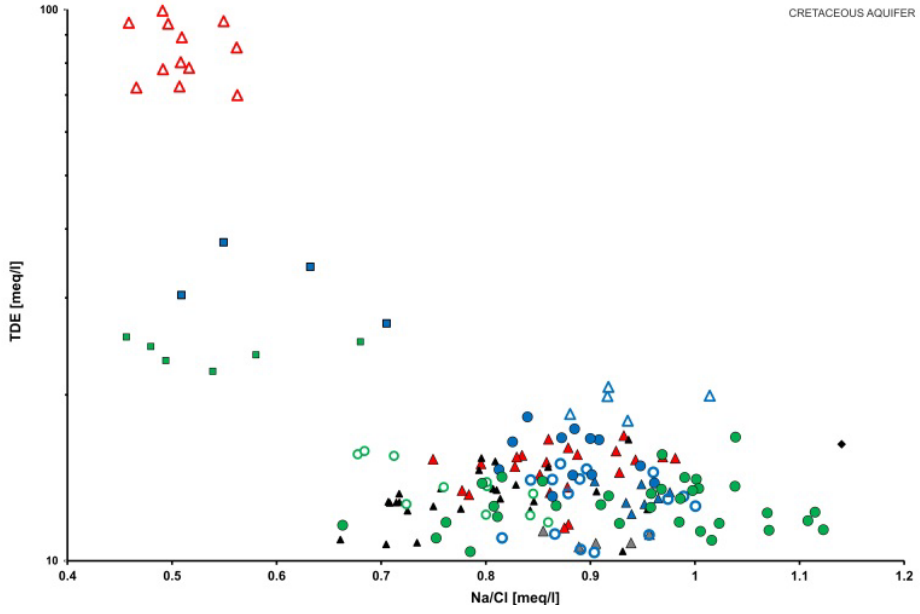

Figure 10 Total dissolved equivalents TDE vs. molar Na/Cl ratios in groundwater, subset of Cretaceous aquifers including a part of Ein Feshkha (Quaternary – springs S) springs with lower TDE, legend corresponds to Figure 9

By means Ca/Sr molar ratios (Figure 11), fresh groundwater from Albian aquifer (Ca/Sr= 190-537) and Upper Cenomanian aquifer (Ca/Sr=537-800) becomes distinguishable (Figure10).Within the Upper Cenomanian aquifer, the northern springs (Ca/Sr=590-1,500), discharging from perched Turonian aquifer and those from the southern springs (Ca/Sr=90-110), emerging from perched Cenomanian Aminadav Fm., form individual subgroups (Figure 10). Irrespective of the producing aquifer, ratios of groundwater within the transition zone (Mizpe Jericho 2, 5, 6) and in well Jerusalem 6 resemble those of the Albian aquifer.

Along the major fault, Ca/Sr values in Jericho wells 2, 4 and 5 are 290-400. The lowest ratios are observed in waters derived from wells east of Jericho (72-275) and in groundwater from Ein Feshkha springs (108-275), which show a distinct mixing trend towards interstitial and Dead Sea brines (109-135), respectively. Considering Ca/Sr ratio combined with Na/Cl ratio (Figure 11), it is shown a clear differentiation between the different groups: Turonian springs (Ein Samia and Auja) and Upper Cennomanian springs with Ca/Sr ratio of 600 to 1500 and its connected springs located in the Quaternary (Sultan and Dyouk) with Ca/Sr of 1200 to 1500 contains the highest Ca concentration in comparison to Sr concentration. Groundwater in the Upper Cenomanian aquifer and Albian aquifer evolve to lower Ca/Sr ratios below 200 combined with almost stable Na/Cl range (0.7 -1.1) indicating intensive dissolution of Sr-rich calcite contributing Sr to the groundwater or saturation of Ca and precipitation of calcite. When Cretaceous groundwater of Upper Cenomanian aquifer and Albian aquifer get input from Quaternary section, the Na/Cl ratio shifts stepwise in direction to Dead Sea brine with low Na/Cl ratios of ~0.2 (as mentioned above).

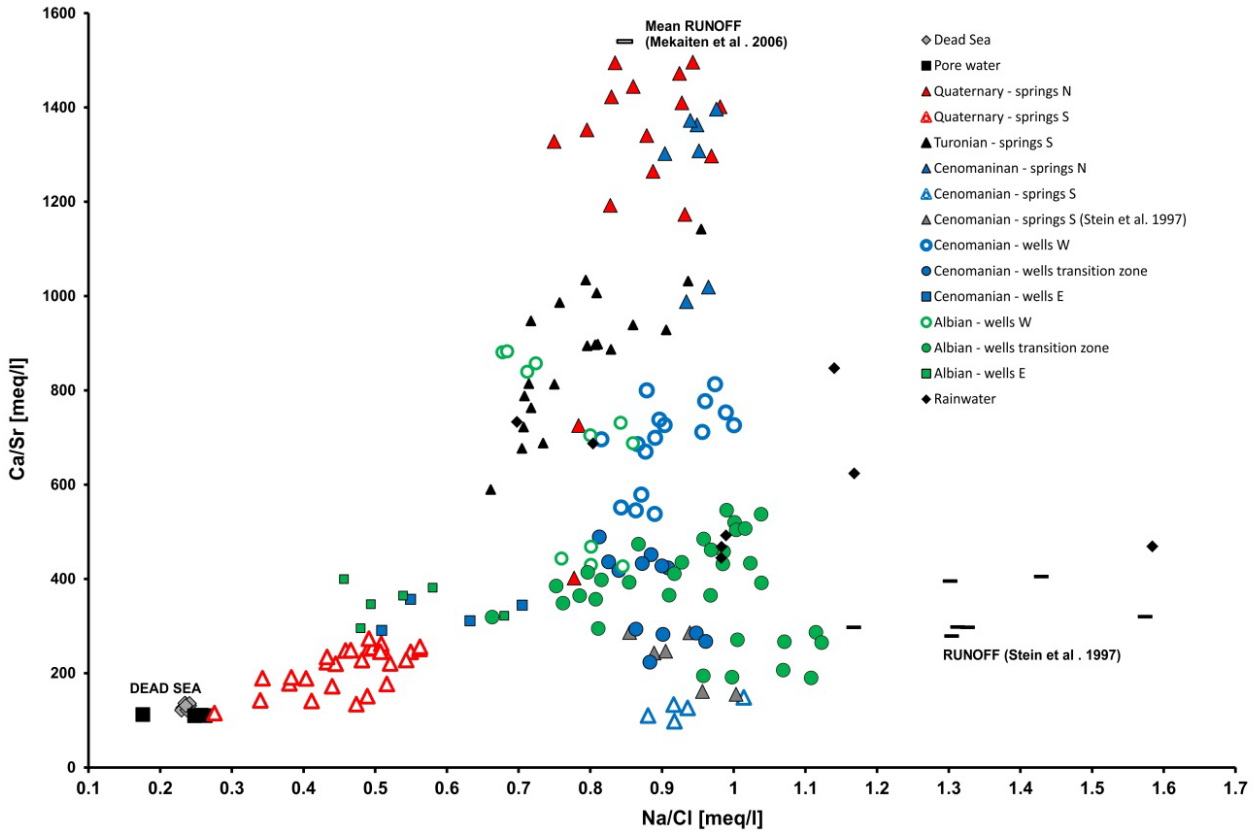

Figure 11 Distinct groundwater groups based on a combination of Ca/Sr ratios vs. Na/Cl ratio (both molar), run - off data from *Stein et al. [1997]*, *Mekaiten* [2006]

4.1.3 Relation of Ca, Sr and Mg

Concentrations of Sr, Ca and Mg in precipitation and in groundwater from the different Cretaceous sub-aquifers vary considerably (Figure 12 & Figure 14). The composition of Levantine rainwater is mainly controlled by uptake of sea spray and washout of dust particles from the atmosphere [*B. Herut et al.*, 1993]. It is characterized by a molar Sr/Ca ratio of 0.002 - 0.004 and Mg/Ca ratio of 0.1-0.36 in rain water analyses [*B. Herut et al.*, 1992] (Figure 14). After infiltration into the Cretaceous formations, mainly composed of calcite and dolomite, water/rock interaction enriches the groundwater with Ca, Mg, and Sr. However, compared to bulk rock composition of the Albian to Turonian aquifer rocks, Sr/Ca and Mg/Ca ratios in groundwater are much larger (Figure 12 & Figure 14), which gives evidence to incongruent release of Sr and Mg, compared to Ca.

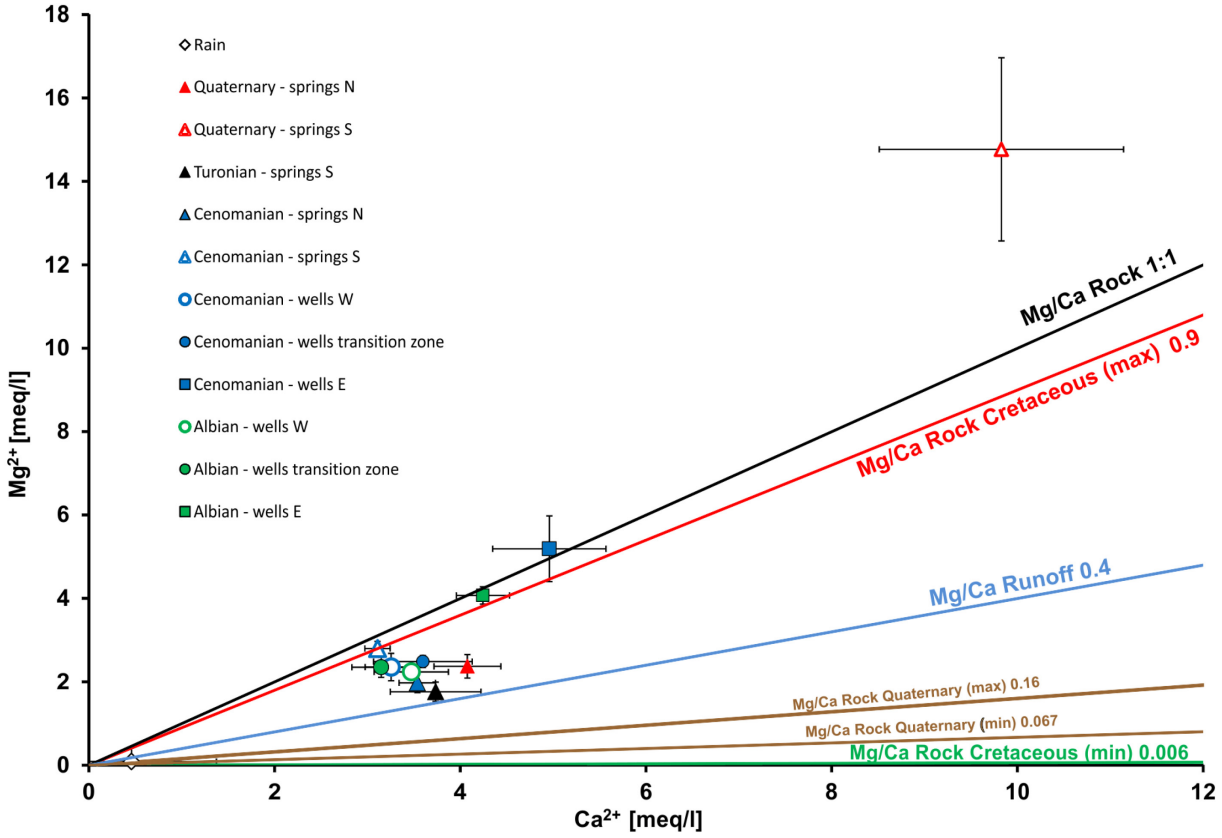

Figure 12 Relation between Ca concentrations and Mg concentrations of the sampled groundwater combined with ratios from local aquifer rock, error bars correspond to standard deviation, run off data from [*Mekaiten*, 2006], Quaternary Springs S correspond to Ein Feshka springs < 100 meq/l TDE representing the main discharge of the fresh water from the Cretaceous aquifers, rock data in appendix A.4

The enrichment of the groundwater in magnesium starts in the springs located in the transition zone (Qilt, Fawwar, Ferat) and the mountain area (Samia and Auja) and develops from ~1 meq/l towards 2.5-3 meq/l in the groundwater of the Upper Cenomanian and Albian layers (Figure 12). The calcium content of groundwater ranges between ~2.5 meq/l and ~5 meq/l. The springs in the transition zone and in the Jordan valley refer to the Turonian formation, where well fissured beds and karst in the mainly limestone layers provide percolation with faster groundwater flow and lower water-rock interaction in comparison to the Upper Cenomanian and Albian layers. Here, the spring waters of the Wadi Qilt still show partly runoff signatures. The slight increase of magnesium and decrease of calcium in the groundwater (UC + Albian) is probably reasoned by incongruent

dissolution of the rock towards calcite saturation under closed system conditions (Figure 12). Regarding to the development of Sr concentrations, the Sr/Ca ratios of the water samples are generally higher than the Sr/Ca ratios of the rock and the runoff with exception of the spring waters (Mountain region, northern Transition zone, Lower Jordan valley), which are controlled by the input signal and reveal runoff Sr/Ca ratios (Table 5, Figure 13). There is an increase of Sr relative to Ca in the water of the Cretaceous from upper to lower aquifer and from discharge to recharge area according to longer water-rock interaction. The springs of the transition zone (Arugot and Ein Gedi) contain the highest Strontium concentration (up to 0.03 meq/l) and built the endmember for the carbonate precipitation and dissolution process in this Cretaceous aquifer system. A strong increase of Ca takes place after admixture of groundwater from the Quaternary sediment fan as it is detected close the graben fault in the wells Jericho 4, Jericho 5 (Lower Jordan valley, Albian) and Jericho 2 (Lower Jordan Valley, UC) with Ca concentrations between 4 and 6 meq/l.

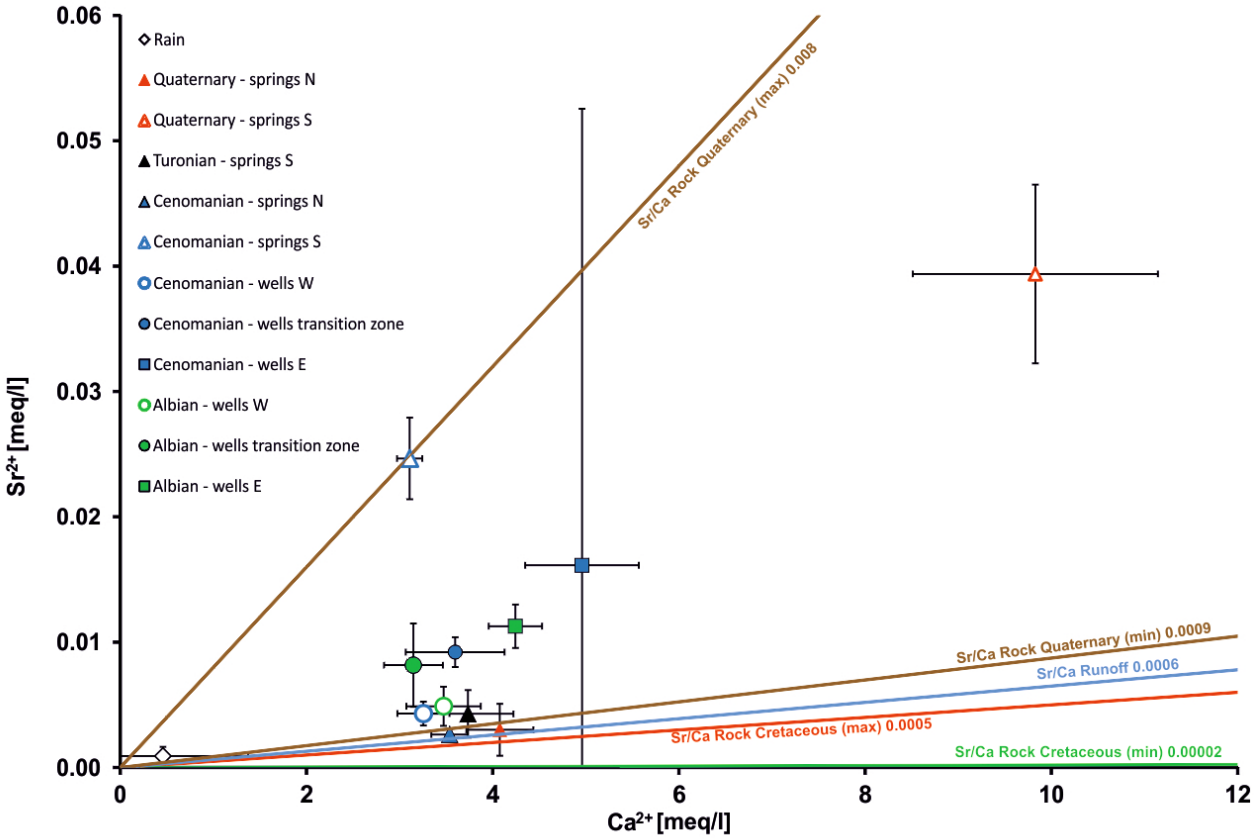

Figure 13 Relation between Ca concentrations and Sr concentrations of the sampled groundwater combined with ratios from local aquifer rock, error bars correspond to standard deviation, run off data from *Mekaiten* [2006], *Stein et al.* [1997], Quaternary Springs S correspond to Ein Feshka springs <100 meq/l TDE representing the main discharge of the fresh water from the Cretaceous aquifers, rock data in appendix A.4

A comparison of the Sr/Ca ratio and Mg/Ca ratio for waters and rocks are given in Figure 14. A low distribution coefficient of Sr and Ca (K_D^{Sr-Ca} of 0.045) is given for carbonate rocks (*Baker et al.* [1982], *A. Katz et al.* [1972]) and the local Cretaceous rocks consist of also low parts of Sr and consequently low Sr/Ca ratios (0.0005- 0.0001 molar, appendix, table A.1). In the Quaternary sediments, the sulphate share is higher than in the Cretaceous rocks. Sr is also related to the sulphate mineral fraction derived from the above mentioned dry-fallen lakebed sediments (*Klein-BenDavid et al.* [2004], *Torfstein et al.* [2005]).

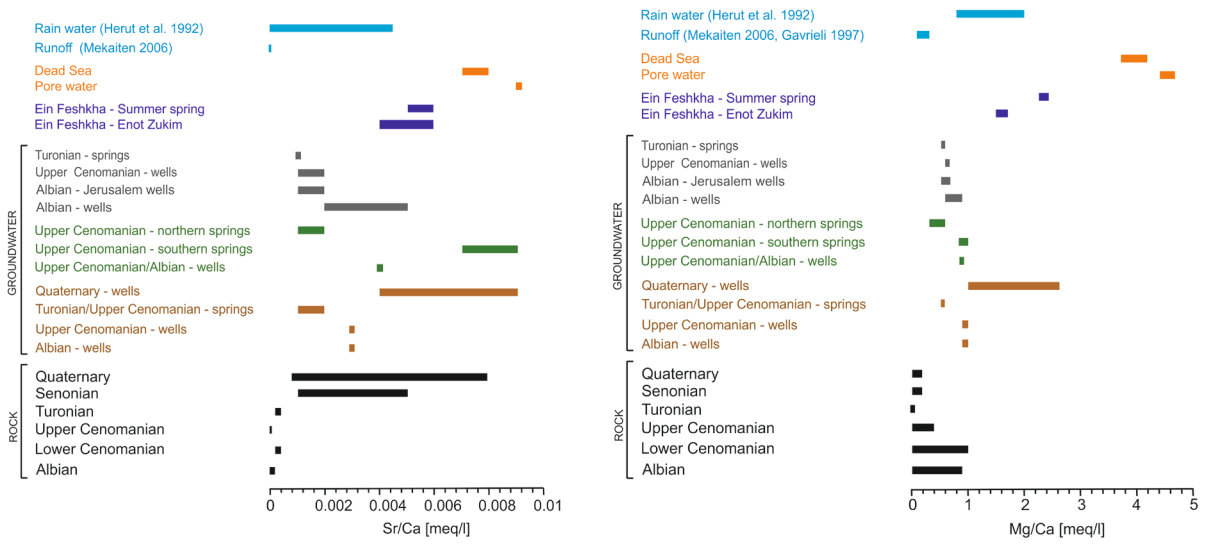

Figure 14 Chart combining rock data (Appendix A.4) and groundwater data (Appendix A.1) (grey: recharge area, green: transition zone, brown: graben area), left plot: Sr/Ca ratio, right plot: Mg/Ca ratio

Regarding the groundwater groups, quite similar Sr/Ca ratios appear in the recharge area including the wells of the Upper Cenomanian, Albian (Jerusalem wells), the northern springs and Jordan valley springs located in the Turonian/Upper Cenomanian. Representative for the discharge area without any influence from the Quaternary are the springs in the Wadi Arugot, which show the highest Sr/Ca ratios of the Cretaceous aquifers (up to ~0.01 meq/l). Together with the strontium isotope ratios, this water is a product of intensive water rock interaction (further discussed in section 4.1.4). The Mg/Ca ratios of Cenomanian and Albian (rocks) range between low Mg-carbonate and dolomite/high Mg-carbonate (0.01 – 1 molar, appendix A.1, Figure 14 Mg/Ca ratio). The Turonian layers are composed of mostly ca-calcite. In the Quaternary sediments, also Mg - sulphate paragenesis with low Mg contents (0.07 – 0.2 molar) occur. The Mg/Ca ratios (Figure 14) in the Cretaceous aquifers show distinct groups with a slight increase from recharge area to discharge area. There are two indicators regulating the Mg/Ca ratio in the groundwater. Due to the fact that the Albian rocks contain higher Mg concentration according to the occurrence of high Mg-carbonate or dolomite, the groundwater in the Albian formations get enriched in Mg relative to Ca. Secondly, when partial CO_2 (P_{CO2}) is lowered under closed system conditions in the aquifer, saturation of calcite could occur, and secondary calcite might precipitates. For both ratios (Sr/Ca and Mg/Ca) (Figure 14), clearly differentiable patterns are identifiable also in the water groups of the Lower Jordan Valley and at the Dead Sea coast. Particularly the waters elevated salinity, e.g. in the Ein Feshkha springs, pore water and the groundwater in the Quaternary sediments (Jericho area) are caused by admixture of brine.

In figure 15, presenting molar Ca/Sr ratios versus Sr-concentrations, freshwaters from both Cretaceous aquifers show an almost linear trend to decreasing Ca/Sr ratios, while Sr-content is increasing. However, both aquifers are differentiable by a threshold of Ca/Sr = 500, being larger in the Upper Cenomanian aquifer. However, the highest Sr-concentrations at lowest Ca/Sr ratios are observable in the springs around Wadi Arugot. Groundwater within the graben follow two distinct trends, which are given by waters from wells in the vicinity of Jericho and the Feshkha springs, respectively. The trends are controlled by admixture of brines.

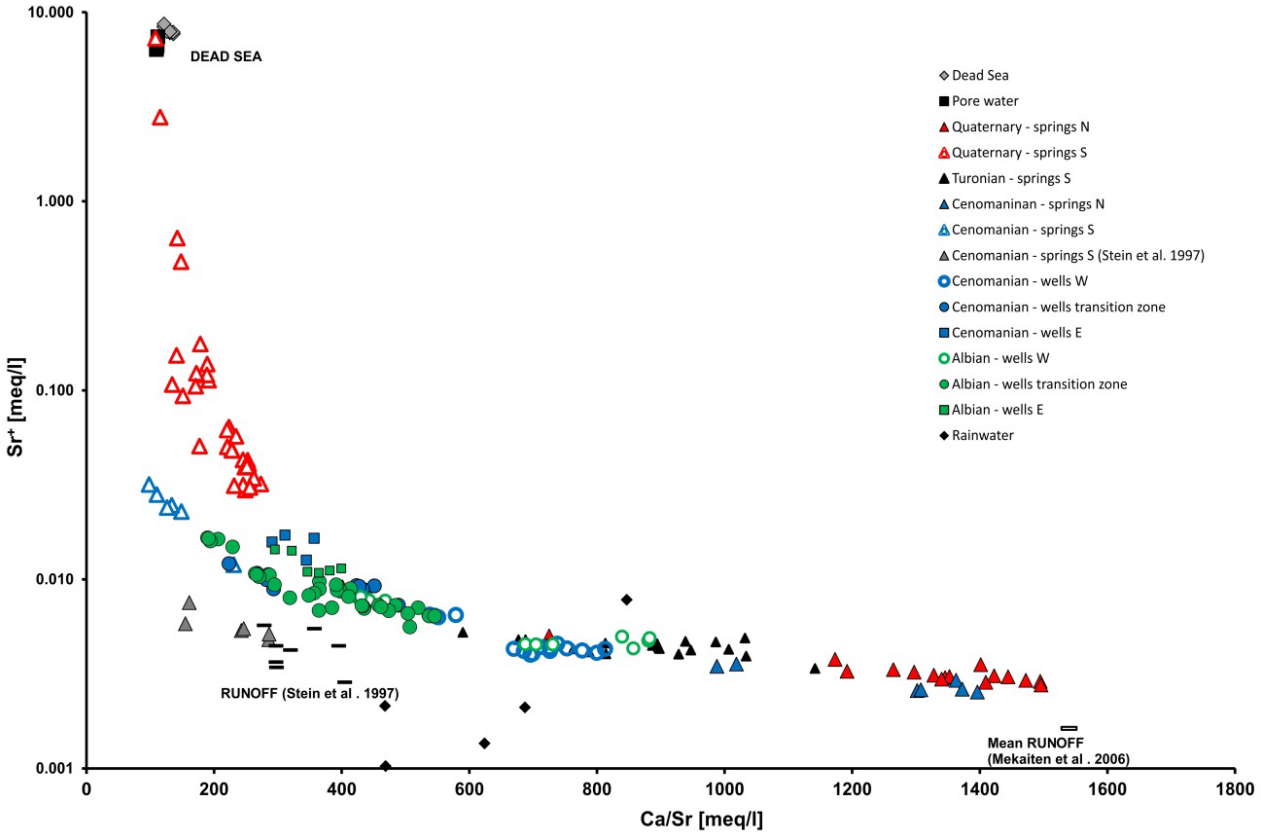

Figure 15 Relation between Ca/Sr and Sr^{2+} concentrations presenting groundwater development from recharge to discharge area, run off data from (*Mekaiten* [2006], *Stein et al.* [1997])

4.1.4 Strontium isotopes

Fresh waters from Cenomanian/Turonian aquifer and the Albian aquifer are characterized by a Na/Cl ratio > 0.8 and show $^{87}Sr/^{86}Sr$ ratios of 0.70814-0.70832 and 0.70759-0.70798, respectively and hence become distinguishable (Figure 16, appendix A.2). According to that separation, wells as Mizpe Jericho 2 and PWA 3 are obviously connected to both aquifers and show seasonal variations in $^{87}Sr/^{86}Sr$ ratios (Figure 16). Although producing water from the Albian section, Jerusalem wells show always high $^{87}Sr/^{86}Sr$ ratios, resembling that of the Upper Cenomanian groundwater, indicating low dissolution of the aquifer rocks during infiltration. The saline end-members, which are both, interstitial and Dead Sea brines, are defined by Na/Cl ratio <0.3 and very low varying $^{87}Sr/^{86}Sr$ ratios of 0.70794-0.7080. Similar narrow is the range of $^{87}Sr/^{86}Sr$ ratios of the Quaternary graben filling, which is 0.70784-0.70804. The lower Na/Cl ratios in most groundwater from wells and springs within the graben the more their $^{87}Sr/^{86}Sr$ ratios become similar to those of the saline endmembers (e.g. brine, quaternary sediments). The only exception of this trend is observable in the southernmost springs of the Ein Feshkha area, which resemble $^{87}Sr/^{86}Sr$ ratios of the Upper Cretaceous aquifer, at comparable low Na/Cl ratios as other springs from Ein Feshkha area.

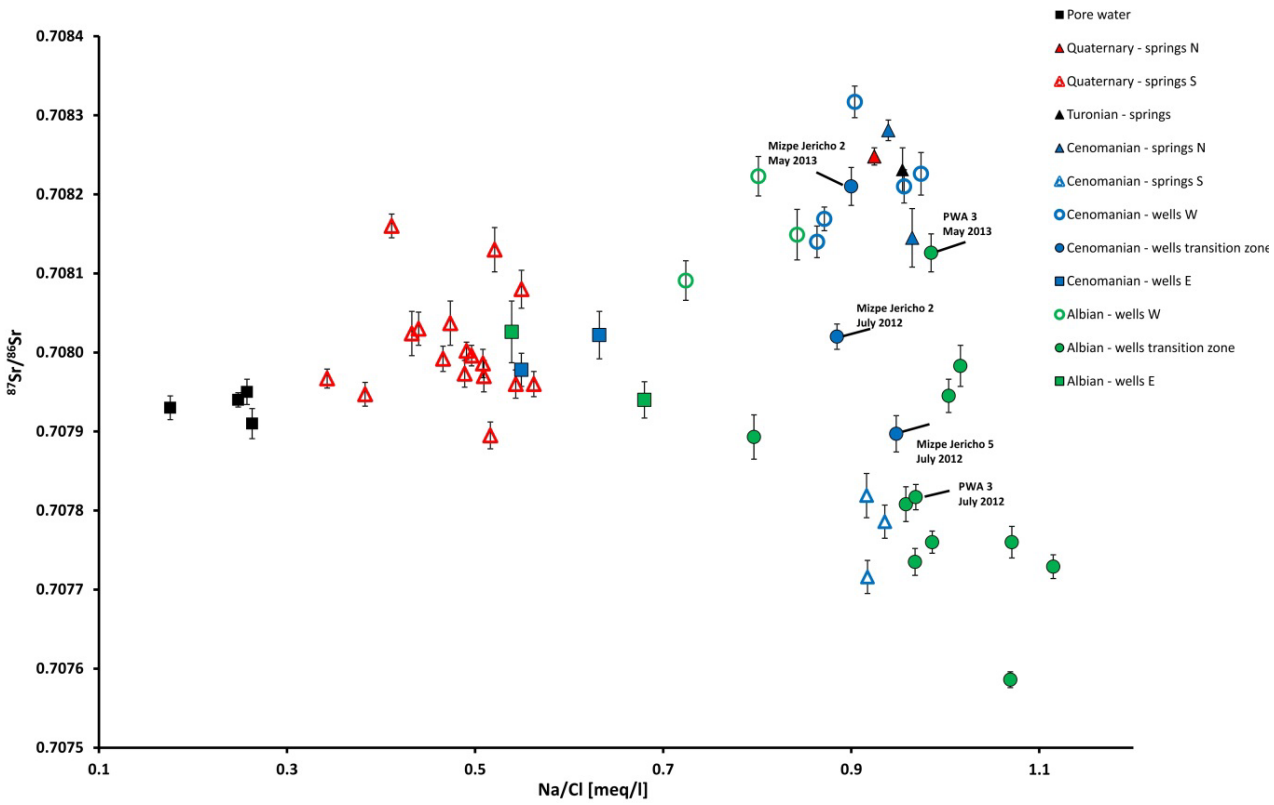

Figure 16 Plot of the $^{87}Sr/^{86}Sr$ ratio vs. the Na/Cl concentration showing the grouping of different aquifers and springs, Sr ratios and uncertainty 2σ in appendix A.2

As for the fresh groundwater from Cretaceous, again a clear trend of $^{87}Sr/^{86}Sr$ versus 1/Sr concentration is given (Figure 17), a correlation that might refer to residence times or intensity of dissolution - re-precipitation processes in the observed groundwater. While waters from Albian wells follow trend 1, those from Upper Cretaceous wells and springs, including Jerusalem wells, but excluding Arugot springs, which follow the much shallower trend (2). Springwater around Wadi Arugot show very low, but variable $^{87}Sr/^{86}Sr$ ratios at almost similar Sr- concentrations. Groundwater within the graben are controlled by the dissolution of Quaternary sediments and admixture of the available brines, resulting in decreasing 1/Sr and converging $^{87}Sr/^{86}Sr$ ratios of 0.7080, comparable to Dead Sea and interstitial brines.

Based on the development of Sr concentration in the Cretaceous aquifers, the evolution of $^{87}Sr/^{86}Sr$ ratios of the groundwater $(^{87}Sr/^{86}Sr)_{groundwater}$ in a carbonate system can further retraced in a dissolution-reprecipitation model, given by *A Starinsky et al.* [1983]:

$$\left(\frac{^{87}Sr}{^{86}Sr}\right)_{groundwater} = \frac{\left(\frac{Sr}{Ca}\right)_{Li}\left(\frac{^{87}Sr}{^{86}Sr}\right)_{Li}\exp\left(-K_D^{Sr-Ca}\left(\frac{Ca_S}{Ca_L}\right)\right) + \frac{1}{K_D^{Sr-Ca}}\left(\frac{Sr}{Ca}\right)_R\left(\frac{^{87}Sr}{^{86}Sr}\right)_R\left(1-\exp\left(-K_D^{Sr-Ca}\left(\frac{Ca_S}{Ca_L}\right)\right)\right)}{\left(\frac{Sr}{Ca}\right)_{Li}\exp\left(-K_D^{Sr-Ca}\left(\frac{Ca_S}{Ca_L}\right)\right) + \frac{1}{K_D^{Sr-Ca}}\left(\frac{Sr}{Ca}\right)_R\left(1-\exp\left(-K_D^{Sr-Ca}\left(\frac{Ca_S}{Ca_L}\right)\right)\right)}$$

Equation 8

The index "Li" of the ratios $(^{87}Sr/^{86}Sr)_{Li}$ and $(Sr/Ca)_{Li}$ ratios refer to the specific input chemistry of rain water or runoff (Table 5). The ratios $(Sr/Ca)_R$ and $(^{87}Sr/^{86}Sr)_R$ belong to the ratios of the carbonate bedrock (Index "R"). The Cretaceous mean of $(^{87}Sr/^{86}Sr)_R$ is used from *Veizer et al.* [1999] ($^{87}Sr/^{86}Sr$ 0.7075). The specific $(Sr/Ca)_R$ ratios are based on the maximum and minimum of the rock analyses from the two main Cretaceous aquifers (Upper Cenomanian $(Sr/Ca)_R$ 0.00046 to 0.00002 and Albian $(Sr/Ca)_R$ 0.00018 to 0.00014, Appendix A.4).

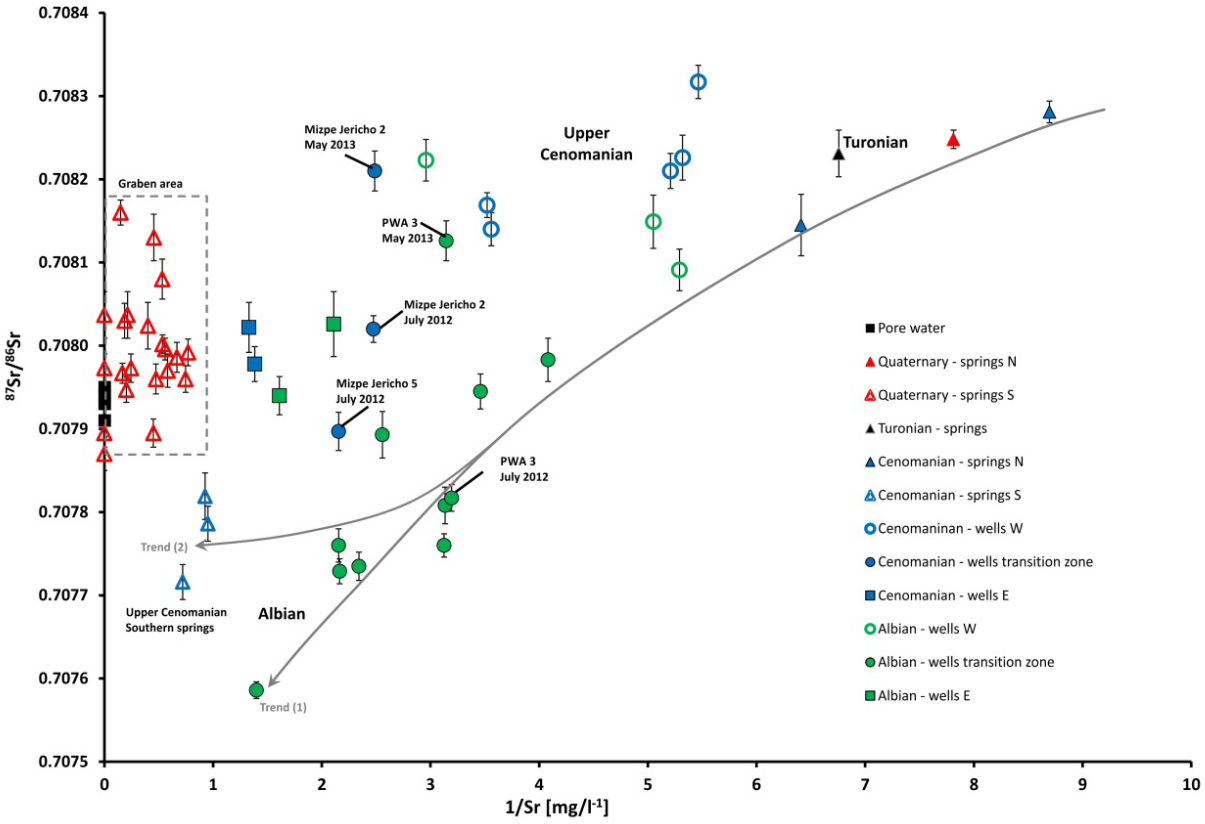

Figure 17 Combination of $^{87}Sr/^{86}Sr$ and 1/Sr concentrations proving dependency of total Sr increase in groundwater with decreasing $^{87}Sr/^{86}Sr$: Trend 1 indicate process of Cretaceous rock dissolution, Trend 2 shows potential groundwater evolvement path to Upper Cenomanian springs (Arugot, Ein Gedi)

The ratio (Ca_S/Ca_L) describes the proportion of Ca in the solution (Index "L") and the proportion of Ca dissipated from the rock (Index "S"). In the calculations this ratio is considered as non-fixed and increases during dissolution–re-precipitation process. The distribution coefficient K_D^{Sr-Ca} of Ca and Sr in carbonates is set to 0.054 for limestone after [*A. Katz et al.*, 1972].

Further on, the $(Sr/Ca)_{groundwater}$ ratio in the groundwater during dissolution–re- precipitation process is calculated in relation to the $(^{87}Sr/^{86}Sr)_{groundwater}$ according to [*A Starinsky et al.*, 1983]:

$$\left(\frac{Sr}{Ca}\right)_{groundwater} = \left(\frac{Sr}{Ca}\right)_{Li} \exp\left(-K_D^{Sr-Ca}\left(\frac{Ca_S}{Ca_L}\right)\right) + \frac{1}{K_D^{Sr-Ca}}\left(\frac{Sr}{Ca}\right)_R \exp\left(-K_D^{Sr-Ca}\left(\frac{Ca_S}{Ca_L}\right)\right)$$

Equation 9

Table 5 Input parameters for runoff and rain water from literature

	Mean $^{87}Sr/^{86}Sr$	Mean Sr/Ca (meq)
Runoff		
Jerusalem Mountains [*Gavrieli et al.*, 1997], [*Mekaiten*, 2006]	0.7083	0.000649
Rain (Herut et al. 1992)	0.7087	0.00203

Both model results calculated after equation 9 with runoff and rain water give indication of the groundwater evolvement in the aquifer. Since the rain water is an endmember for runoff, it bases also the groundwater chemistry. By application of both models can be shown that the groundwater approaches the low $^{87}Sr/^{86}Sr$ ratio of the aquifer work via dissolution - re-precipitation processes.

Thus, by application of the minimal and maximal molar Sr/Ca ratio of the analysed Cretaceous formations, the model shows the dependency of the dissolution process in the aquifer matrix. An increase of molar Sr/Ca ratio in the rock formation forms groundwater of higher Sr/Ca ratios as function of water rock interaction: groundwater in the recharge area of the Upper Cenomanian and Upper Cenomanian - Turonian springs exhibit the lowest Sr/Ca ratio and the highest $^{87}Sr/^{86}Sr$ values originating from the rain water composition, which in term reflect the recent isotope ratio of Mediterranean Sea (~0.709 in *B. Herut et al.* [1993]). All values plot in the calculated model (Equation 9) of the maximum and minimum Sr/Ca rock ratio (Figure 19). The progressive dissolution of the aquifer rock ($^{87}Sr/^{86}Sr$ ratios (0.7075)) result into $^{87}Sr/^{86}Sr$ ratios of the lower aquifers. The Upper Cenomanian spring “Arugot uppermost” in the southern part is shifted to higher Sr/Ca ratios. Two reasons can be mainly discussed: Precipitation of Ca as calcite in saturated groundwater result into a low Sr-Ca- distribution coefficient in the re- crystallised minerals [*A. Katz et al.*, 1972]. This results into a rising Sr/Ca ratio in the groundwater during the groundwater flow, which goes along with continuous input of dissolved Sr originating also from Sr-sulphate sources (e.g. Celestine). Additionally, the Sr/Ca ratio in the southern springs could be influenced by rock formations of higher Sr/Ca ratios (0.0012, Appendix A.4), which are abundant in the overlaying layers of the upper Cretaceous (Menuha to Gahreb formation).

The modelled results of the runoff simulation (Figure 18) show in general a lower Sr/Ca ratio in comparison to the groundwater samples. The groundwater development from recharge area/ Upper Cenomanian aquifer to Albian aquifer is directed to increasing Sr/Ca ratios and lower $^{87}Sr/^{86}Sr$ ratios in the water. The spring waters find their origin in the runoff composition or fall along the upper part of the model line of the aquifer rocks. However, the elevated Sr/Ca ratio in the groundwater of the Upper Cenomanian aquifer and Albian aquifer in comparison to the simulation indicate calcite saturation. By the precipitation process, the waters get enriched of Sr relative to Ca.

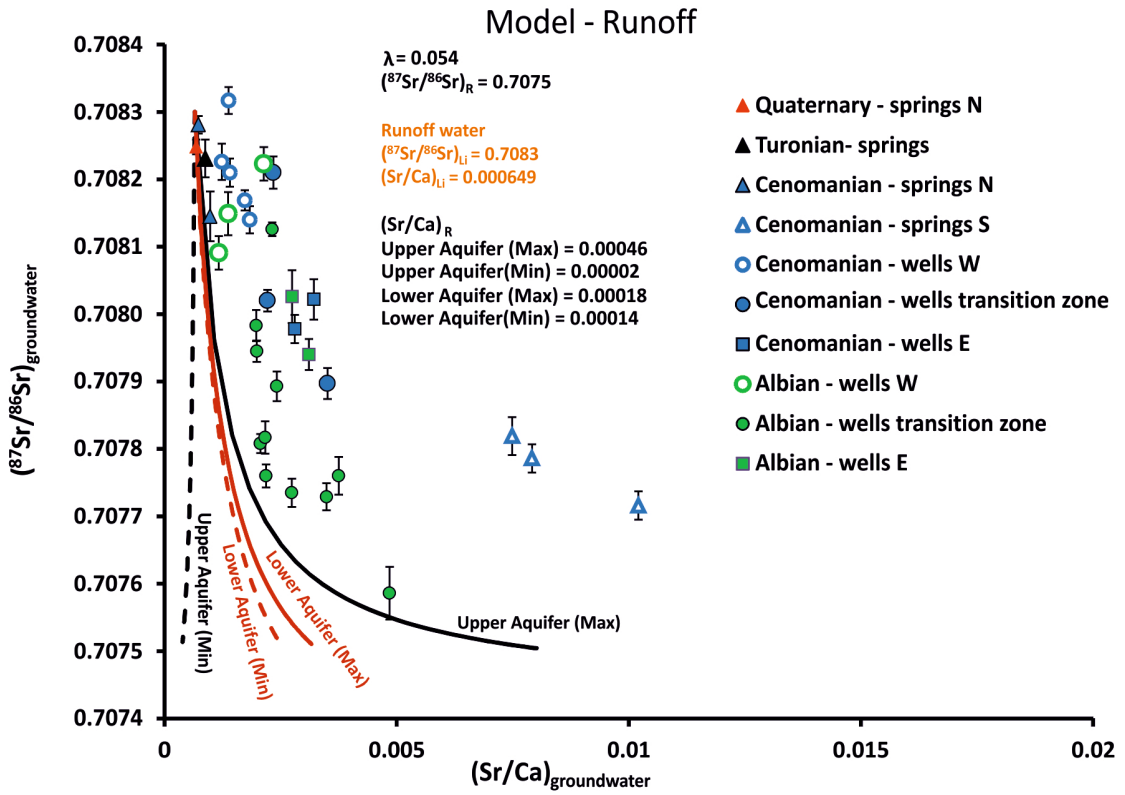

Figure 18 Model results calculated based on run off according to equation 9

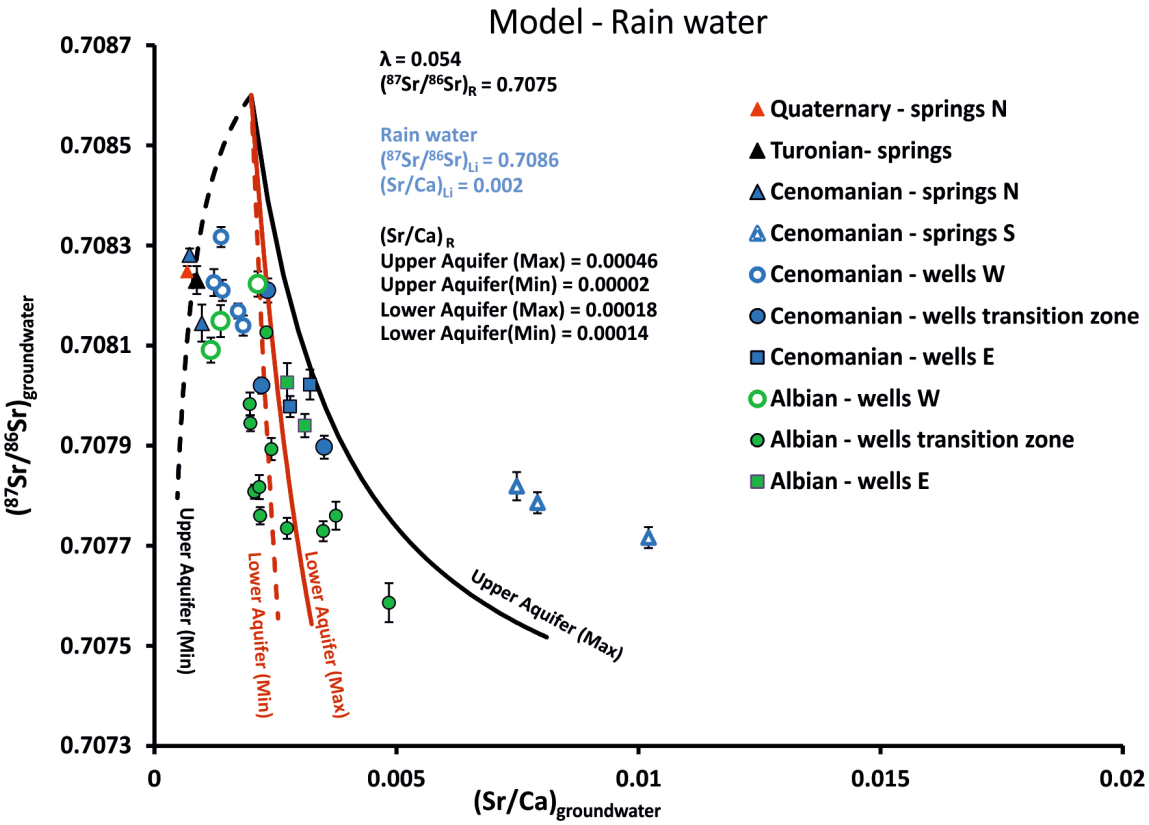

Figure 19 Model results calculated based on rain water according to equation 9

4.1.5 Stable isotopes patterns - $\delta^{13}C_{DIC}$

The Cretaceous aquifers consisting of carbonate minerals provide an inorganic environment for dissolution process of carbonate. Consequently, sources of carbon refer to the main carbonate minerals as calcite, aragonite, dolomite and strontianite and CO_2 produced by microorganisms in the soil. Incongruent and congruent dissolution of soluble carbonate fraction would affect an enrichment of $\delta^{13}C$ and therefor it is a result from the aquifer matrix [*Clark and Fritz*, 1997]. During incongruent dissolution in the saturated zone, calcite precipitates as function of calcite saturation, while the precipitate reflects the $\delta^{13}C$ ratio of the groundwater in relation to slow fraction during precipitation processes [*Clark and Fritz*, 1997].

In figure 20, an overview is given of the $\delta^{13}C$ of the different groundwater groups in the local Cretaceous aquifers, $\delta^{13}C$ of the rock formations, $\delta^{13}C$ for calcite and dolomitic from *Kroitoru* [1987] and *Margaritz* [1974] and the interval of global $\delta^{13}C$ of Cretaceous deposits given by [*Veizer et al.*, 1999]. Bedrock analyses of the Albian aquifer reveal similar ratios as global $\delta^{13}C$ from [*Veizer et al.*, 1999]. $\delta^{13}C$ of Kefira Formation tends to isotope ratios of dolomite from *Kroitoru* [1987] and *Margaritz* [1974]. Groundwater of Upper Cenomanian and Albian formation can be characterized by similar $\delta^{13}C$ ratios (-8.8 to -11.7‰ VPDB). However, less enriched groundwater in the Turonian springs (Samia, Auja and Dyouk spring) refer to rain water input and congruent dissolution of the carbonates, respectively.

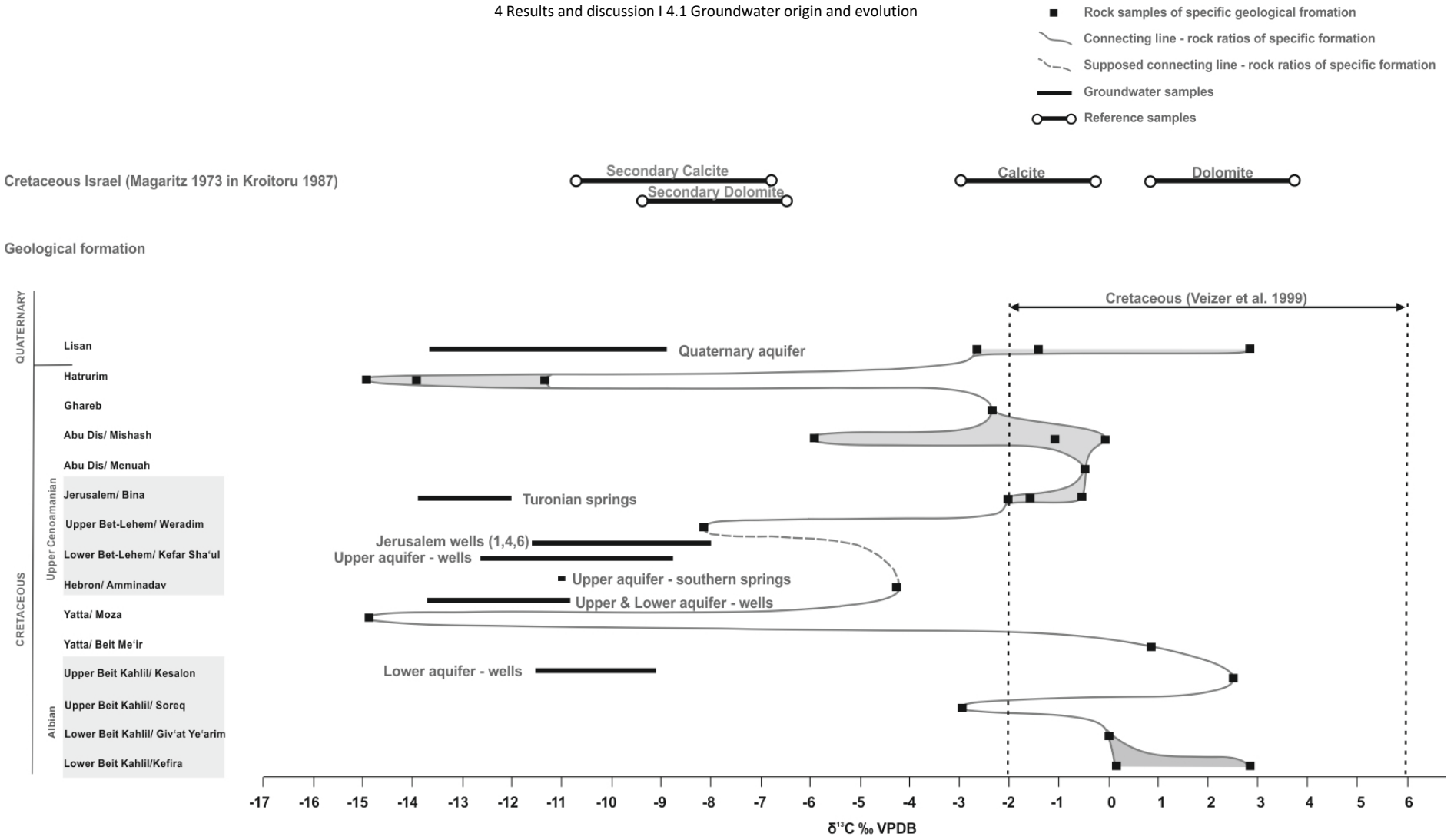

Figure 20 $\delta^{13}C$ distribution of rock samples representing local litho - stratigraphy including groundwater ratios and global $\delta^{13}C$ Cretaceous ratios [*Veizer et al.*, 1999] and ratio of sampled surface water

4.1.6 Proving groundwater origin with REE+Y

Results of the REE+Y in the aquifer lead to following differentiation: Based on Mg/Ca ratio in rocks, a differentiation of calcite- rich or dolomite- rich carbonates in the rock is shown (Figure 14, Appendix A.6). In Figure 14, it is discussed that the Upper Cenomanian and Albian aquifer layers show Mg/Ca ratio ~0.8 meq/l or 0.6 mg/g. REE+Y in the aquifer with varying calcite and dolomite fractions exhibit also different enrichment of REE+Y – integration of REE+Y in calcite or dolomite during sedimentation depending on the crystal structure of each mineral phase. Preferable they could be substituted for Ca [*Stosch*, 2000].

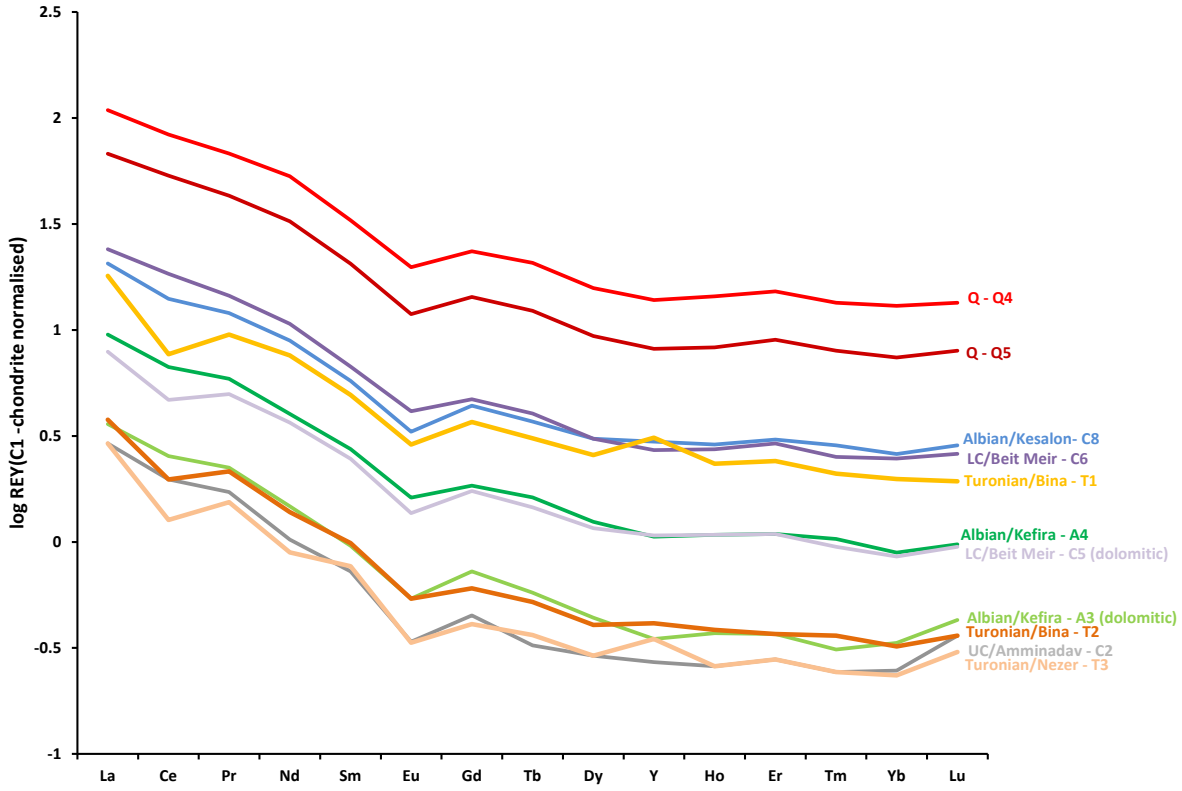

Figure 21 REE +Y patterns - results of total digestion of rock sample from Quaternary, Turonian (Bina and Nezer Fm.), Upper Cenomanian (Amminadav Fm.), Lower Cenomanian (Beit Meir Fm.) and Albian (Kesalon and Kefira Fm.) (Appendix A.5)

Turonian rocks show decreasing distribution from light to trace elements. However, in comparison to the early Cretaceous layers (Upper Cenomanian to Albian), this lithology is characterized by a negative Ce and EU anomaly and positive Y anomaly (Figure 21). The REE+Y patterns of the analysed rock samples from the main two aquifers (Upper Cenomanian and Albian) of Cretaceous layer show similar trend of REE+Y concentrations. There is a decrease by one order of magnitude from La to Eu (negative anomaly) followed by a slight decreasing trend. In rock samples of Beit Meir (Lower Cenomanian) and Kefira (Albian), two types of samples (dolomite enriched, and calcite enriched) showed less enrichment of REE+Y in the dolomite rock sample.

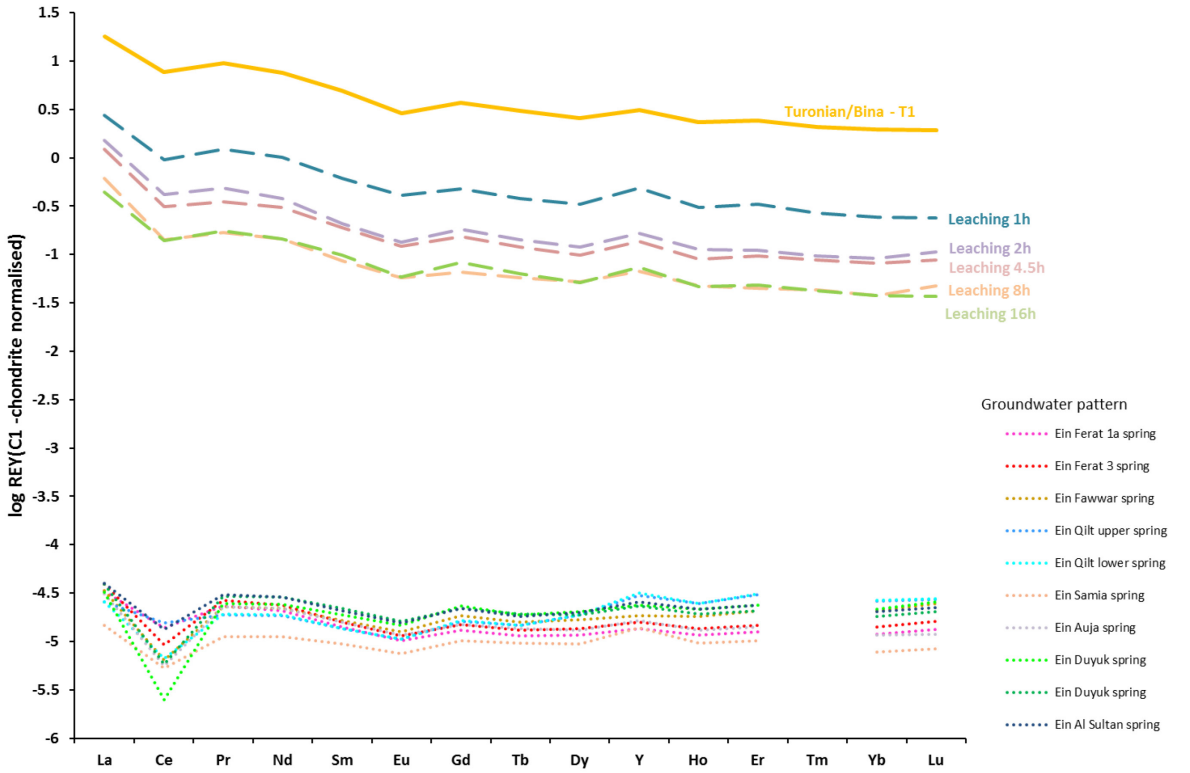

Figure 22 REE+Y patterns - results of total digestion of Turonian Bina Fm. including the leaching results (1h, 2h, 4.5h, 8h and 16h) and the REE+Y groundwater pattern referring to Turonian layers

Pointing on the dissolution of the rock samples in the leaching analyses, it can be shown that less enriched rock of REE+Y contribute less REE+Y to the leachate. In addition, the pattern of the total content in the rock is reproduced in a similar shape in the leachate, which was also shown by *Möller et al.* [2003]. In Figure 23, rock analyses of Beit Meir and Kefira Fm. for calcite and dolomite samples show similar REE+Y patterns. There is a decrease from light to trace elements as described above and REE+Y are less enriched in the dolomites. The leaching results of both rock types are less enriched in comparison to the results of the total digested rock. In the here presented examples (Beir Meir Fm. and Kefira Fm.), the leaching results exhibit the highest enrichment in the leachate of 1h, lowest in 16h leachate. It would be expected, the highest enrichment of REE+Y would be for the 16h experiment due to the longest reaction times and therefore potential longer dissolution process. Reasons for lowest enrichment of REE+Y with increasing leaching times could be re-precipitation processes of carbonates (including the dissolved REE+Y) due to changing pH conditions in atmospheric temperature and air pressure conditions during dissolution.

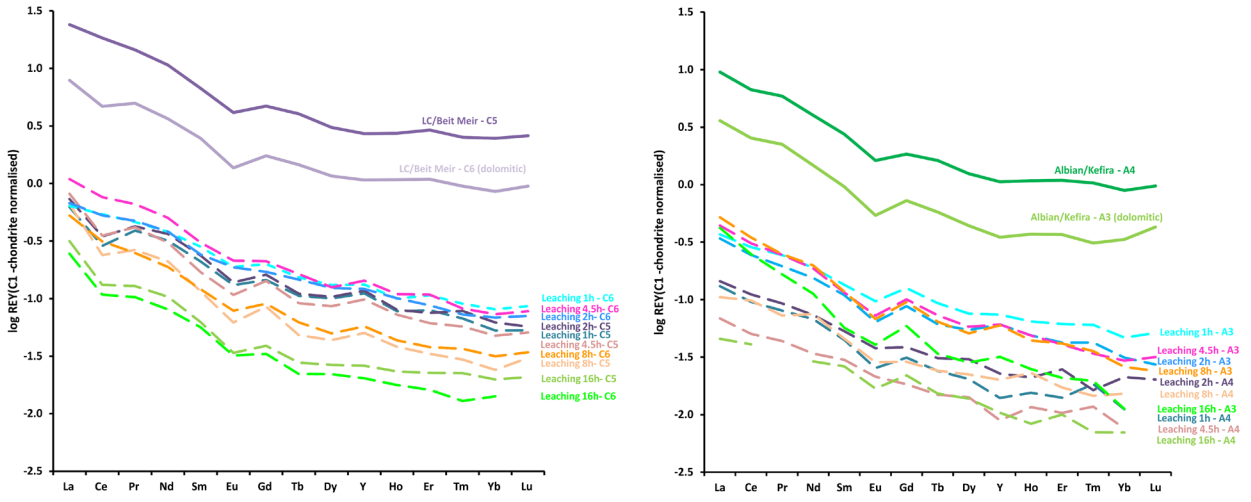

Figure 23 REE+Y patterns of Beit Meir Fm. and Kefira Fm.; comparison of dolomite – enriched carbonate and calcite - enriched carbonate of Beit Meir Fm. (left) and Kefira Fm. (right) ; total digestion (solid lines) and leachings of 1h, 2h, 4h, 5h, 8h and 16h (dashed lines)

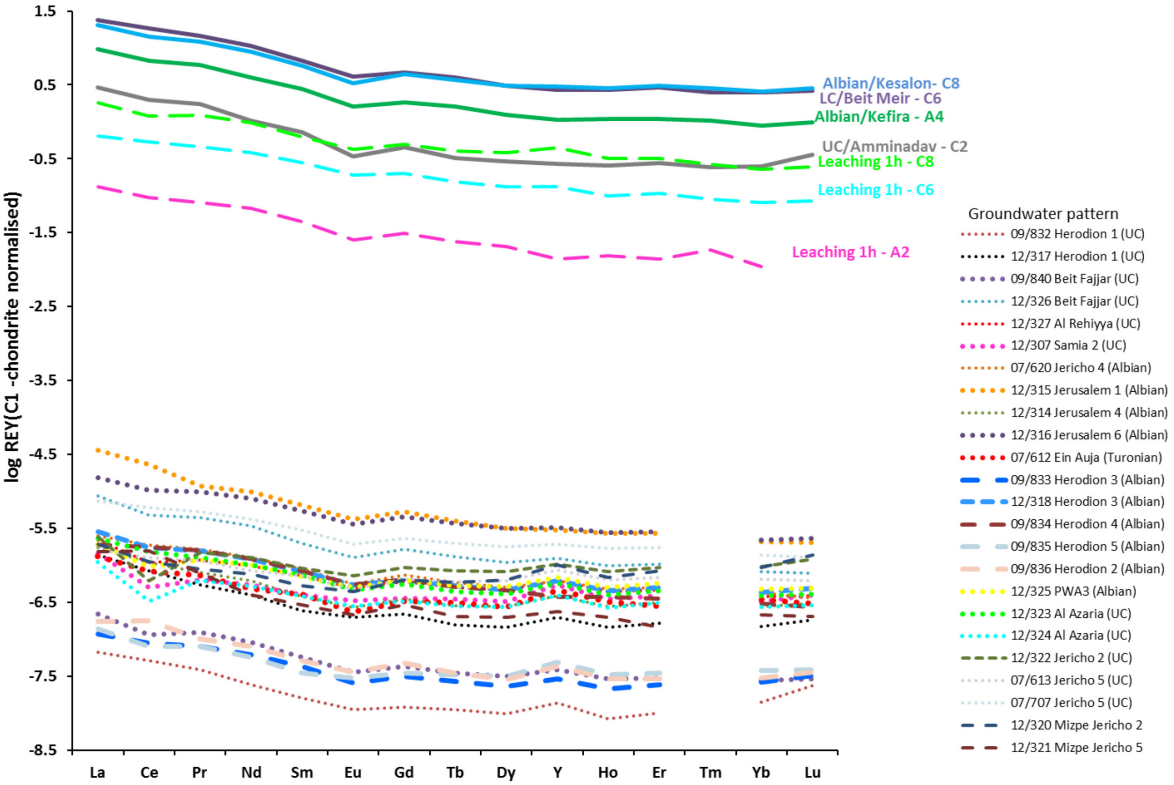

Figure 24 REE+Y patterns - results of total digestion of Kesalon Fm., Beit Meir F m. and Aminadav Fm. including the leaching results (1h, highest enriched with REE+Y) and REE+Y groundwater patterns from wells of UC and Albian except for Ein Auja spring (Turonian), data in Appendix A.5 and A.6

Combining groundwater samples of Upper Cenomanian and Albian aquifer with REE+Y patterns of the host rock including their 1h leachates (highest enriched of REE+Y) (Figure 24), it can be extracted that mostly all groundwater of UC an Albian aquifer show similar REE+Y patterns like the host rocks, only with 3-4 orders of magnitude lower enriched. There are some well like al Azaria 3, Samia 2, Al Rehiyya, Beit Fajjar and Mizpe Jericho 2 which contain a negative Ce anomaly and positive Y anomaly (as it is characteristic for Bina Fm.) indicating groundwater input from the Turonian layers.

4.1.7 Conclusions

A combination of stable isotopes $^{87}Sr/^{86}Sr$, REE+Y and major ion chemistry are applicable to distinguish between the Cretaceous aquifers of the north western Dead Sea aquifer system and to face the evolution process of groundwater:

1. $^{87}Sr/^{86}Sr$ in the Upper Cenomanian aquifer and springs of the Turonian comprises a higher radiogenic $^{87}Sr/^{86}Sr$ ratios compared to the Albian aquifer. Lower Strontium concentrations and higher $^{87}Sr/^{86}Sr$ signatures in the Turonian originate from partly preserved rain water patterns due to fast groundwater flow velocities in the occurring karst layers of the Turonian.
2. The dissolution processes for each aquifer from recharge area to discharge area can be followed by the Sr/Ca ratio development. Groundwater evolvement in the Cretaceous aquifers is mainly formed by water-rock interaction in the aquifer. Mg^{2+}, Ca^{2+}, Sr^{2+} converge to the carbonate composition of the aquifer matrix during incongruent dissolution processes and re-precipitation of calcite in the saturated zone.
3. Discharge area in the Quaternary section act as clearly identifiable endmember to the groundwater in Cretaceous aquifers due to admixture signatures representing saline sources. Groundwater from the Quaternary section is influenced by saline components resulting into an increase of salinity. However, sampling locations (e.g. Ein Sultan or western Jericho wells in the Quaternary section) close to the graben fault are fed by groundwater from the Turonian showing similar $^{87}Sr/^{86}Sr$ ratios (e.g. from Ein Qilt).
4. Groundwater origin according to aquifer rock can be identified with results of the REE+Y pattern. Particularly rocks of the Turonian layer including here infiltrating water resources show a specific REE+ Y pattern, which is preserved in the Upper Cenomanian and Albian groundwater. Groundwater input to from the Turonian layers can be retraced.

4.2 Modification of Cretaceous groundwater in the Lower Jordan Valley

The groundwater flow mechanism in the transition zone of the graben fault and within the Quaternary graben sediment is still under continuous investigation due to the inhomogeneity of sediments and the dynamics of the connected Cretaceous aquifer system triggered by the decreasing Dead Sea water level. For this, complex groundwater flow models were created in several studies to investigate the groundwater hydraulics by a combination of geological profiles and an interpretation of the groundwater levels (*Gräbe et al.* [2013], *Laronne Ben-Itzhak and Gvirtzman* [2005], *SUSMAQ* [2001], *Yellin-Dror et al.* [2009]). However, questions about the groundwater movement and quantity within the Quaternary in the Lower Jordan Valley remain still unanswered. For a further understanding of groundwater flow mechanism in the Quaternary sediment fans and evaporates, geochemical investigations of the groundwater resources and exploration of the geometry of depositions and flow mechanism is supposed to be an appropriate tool.

Previous studies of the Ein Feshkha region focussed on the spring water chemistry regarding water origin and water age. In 1972,[*Mazor and Molcho*]separated the Ein Feshkha waters into two groups, which were related to the water types of the Tiberias and Noit springs and a combination of Zohar spring water and Yesha well water with a saline end member (Dead Sea). *Hasan* [2009] investigated also the geological underground of the spring region with electromagnetic measurements beside the spring water chemistry. In his study, a salt diapir was investigated in the Ein Feshkha region, which contributes in addition to the paleo-brines to the increased salinity in the spring water. Stable isotopes $\delta^{34}S$ and $\delta^{18}O$ of sulphate contributes to a differentiation of sulphur sources in minerals occurring in the Quaternary sediments and tracing fractionation processes of redox reaction, precipitation and dilution, and organic degradation by organism activity (e.g. *Krouse and Mayer* [2000]).

Sulphur

Sulphur in the local groundwater system depends on three main input sources: (i) sulphur is contributed to the groundwater via rain water in form of sulphate. The regional precipitation pattern is composed of air masses coming from Mediterranean Sea including sea spray and dust from the exposed Cretaceous rock formations. *B Herut et al.* [1995] investigated rainwater patterns in Israel showing of sulphate concentrations from 0.1 to 2.6 meq/l and $\delta^{34}S$ from 0 - 15‰. (ii) As it is mentioned for the strontium isotopes and for the Mg/Ca and Sr/Ca ratios in seawater (4.1.3), there is variation of $\delta^{34}S$ over time in seawater reflected in marine carbonate deposition [*Prokoph et al.*, 2008]. For the Cretaceous, $\delta^{34}S$ in sulphate (barite or structurally substituted sulphate, [*Prokoph et al.*, 2008] range between 12 to 25 ‰ and particularly in the late Cretaceous ~ 18‰. During sedimentation of the Lisan formation (Quaternary) sulphur was deposited in different mineral phases in up to 35 m sediment thickness [*Begin*, 1974] extending to the Jordan river. *Torfstein* [2008] classified the deposition into (i) gypsum layers (10 -20 m thickness) consisting of Lower Gypsum Unit and Upper Gypsum Unit, (ii) thin gypsum laminae, (iii) native sulphur in concretions and (iv) carbonate associated sulphate. These formations differ in $\delta^{34}S$ signature [*Torfstein*, 2008]:

Primary gypsum layer (10-20 m)	$\delta^{34}S$ ‰ VCDT
- fine crystalline gypsum with little lamination	14 to 28‰
- laminar gypsarenite, sporadic aragonite	14 to 28‰
- Lower gypsum unit	16 to 20‰
- Upper gypsum unit	25 to 28‰
Silty detritus	-26 to 1‰
Native Sulphur	-20 to -10‰
Carbonate associated sulphate (sulphate co-precipitated with aragonite)	-2.5 to 26‰
Dead Sea – Sulphate	15‰
Dead Sea – Sulfide	~ -22‰

(v) A further sulphate source is formed by anthropogenic input. Aspects like e.g. atmospheric air contamination by industry result into sulphur compounds in air masses and leaching of fertilizer as well as degradation in soil effects further sulphate input to groundwater [*Matthess*, 2005].

4.2.1 $\delta^{34}S$ pattern in the Cretaceous groundwater and springs

Sulphate concentrations range from ~0.2 meq/l (recharge area) to ~10 meq/l in the discharge area (Lower Jordan valley) (Figure 25, Appendix A.2).

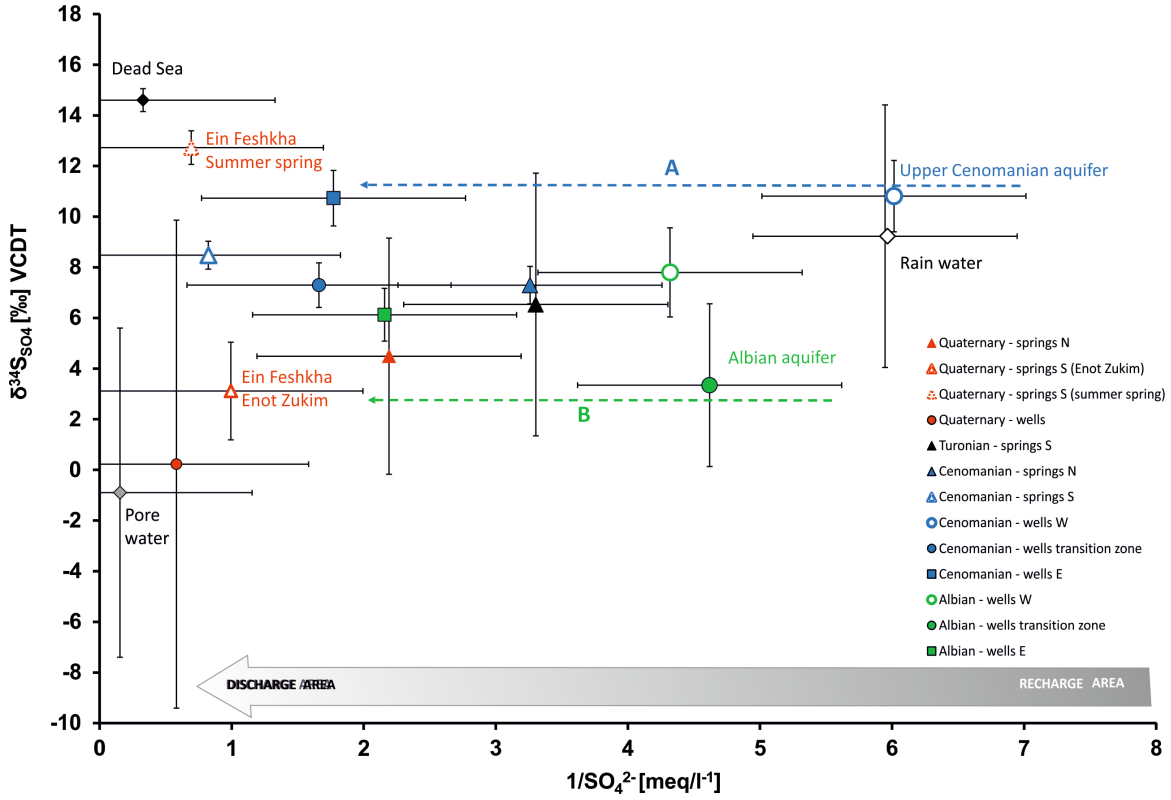

Figure 25 Mean of $\delta^{34}S$ ratios of groundwater in combination with the inverse sulphate concentrations (standard deviation as error bars), from recharge to discharge area, course A and B indicate conservation of $\delta^{34}S$ ratio from recharge to discharging springs with increasing sulphate (Ein Feshkha)

Groundwater of the Upper Cenomanian aquifer in the recharge area corresponds to rain water composition (Mean ~10‰ for $\delta^{34}S$ and ~0.2 meq/l sulphate). In the lower aquifer (Albian), the sulphate concentrations increase (0.3 meq/l, Appendix A.1) with a shift to lighter $\delta^{34}S$ ratio values (~8‰). Groundwater of the Albian aquifer in the transition zone develops further to $\delta^{34}S$ ratios of ~3‰. This can be reasoned by two main aspects: (i) The lower aquifer preserves a range of precipitation events with varying $\delta^{34}S$ ratios depending on seasonal input times (see standard deviations of rain water signal) and (ii) dissolution of aquifer rock result into mixture processes between rock isotope ratios and groundwater ratios. There is no fraction of $\delta^{34}S$ and therefore the water evolvement from recharge to discharge area depend on the input signal like rain water composition and contributing sources like the aquifer rock. Consequently, sulphate concentrations increase in the groundwater of the Cretaceous aquifers while the $\delta^{34}S$ signal is almost preserved depending on sulphate amount in aquifer matrix (Figure 25).

The Turonian springs Auja and Samia (north) and Cenomanian springs (e.g. Qilt, Ferat, Fawar) cover a wide range of sulphate concentration and $\delta^{34}S$ values as a function of rain water input, fast flow velocities and aquifer rock dissolution in the aquifer. The Dead Sea is one of the mixing endmembers of the system. After the fresh groundwater from the Cretaceous aquifer enters the Quaternary sediment section the groundwater gets mixtured. That means, the wells in Quaternary section are shifted to lighter $\delta^{34}S$ vaulues including negative values as a result of sulfide oxidation and heavier isotope ratios from the e.g. gypsum units as well as Dead Sea sulphate [*Torfstein*, 2008]. The Ein Feshkha springs are differentiable into two groups based on the $\delta^{34}S$ values and TDE (Figure 25). The Ein Feshkha “summer spring” contain a TDE > 110 meq/l and show a mean $\delta^{34}S$ value of ~13‰ indicating a mixture of upper Cenomanian aquifer and strong saline sources like Dead Sea water. In comparison the brackish spring “Enot Zukim” in Ein Feshkha show a lighter $\delta^{34}S$ value of (~3‰) in combination with <110 meq/l TDE indicating groundwater from the Albian aquifer mixed with pore water of the Quaternary section or at Albian groundwater in the first step of dissolution of Quaternary saline sediments.

Further indication of water evolvement towards the discharging springs in Ein Feshkha can be obtained from $\delta^{18}O_{SO4}$: A differentiation of the groundwater in the upper Cenomanian aquifer and Albian aquifer is given by an enrichment of $\delta^{18}O_{SO4}$ values towards the lower aquifer. $\delta^{18}O_{SO4}$ is also a stable isotope ratio and is specific for the source of origin (e.g. dissolution of gypsum or oxidation of H_2S). In this context, both aquifers show the continuously dissolutions of sulphate mineral fraction in the carbonate aquifers. The development of the groundwater in upper Cenomanian aquifer is presented by the well Jericho 2 (transition zone) and the discharging springs Arugot and Ein Gedi. They show ~9‰ for $\delta^{34}S$ and an enrichment of $\delta^{18}O_{SO4}$ to ~8 -13‰ indicating water development from Upper Cenomanian groundwater to Ein Feshkha summer spring (Trend A, Figure 26). Further enrichment of heavier isotopes in sulphur and oxygen and total dissolved solids in the Ein Feshkha springs are strongly influenced by the saline pattern of the Quaternary sediments and the Dead Sea brine (~ 15‰ $\delta^{34}S$ for sulphate, *Torfstein* [2008]). In the Ein Feshkha springs of Enot Zukim, the $\delta^{34}S$ and $\delta^{18}O$ values point to an origin from the Albian aquifer (Trend B, Figure 26). Groundwater in the Quaternary sediments, which originates from the Cretaceous aquifers, span a wide range of oxygen (5-18 ‰ $\delta^{18}O$) and sulphur isotopes (-15 – 15‰ $\delta^{34}S$) according to the contacting sediment layers including sediments with sulfide oxidation with negative $\delta^{34}S$ ratios.

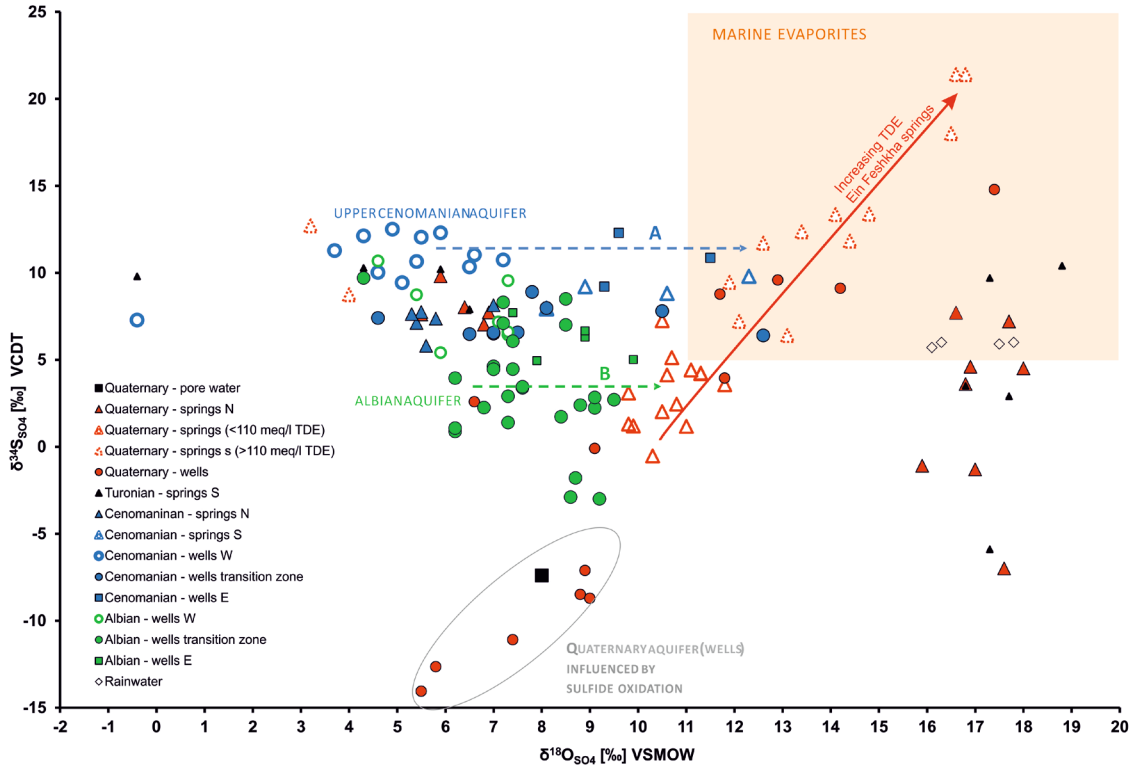

Figure 26 Distinct groundwater groups of $\delta^{34}S$ ratios and $\delta^{18}O$ ratios in investigated waters; Trends A and B show indication of water development from Cretaceous aquifers in direction of Ein Feshkha springs; field of marine evaporates refer to *Krouse and Mayer* [2000]

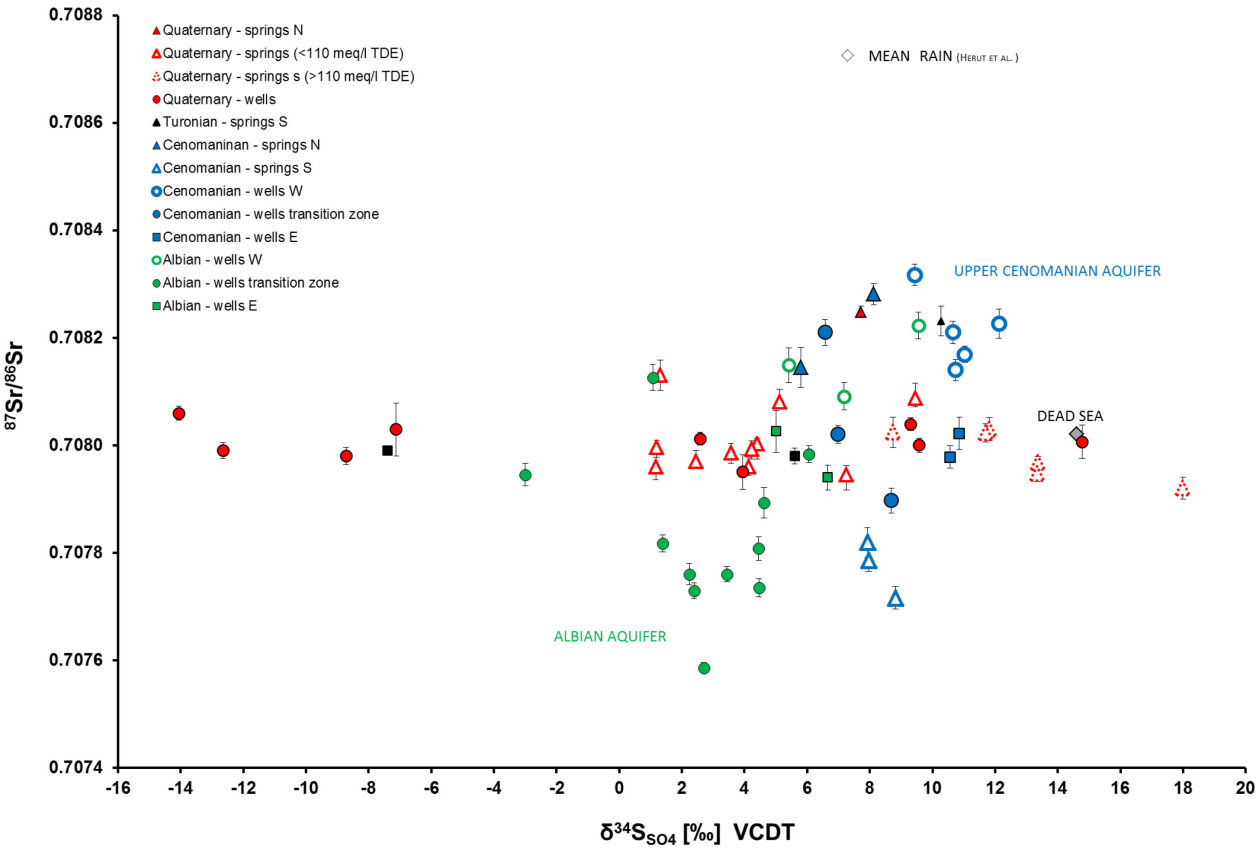

Figure 27 Distinct groundwater groups plotting $^{87}Sr/^{86}Sr$ ratios (including σ2 measurement error) and $\delta^{34}S$ ratios of sulphate: isotope data show distinct groups of upper and lower aquifer (Cretaceous) and indicate spring water origin of Ein Feshkha via mixing of Cretaceous groundwater and brine of saline Quaternary water reservoirs or Dead Sea, mean rain water values after [*B. Herut et al.*, 1993; *B Herut et al.*, 1995]

The enriched $\delta^{18}O$ values in the northern Quaternary section and partly in the Turonian springs depend on the rain water isotope variations since those springs are correlated to rain water events. Combination of $\delta^{34}S$ results and $^{87}Sr/^{86}Sr$ ratios (Figure 27) shows a distinct separation of all aquifer groups (Upper Cenomanian and Albian aquifer) including the Ein Feshkha springs and Quaternary groundwater. From the Upper Cenomanian to the Albian aquifer, the groundwater evolves from rain water composition and gets modified by continuing water- rock interaction. The typical above mentioned $\delta^{34}S$ values and $^{87}Sr/^{86}Sr$ ratios in the Upper Cenomanian (lower water-rock interaction) and Albian aquifer (higher water-rock interaction) can be identified in the two main Ein Feshkha groups (represented by Enot Zukim and Summer spring). Isotopic patterns in the Ein Feshkha spring are additionally modified in direction to saline endmembers in the graben, e.g. sediment composition and Dead Sea.

4.2.2 Trace elements - Identification of saline patterns in Cretaceous and Quaternary aquifers

Box plot analysis

Characterization of the investigated aquifer groups is examined by calculation the statistical parameters median, maximum, minimum, 25%- and 75% - quantile presented in a boxplot. The data set of As, Ni, Cu, Cr, V, Mo, Rb, Sr, U ("diluted" and "suspended" (solid)) are given in the following figures.

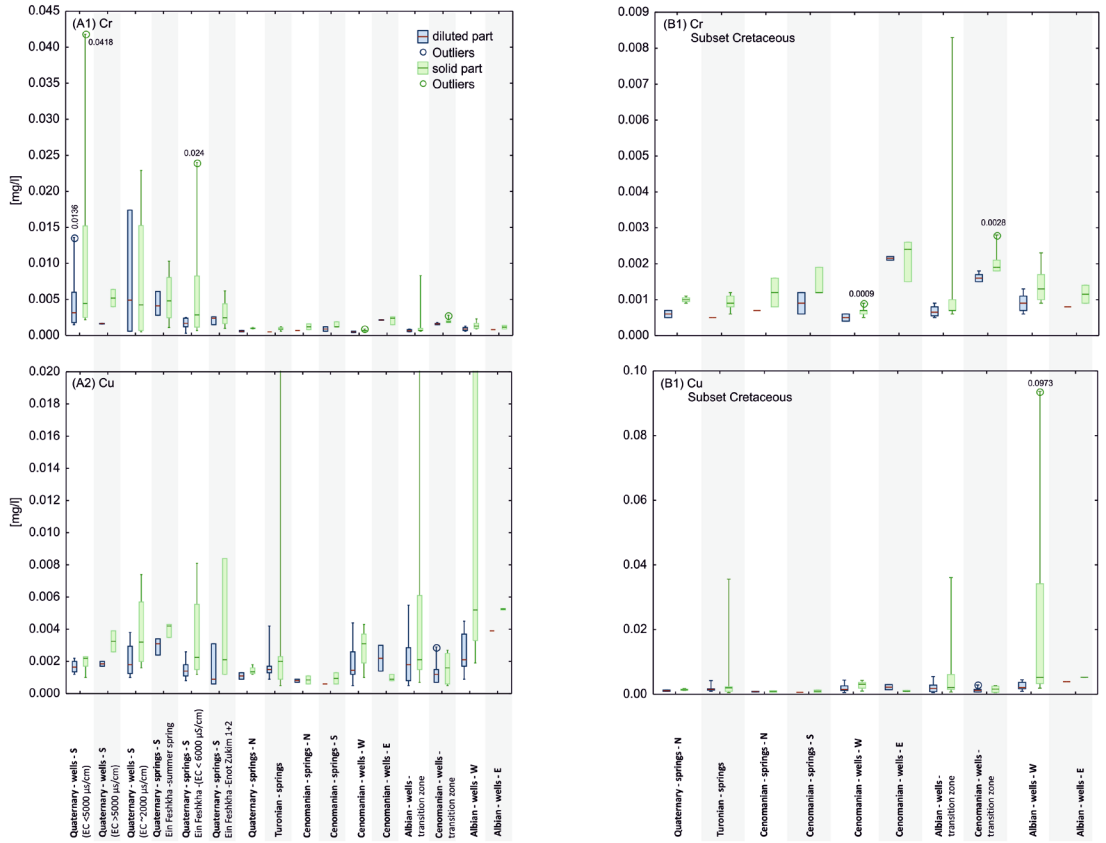

Figure 28 Box plot from trace elements (Cr, Cu) of "diluted" samples (blue boxes) and "suspended" samples (green boxes) from each groundwater/ spring group sorted by geology and regional pattern (N, S, W, E). Left side presents the subset of the groundwater groups coming from the Cretaceous with adjusted y - axis. Boxes show the median and 25/75 percentile, whiskers maximum and minimum, open dots are outliers.

Groundwater of the Cretaceous layers contain low Cr concentrations (<0.003 mg/l), except in the well of transition in the lower aquifer (Albian) (up to 0.008 mg/l). Occurring forms of Cr in water (EH depend on pH and redox conditions [*Matthess*, 2005]. In neutral water with neutral water and positive redox potential (~100- 1000 mV for all sampled waters) $Cr(OH)^{2+}$ is the dominant species [*Matthess*, 2005]. In the Quaternary sediments, Cr reaches up to 0.04 mg/l in the suspended part and dissolved Cr is higher than in the Cretaceous groundwater. The Ein Feshkha spring contain low dissolved concentrations (<0.005 mg/l) with higher suspended concentrations (up to 0.024 in summer spring) indicating contributions of low dissolvable Cr minerals of the Lisan sediments. Similar to Cr, Cu concentration are low in "diluted" and "suspended" parts (<0.1 mg/l). Only Cu concentrations in the Ein Feshkha springs tend to higher concentrations except of outliers in the Turonian springs and Albian wells (transition zone and W).

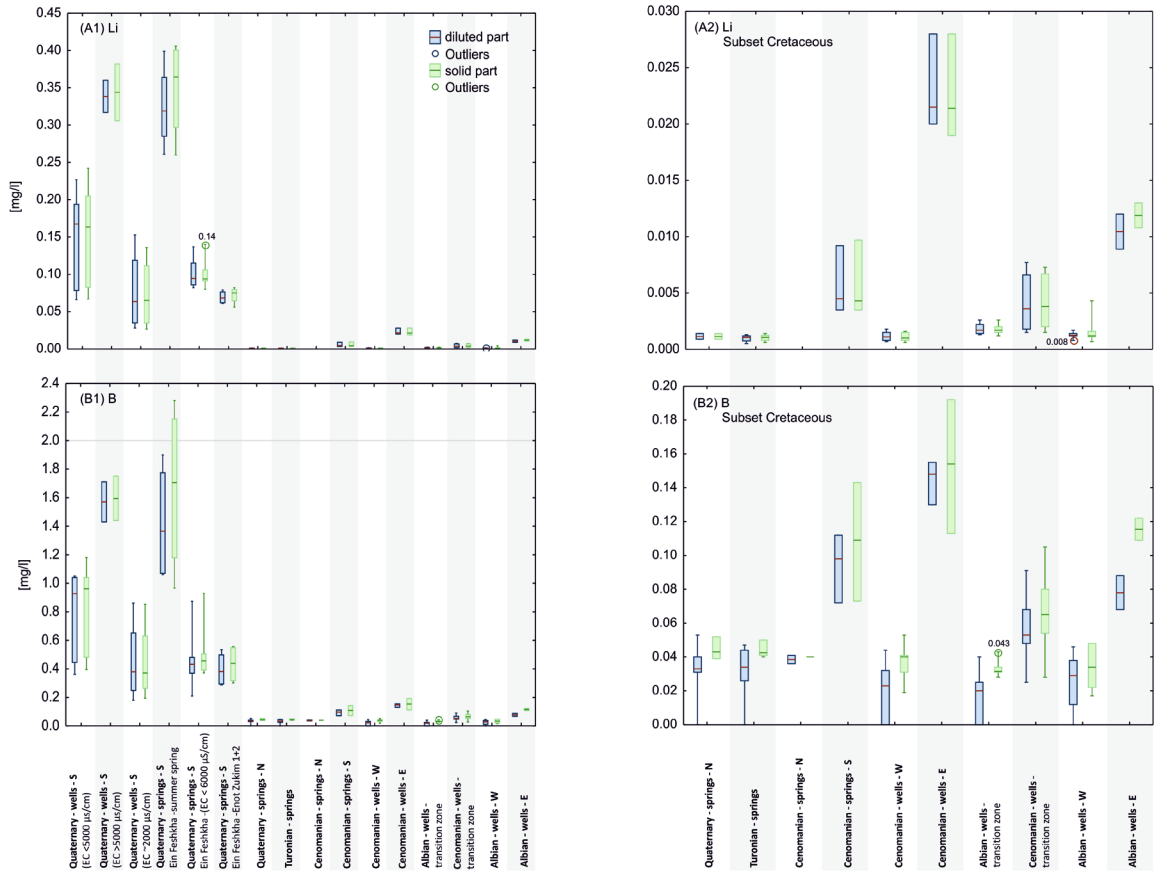

Figure 29 Box plot from trace elements (Li, B) of "diluted" samples (blue boxes) and "suspended" samples (green boxes) from each groundwater/ spring group sorted by geology and regional pattern (N, S, W, E). Left side presents the subset of the groundwater groups coming from the Cretaceous with adjusted y - axis. Boxes show the median and 25/75 percentile, whiskers maximum and minimum, open dots are outliers.

Li is also enriched in local brines in the Quaternary section, e.g. Dead Sea, and high Li concentrations in the water corresponds to high electrical conductivity, e.g. in the summer spring and Quaternary wells with EC >5000µS/cm up to 0.4 mg/l (Figure 29). In the groundwater of the Cretaceous layers, Li concentrations range below 0.03 mg/l. Here, groundwater with longer flow paths and intensive water rock interaction like the Arugot and Ein Gedi discharging the upper aquifer close to the graben fault as well as the wells in the transition zone. B contents in the

investigated groundwater show similar distribution pattern like Li. It is associated with Li in brines of the Quaternary deposits.

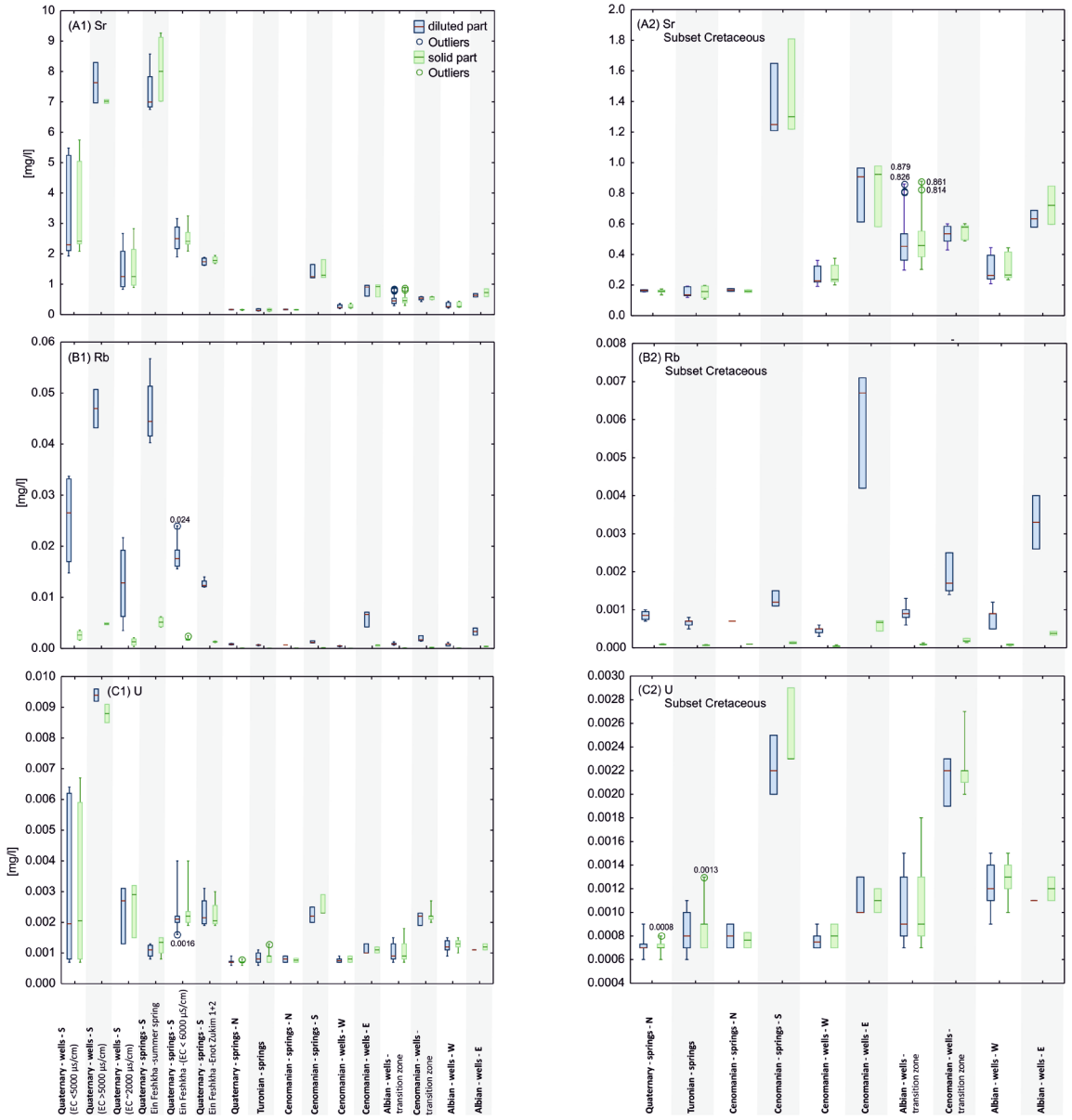

Figure 30 Box plot Sr, Rb,U of "diluted" samples (blue boxes) and "suspended" samples (green boxes) from each groundwater/ spring group sorted by geology and regional pattern (N, S, W, E). Left side presents the subset of the groundwater groups coming from the Cretaceous with adjusted y - axis. Boxes show the median and 25/75 percentile, whiskers maximum and minimum, open dots are outliers.

U concentrations range between 0.0005 and 0.003 mg/l in the groundwater in the Cretaceous rocks originating from dissolution of carbonates (Figure 30). U forms readily the Uranyl complex (UO_2^{2+}) when the groundwater show positive redox potential [*Matthess*, 2005]; most dominant in groundwater is the anion $UO_2(CO_3)_2^{-2}$ (*Matthess* [2005], *Merkel et al.* [2005]). The southern spring Arugot and Ein Gedi emerge from Cenomanian layers and in the transition zone Mizpe Jericho 2 (Upper Cenomanian) form distinct groups indicating U enrichment caused by more dissolution along the flow path or local contamination of the upper aquifer. The wells, which are frequently used for agricultural irrigation (Arab project well 66), show the highest U concentration up to

~0.009 mg/l corresponding to highest dissolved suspended content. Rb occurs mainly dissolved in the investigated waters. Suspended parts of rubidium, meaning adsorbed Rb is very low (<0.001 mg/l for Cretaceous groundwater and <0.005 mg/l for Quaternary waters). Highest Rb content occurs in the Ein Feshkha Summer spring and in the Quaternary wells with EC >5000µs/cm. Higher Rb concentrations in the Cretaceous groundwater are given in the Cenomanian wells E, Cenomanian wells transition zone and Albian wells E forming distinct groups of different Rb enrichment (up to 0.007mg/l in Cenomanian wells E).

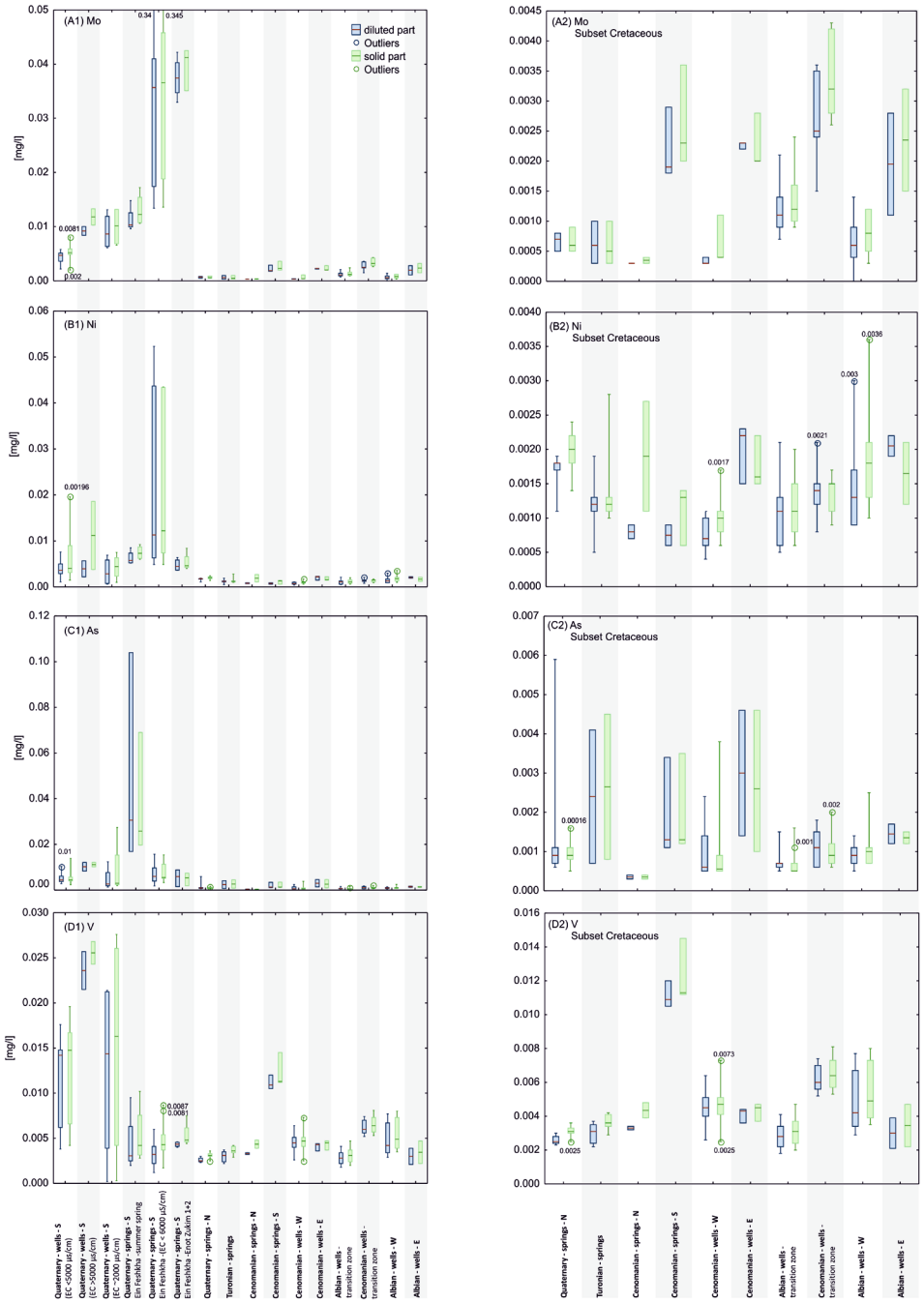

Figure 31 Box plot from trace elements (Mo, Ni, As, V) of "diluted" samples (blue boxes) and "suspended" samples (green boxes) from each groundwater/ spring group sorted by geology and regional pattern (N, S, W, E). Left side presents the subset of the groundwater groups coming from the Cretaceous with adjusted y - axis. Boxes show the median and 25/75 percentile, whiskers maximum and minimum, open dots are outliers.

Sr concentrations in the groundwater of the Cretaceous show a clear increasing trend for recharge to discharge area and from upper to lower aquifer (up to 9 mg/l in Ein Feshkha summer spring and up to 0.007 mg/l in the Cretaceous subset, the southern Cenomanian springs). This pattern refers to progressing dissolution of the carbonates including overprinting rainwater signature with aquifer rock signature and admixture of saline suspended from and in the Quaternary section (as discussed before). Mo occurs under oxidized conditions as $HMoO_4^-$ and MoO_4^{2-} (Matthess [2005], Merkel et al. [2005]). Under neutral pH $HMoO_4^-$ is the dominant species. The concentrations in the groundwater located in the Cretaceous layers exhibit very low concentrations of Mo (up to 0.0045 mg/l), where the lowest occur in the "springs N" emerging in the Quaternary section (Dyouk and Sultan), Turonian and Cenomanian springs located in the northern part of the investigation area (Figure 31). Here water chemistry tends in general to the rain water composition with low mineralisation. For the rest of the groundwater in the Cretaceous, there is only minor variation with increasing trend in the wells of the transition zone. Sampled wells and springs and springs in the Quaternary section contain higher concentrations in comparison the groundwater in the Cretaceous (~0.003 to 0.345). The highest Mo concentration arises in the Ein Feshkha springs with electrical conductivity <6000 µs/cm. The increase of the Mo concentrations in the Quaternary refers to the saline depositions in the Lisan sediments (deposition of the Dead Sea precursors). Likewise, Mo, Ni concentrations are very low and with little variation in the groundwater of Cretaceous layers (0.0005 – 0.0036 mg/l Ni) and higher in the groundwater of the Quaternary (Figure 31). The Ni content in all sampled waters is mainly dissolved as Ni2+ ("diluted" and "suspended" part are mainly equal). The highest Ni concentration occur in the Ein Feshkha spring "stream", which is a confluence on-site of the emerging less saline springs (<6000µs/cm). Concentrations range between <0.001 –0.006 mg/l in the groundwater of the Cretaceous layers. Water in the Quaternary contain up to 0.02 mg/l. Under neutral pH and oxidizing conditions $H_2AsO_4^-$ and $HAsO_4^{2-}$ are the dominant species. The Ein Feshkha summer spring forms a distinct group with the highest dissolved concentration ranging between 0.017- 0.1 mg/l. Contents of V show similar concentration patterns like V for the groundwater in the Cretaceous. $VO_2(OH)_2$- is the dominant anion under neutral pH and oidizing conditions- The springs Arugot and Ein Gedi (Cenomanian springs S) form a distinct group with higher concentrations than Ein Feshkha springs and correspond to V content of water in the Quaternary wells. Vanadium can be removed from solutions via sorption in particular on FeOOH because it occurs similar to As, Mo, and U as anion (Krauskopf [1956], Matthess [2005]). Higher V concentration in the Quaternary wells (>5000 µS/cm) reach values of ~0.025mg/l referring to contact dissolution of saline sediments of the Quaternary.

Cluster analysis of hydrochemical data – trace elements

Application of Cluster analysis was based on z-score normalised data matrix. Data matrix consists of calculated means for location (in case of more than one sample from a certain point). According to the existence of Cretaceous aquifers and Quaternary aquifers, the cluster analysis separates into main cluster (Figure 32). Further sub groups represent a refinement. The main cluster (A) consists of an accumulation of the upper aquifer (first group) and lower aquifer (third group). The second group represents wells situated close to the main fault in the Cretaceous aquifers (transition zone: Jericho 2, 4, 5). A cluster combination of Arugot, Mizpe Jericho 2 and 5, as well as the lower aquifer wells Al Azaria 3 and Jerusalem 6 refer to similar tracer pattern indicating

connatural maturity. This can be reasoned by similar intensity of water rock interaction via long flow path in Arugot and Mizpe Jericho 2 and 5 and via admixture of mature water in the lower aquifer (Al Azaria 3, Jerusalem 6). A higher chloride content and higher TDE in comparison to the other groundwater groups other Cretaceous aquifer are given by the fifth sub cluster. Here, the origin from the Cretaceous aquifer is indicated as well as separation via admixture of different saline sources.

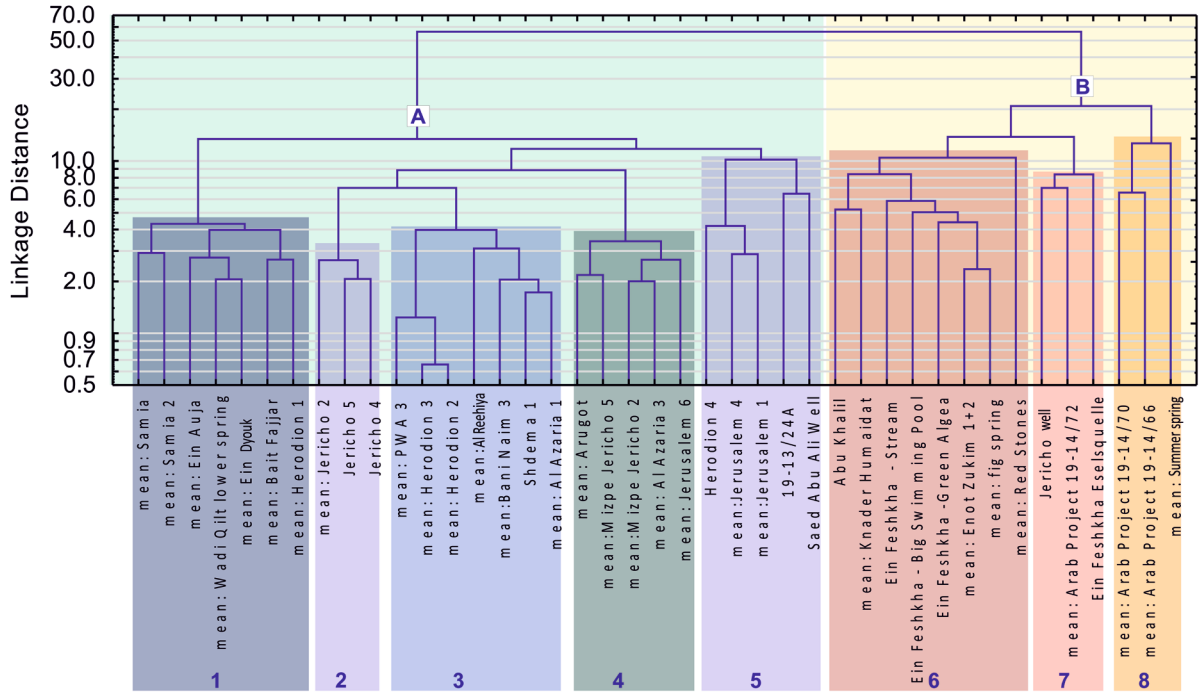

Figure 32 Tree plot of all sampling locations and sampling times using Ward` s method and Euclidian distances, linkage distances are presented logarithmic

For Jerusalem 4 and 6, Herodion 4, it can be assumed that there is an addition from enriched surface water and the Jericho wells (19-13/24A and Saed Abu Ali) from dissolution of saline deposits or admixture of brine. The second main cluster (B) comprises all sub groups located in the Quaternary section from low to high TDE: sub group (6) of Enot Zukim, sub group (7) Ein Feshkha “Eselsquelle” and sub group (8) around summer spring. This 2nd main cluster represents a group referring to different stages of saline patterns including three TDE levels. Focussing on cluster 1 of tree plot in Figure 32, which is mainly representative for the Upper Cenomanian aquifer, the trace elements cluster combined with anion are almost similiar (Figure 33). Sulphate and nitrate are combined with Ni, Mn, As, Fe, V in one cluster and Cl is clustered with Mg, B, Cr, Na, K. Considering the suspended fraction, nitrate is similar clustered with As, Ni and Fe, rest of cations were not analysed in the suspended fraction.

Cluster 3 (Albian Aquifer) of Figure 32 show three main clusters according nitrate, bicarbonate and chloride concentrations in the diluted fraction (Figure 34). Sulphate is clustered with Rb, K, Mo, Ba and Li and nitrate is combined with Mn, Mg, As and Cs. Bicarbonate and chloride are combined in one cluster with V, F, Na and Ni. The suspended fraction shows different sub cluster with sulphate (Li, Rb, Mo) and chloride and bicarbonate (Sr, B).

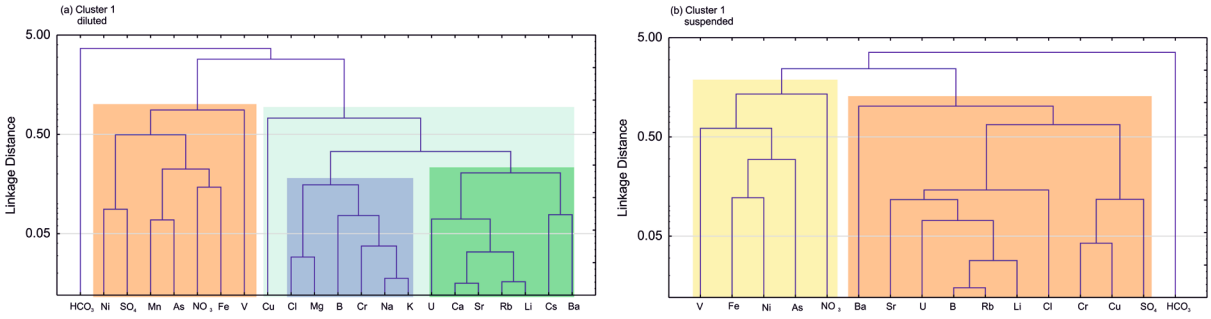

Figure 33 Tree plot of groundwater of cluster 1 from figure 32 (wells and springs) and all sampling times using Ward`s method and Euclidean distances, linkage distances are presented logarithmic, left: " diluted" samples, right: "suspended" samples

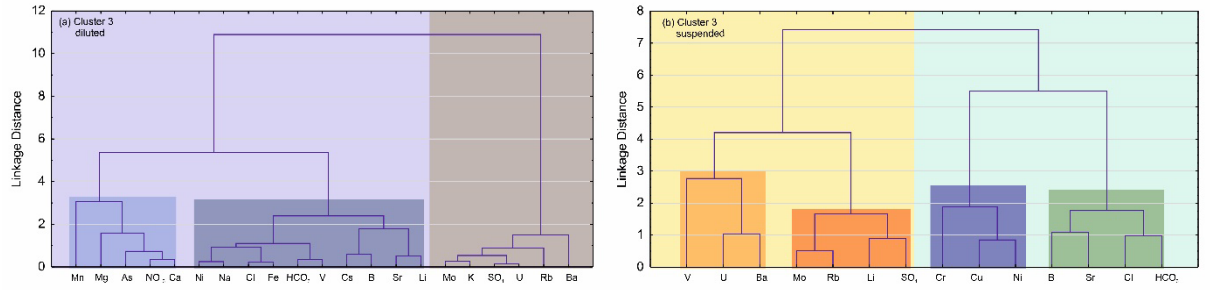

Figure 34 Tree plot of groundwater of cluster 3 from figure 32 (wells and springs) and all sampling times using Ward`s method and Euclidean distances, linkage distances are presented logarithmic, left: "diluted" samples right: "suspended" samples

Quaternary aquifer

Results of cluster analysis for the sampled groundwater in the Quaternary sediments are presented in the following section. There are two main clusters for the groundwater in the Quaternary wells (A and B in Figure 35). Cluster "A" comprises groundwater clusters of Arab well 70 (~100 meq/l TDE) and Arab well 66 (>100 meq/l). The second cluster "B" includes groundwater with TDE <100 meq/l.

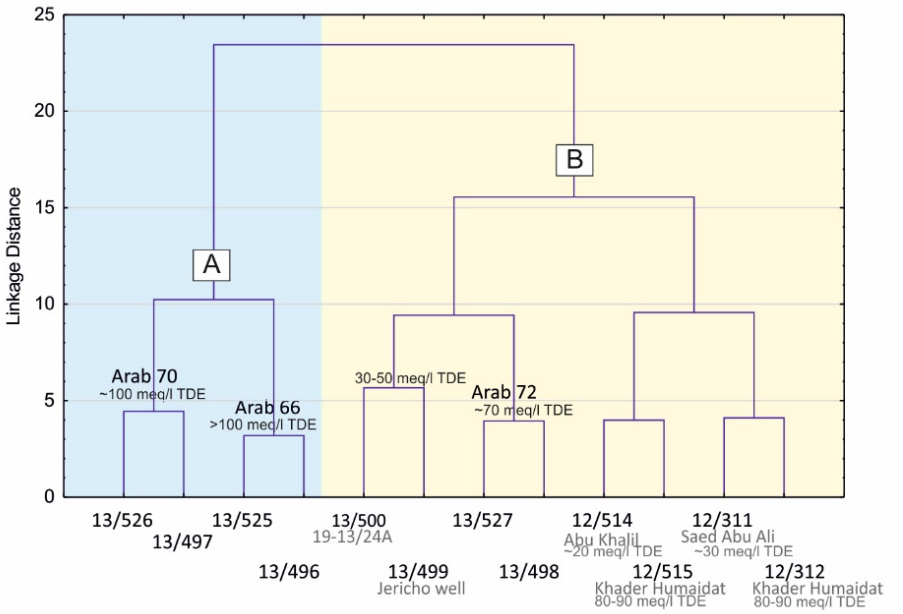

Figure 35 Tree plot of wells in the Quaternary sediments using Ward`s method and Euclidean distances, linkage distances are presented logarithmic; cluster A includes mainly the higher saline wells (Arab well 66 and 70), whereas cluster B is characterizes the lower saline wells in the Jericho area

Cluster B in Figure 35 consists also of two groups, which is caused by different contribution of Cretaceous fresh water input for the wells closer to the main fault (Abu Khalil, Saed Abu ali well & Khader Humaidat). The groundwater cluster of the Jericho well, Arab 72 and well 19-13/24 (situated on the eastern side of Jericho) could be a result of low admixture of brine in the Quaternary sediments. Element distribution in the Quaternary groundwater within a cluster plot show nearly similar patterns for the analyses of the sloid parts and “diluted” part in the samples Figure 36. Bicarbonate builds a group with V, Cr and Mo. Nitrate is combined with Ba, Li, Rb, B and K (only “diluted” samples). Sulphate and chloride build each sub group, where sulphate is combined with U and Sr. In the analyses of the “diluted” samples, chloride is clustered with Na, Mg and Cs and Ca. In comparison, in the “suspended” samples, trace element like Ni correlates with chloride. A main difference between analysis of “suspended” and “diluted”samples is that in Mn, Fe, Cu, Ni, As build a separate cluster in the diluted part.

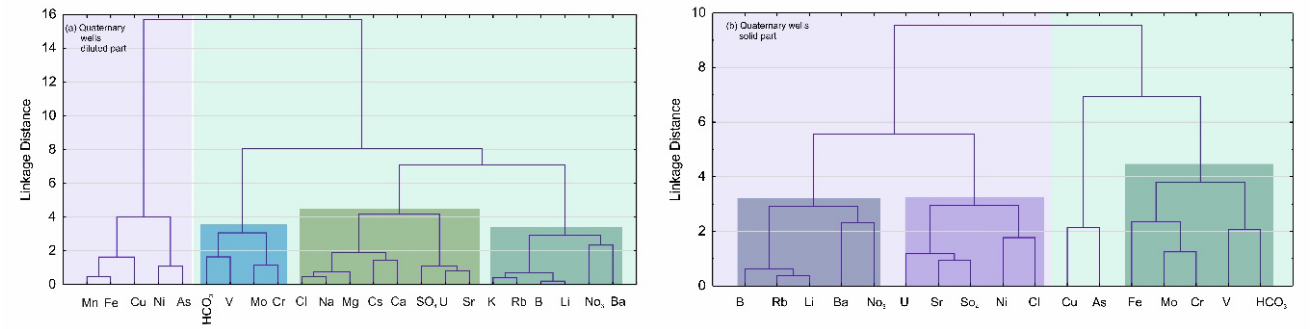

Figure 36 Tree plot of trace elements based on the analyses of the groundwater in the Quaternary using Ward`s method and Euclidean distances, left side: “diluted” samples, right side: “suspended” samples

The solubility of these elements strongly depend on pH conditions means that neutral pH in the waters triggers low mobility and therefore occur low concentrations of those elements in the “diluted” samples caused by naturally higher dissolution with lower pH conditions [*Matthess*, 2005].

Ein Feshkha

Cluster analysis applied for the spring waters of Ein Feshkha result into two main groups: one group consists of Ein Feshkha summer spring with higher electrical conductivity of >6000 µS/cm (TDE >110meq/l) and the other group is characterized by lower electrical conductivities, whereas the analyses of the “Enot Zukim” spring water form a sub group (TDE< 110meq/l, EC <4000µS/cm) (Figure 37). Cluster results of trace elements including analysed main anions (chloride, sulphate and bicarbonate) result into three main groups according to the main anions for the “diluted” content in the Ein Feshkha “Summer spring” (Figure 38). Bicarbonate is grouped with Mo, Ni, V, U. Chloride is grouped with Sr, Mg, Ca, Rb, Li, K, Cs, Na and B. Sulphate is combined with Cu, Fe, Mn, Ba. Groups of chloride and sulphate are part of one big cluster (Figure 38). Analyses of the suspended samples of Ein Feshkha summer spring are clustered into two main clusters chloride and sulphate with bicarbonate. In difference to the “diluted” part is that Mn and Fe built an own group in the cluster of chloride.

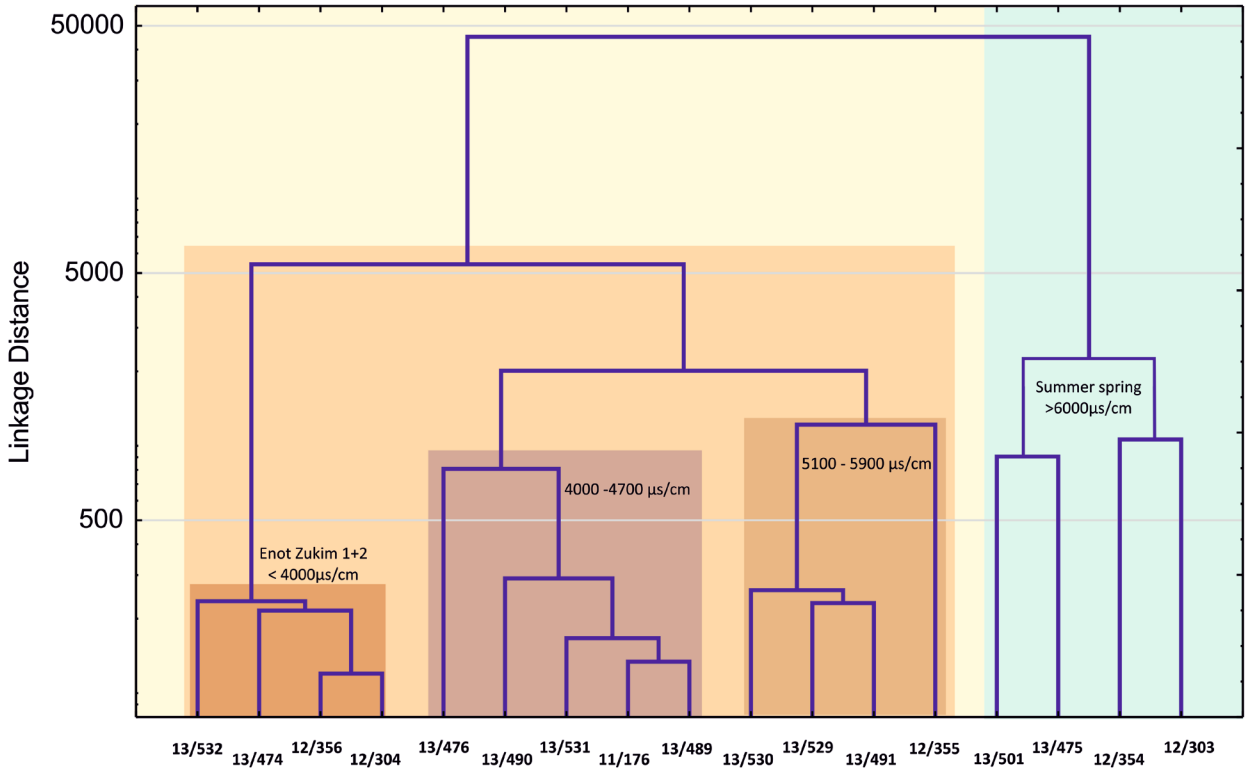

Figure 37 Result of cluster analysis of Ein Feshkha springs using Ward`s method and Euclidean distances, cluster separates distinct hydrochemical spring groups, which are here differentiated by electrical conductivity [µS/cm]

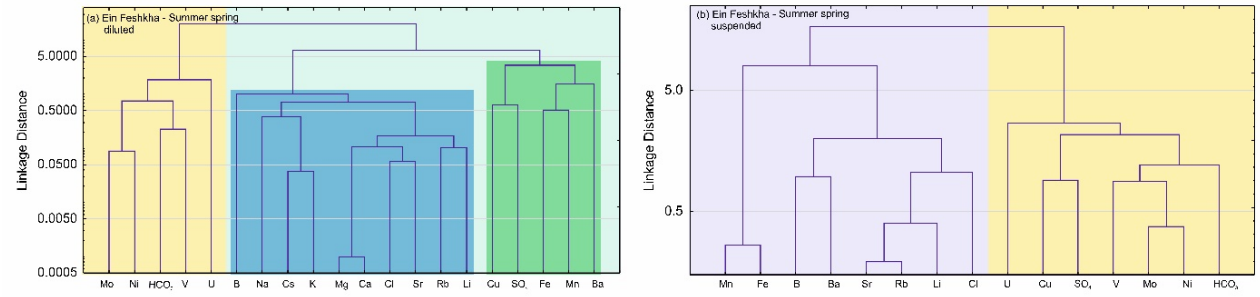

Figure 38 Tree plot of trace elements based on the analyses of the groundwater in Ein Feshkha "Summer spring" using Ward`s method and Euclidean distances, left side: "diluted" samples, right side: "suspended" samples

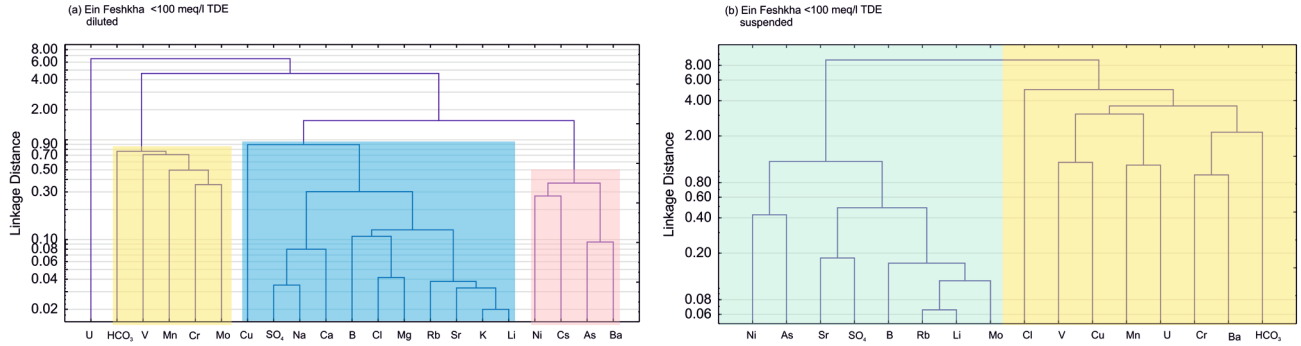

Figure 39 Tree plot of trace elements based on the analyses of the groundwater in Ein Feshkha "Enot Zukim" using Ward`s method and Euclidean distances, left side: "diluted" samples, right side: "suspended" samples

Considering the cluster results of the Ein Feshkha “Enot Zukim” (“diluted” samples), bicarbonate is grouped with V, Mn, Cr and Mo. There is a second cluster, which consists of sulphate, Na, Ca, B, Cl, Mg, Rb, Sr, K, Li, and Cu. A third group contains of Ni, Cs, As and Ba. Results of the suspended content in the Ein Feshkha “Enot Zukim” springs show two main cluster: sulphate with Sr, As, Ni, B, Rb, Li and Mo and bicarbonate with Ba, Cr, U, Mn, Cu, V and chloride.

4.2.3 Conclusion

Application of sulphur isotopes and trace elements in the aquifer system of the Dead Sea let us step further into understanding of mixing processes and contributions of individual saline patterns coming from the Quaternary sediments and interstitial brines.

1. The $\delta^{34}S$ and $\delta^{18}O$ in the sulphate of the groundwater show a specific signature for the main Cretaceous aquifers. In comparison to the lower aquifer, the upper aquifer shows heavier $\delta^{34}S$ ratios showing an origin of rain water.
2. No reduction processes of $\delta^{34}S$ and $\delta^{18}O$ in the investigated system are relevant. The dominant process of $\delta^{34}S$ development is mixing. Ein Feshkha`s spring “Enot Zukim” contains similar pattern $\delta^{34}S$ like the lower aquifer. The “Summer spring” in Ein Feshkha, which only occurs during the summer time, shows isotopic pattern of the upper aquifer. The increase of sulphate in the springwater is a contribution of saline sources. Endmembers for the “Summer spring” is indicated by the Dead Sea brine and pore water could attributed to “Enot Zukim”.
3. Combination of $^{87}Sr/^{86}Sr$ with $\delta^{34}S$ describes the water evolvement within the Cretaceous aquifers towards the discharge area. Every aquifer group is differentiable based on the isotopic pattern of $^{87}Sr/^{86}Sr$ and $\delta^{34}S$.
4. Trace element distributions in the aquifer system are characteristic for the Cretaceous and Quaternary aquifers. Particularly there are specific trace element patterns, which are identifiable for dissolution of saline sources or brine contributions in the Quaternary sediments. They are mainly associated with chloride and sulphate.

4.3 Groundwater dating of W Dead Sea aquifer system

Karst systems represent abundant, but highly variable water resources whose extremely heterogeneous and anisotropic flow behaviour prevents exact predictions regarding the available quantities and mass transport. However, such an understanding of the system is the basic requirement for the sustainable management and protection of water resources. Estimation of groundwater infiltration times and groundwater age compositions play an important role in groundwater resources studies. In arid/semiarid regions water scarcity is serious problem manifesting itself in limited groundwater recharge with low amounts of water that can be sustainably extracted and an increasingly high-water demand. Sustainable water management strategies need detailed information about yearly groundwater recharge rates, groundwater flow velocity and quantity (volume) of the groundwater reservoirs. It is therefore essential to quantify infiltration rates and mean residence times of the groundwater system. Karst aquifer reservoirs consist of billions of water molecules from different precipitation events. Inside the water reservoir the water flows rapidly through conduits and fractures and very slowly through the small pores and fissures where most of the recharged water may be stored for a long period. Consequently, wide ranges of residence times are observable. The residence-time distribution represents the distribution of different groundwater ages. The term groundwater age is often understood as the time span of an imaginary water parcel between infiltrating at the groundwater surface and being sampled at a well or spring. This was defined as “idealized groundwater age” [*A Suckow*, 2012]. The idealized age is not directly measurable; therefore, tracers are used, which are isotopes of the water molecule or substances transported with the fluid. In practice measured tracer concentrations are compared to the output of simplified, often zero-dimensional models that assume a defined age distribution. This age distribution can be inherent in the transport mechanism, e.g. advection – diffusion – dispersion, and/or caused by sampling, e.g. of a groundwater sample taken from a well with a long filter screen or a karst spring where many flow lines meet. In addition to impeding the determination of groundwater age, the transport through the unsaturated zone has an effect. The transport of the gas tracers via the unsaturated zone is delayed by diffusion in the gas phase of soil air [*P G Cook et al.*, 1995]. Gas tracers like CFCs and SF_6 move through the unsaturated zone primary by diffusion, this leads to a time lag of gas concentrations in the unsaturated zone compared to the atmosphere. A time lag is also possible for the water bound tracer’s tritium and ^{36}Cl since the advection through the unsaturated zone may take decades (*Lin and Wei* [2006], *A. Suckow et al.* [1993]). In infiltration areas dominated by sand or clay water bound tracers are generally slower than gas tracers. This can be very different in karst systems, where preferential flows in karst “tubes” allow fast recharge to the water table. This part deals with age estimations of the stressed Eastern carbonate aquifer system in the western Dead Sea catchment. Over 5 Million people are reliant from the karst resources, which are divided in Lower and Upper Cretaceous Aquifer. Previous studies consider different age dating tracers to quantify water movement and flow velocity between the infiltration area and the sampling points in the different aquifers. *Yechieli et al.* [1996] and *Paul et al.* [1986] studied $^{36}Cl/Cl$ ratios to detect saline sources of groundwater brines in the Dead Sea area.

Groundwater age investigations of the main Cretaceous aquifers in the western Dead Sea catchment tried to quantify the duration of water flow from the recharge area to the springs in the mountain region. In this context, young-age dating tracers such as Tritium were used to estimate

the time of groundwater recharge for the Ein Gedi spring area at the Dead Sea coast [*Yechieli et al.*, 1994]. Groundwater recharge of the Upper Cretaceous aquifers was investigated with the use of anthropogenic gases (CFCs and SF_6) and Tritium by *Lange* [2012]. These studies demonstrated that there is a young component of water from the Upper Aquifer (Upper Cretaceous) with a mean residence time (MRT) of less than 30 years in the springs of the mountain region and therefore fast connections to the recharge area. The results demonstrate an extremely heterogeneous distribution of different groundwater ages in Lower and Upper Cretaceous aquifer. To better quantify the groundwater flow velocities from the recharge area to the spring outlets at the Dead Sea, specifically this work aims to (i) validate young rainwater input and fast groundwater movement via karst conduits, related to rapid flow paths from the recharge area, (ii) to quantify groundwater mixing of several groundwater components via lumped parameter models and (iii) to estimate groundwater recharge and to support future groundwater development scenarios using age dating tracers for "young" water (<70y) like the anthropogenic gases SF_6 and Chloroflourocarbons (CFC`s) and the anthropogenic bomb introduced isotopes tritium and ^{36}Cl. This tracer combination allows assessing contributions from the last decades until ~1950. Lumped parameter models (piston flow, dispersion and partial exponential) were applied to approximate the age distribution in groundwater samples. Using different model approaches, it is possible to test for different flow mechanism in the main Cretaceous limestone aquifer and draw conclusions on a wider range of the age distribution.

4.3.1 Dating parameters

The assessment of groundwater flow velocities using environmental tracers is based upon the input function (Figure 40) of the investigated tracers which is well constrained from precipitation samples since the 1960s (e.g. *Synal et al.* [1990], [*L Plummer et al.*, 2006], [*IAEA/WMO*, 2017]).

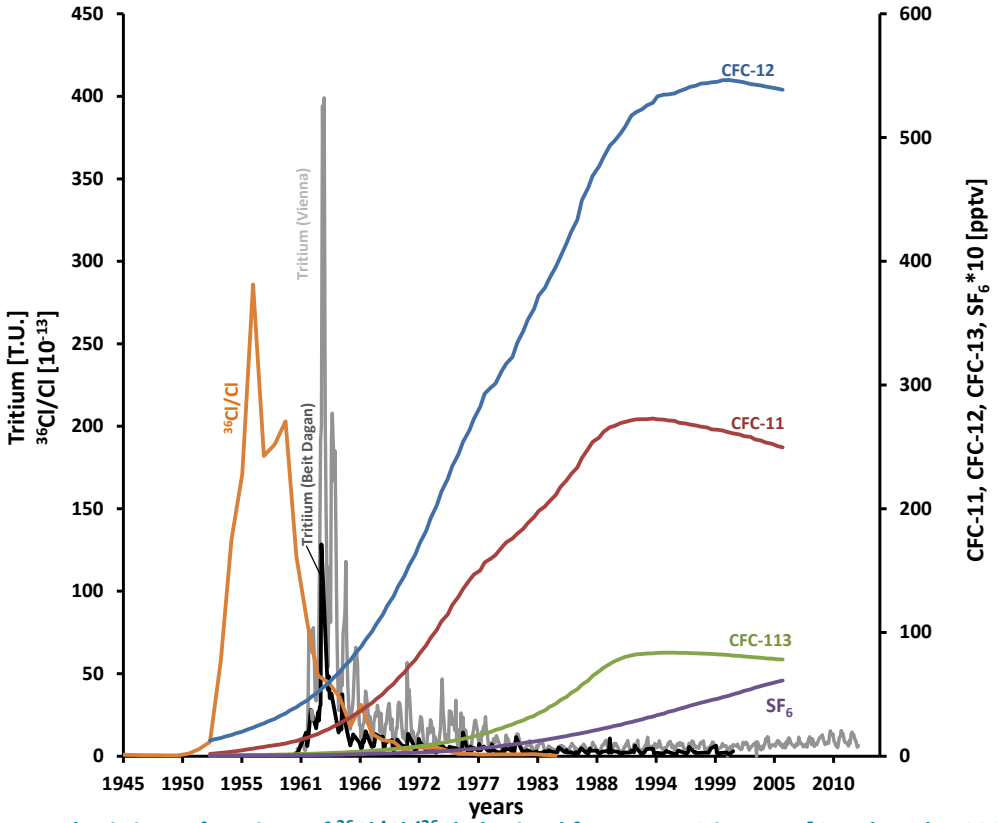

Figure 40 Atmospheric input functions of $^{36}Cl/Cl$ (^{36}Cl obtained from Dye - 3 ice core [*Synal et al.*, 1990], SF_6 and CFCs [*L Plummer et al.*, 2006] and decay - corrected Tritium in rain water of Beit Dagan (Israel) and Vienna (Austria) [*IAEA/WMO*, 2017]

The tracers Tritium and ^{36}Cl enter the unsaturated zone by means of precipitation events as part of the infiltrating rainwater. The anthropogenic gases SF_6 and the CFC`s in turn are transported by rainfall and gas diffusion through the unsaturated zone. The diffusive transport is parameterized by temperature, water content and pressure of the unsaturated zone. Tracers from treated and untreated waste water discharge and agricultural activities used in this study are the artificial sweetener Acesulfame K, the drug Naproxen, the pesticide Simazine and the fertilizer nitrate to prove further groundwater recharge in the last decades.

^{36}Cl as age tracer

^{36}Cl is a cosmogenic radioactive isotope with a half-life of 301,000 years and as such contained in infiltrating rain water. In the atmosphere, 36Cl derives naturally via cosmic ray spallation of ^{40}Ar in the atmosphere and ^{35}Cl in marine aerosols [*Alvarado et al.*, 2005]. Nuclear industry and the nuclear weapon tests starting in 1945 had a major impact on ^{36}Cl abundance in the atmosphere. Between 1950 and 1955, the deposition of "bomb" ^{36}Cl peaked with 400 x 105 atoms/cm^2y [*Elmore et al.*, 1982] in Greenland ice and this bomb ^{36}Cl was washed out from the atmosphere until the end of the 1960s (Figure 40). Local nuclear weapon tests have led to an inhomogeneous decreasing distribution in the atmosphere, depending on latitude and longitude [*Cornett et al.*, 1997]. The natural ^{36}Cl flux in the global atmosphere, particularly the latitudinal differences, are still investigated, e.g. by *Heikkilä et al.* [2009] and in precipitation over Europe by *Johnston and McDermott* [2008]. *Heikkilä et al.* [2009] combined ^{36}Cl results of atmospheric deposition of different locations and modelled ^{36}Cl fall out for different latitudes. Most age estimates of groundwater with ^{36}Cl are based on the half-life of ^{36}Cl (301 000 years) and consider time frames >100,000 years (*Bentley et al.* [1986]; *Davis et al.* [1983], *Love et al.* [2000], *Mahara et al.* [2012]; *Müller et al.* [2016]. The use of ^{36}Cl from the atmospheric bomb peak and groundwater age estimations of the last decades are much less frequent and were applied by e.g. *Alvarado et al.* [2005]; *Lavastre et al.* [2010]; *Rebeix et al.* [2014]; *Tosaki et al.* [2010]; *Tosaki et al.* [2007].

Tritium as age tracer

Tritium (^3H) is the naturally occurring radioactive isotope of hydrogen and enters the hydrological cycle as part of the water molecule (^3HOH). Concentration of Tritium in water is given in Tritium Units (TU) where 1TU corresponds to an isotope ratio $^3H/^1H$ of 10^{-18}. It is produced naturally by neutrons from cosmic radiation via the $^{14}N(n,^3H)^{12}C$ reaction [*Clark and Fritz*, 1997]. However, since 1960 atmospheric Tritium is dominated by fallout from the thermonuclear bomb tests between 1951 and 1980 and releases from the nuclear industry [*Clark and Fritz*, 1997]. In 1963, the Tritium annual precipitation weighted average concentrations reached a peak of 400 TU in Vienna (Austria) and 130 TU in Bet Dagan (Israel) (Figure 40). The global atmospheric distribution shows higher concentrations in the northern hemisphere and latitudinal and longitudinal differences since testing occurred mainly in the northern hemisphere. In addition, latitudinal dependencies of Tritium precipitation concentrations are influenced by varying precipitation and re- evaporation processes on a regional scale similar to the stable water isotopes δ^2H and $\delta^{18}O$ (e.g. *K Rozanski et al.* [1991]; *K. Rozanski et al.* [1993]). Tritium decays with a half-life of 12.32yeras (4500 days) to ^3He [*Lucas and Unterweger*, 2000]. The ratio between Tritium and its decay product

^{3}He is used for groundwater age dating in a time frame of 1-40 years (*P Cook and Solomon* [1997]; *Schlosser et al.* [1988]; *Solomon et al.* [1992]; *Sültenfuß and Massmann* [2004].

SF_6 and CFC`s as age tracer

Types of chlorofluorocarbons (CFCs) are the gas molecules CFC-11 (trichloroflouromethane $CFCl_3$), CFC-12 (dichlorodifluoromethane, CF_2Cl_2) and CFC-113 (trichlorotriflouroethane, $C_2F_3Cl_3$). They are volatile and synthetic and mainly produced since the 1930s as freezing agent and solvent for e.g. refrigerators. Their concentration in atmosphere increased since the 1950s with a life time of about 3000 years. These CFCs have a destructive effect on the ozone layer that resulted in a production moratorium and since the late 1980ies in a decrease of the atmospheric concentrations (Figure 40). Also, the anthropogenic trace gas SF_6 can be actively applied for age-dating of groundwater. SF6 is mainly used as electrical insulator in high-voltage technology and as inert gas during production of glass, aluminium, and magnesium. SF_6 concentrations in the atmosphere still increase exponentially with a rate of ~5%/a. Recently, a SF_6 concentration of 7 pptv in atmosphere has been reported. The distribution of CFCs and SF_6 in the atmosphere is nearly homogeneous due to the worldwide continuous emission with a well-defined time lag between the northern and southern hemisphere. Input curves from 1953 to 2006 can be found in *L Plummer et al.* [2006]. All anthropogenic gases were intensively studied by *Busenberg and Plummer* [2000]; 2008]; 2010]; *L Plummer et al.* [2006].

In groundwater, combinations of these gases with other environmental tracers were applied in order to distinguish e.g. local contaminations or time lags in the unsaturated zone (*Busenberg and Plummer* [1992]; *P G Cook et al.* [1995]; *Dunkle et al.* [1993]; *L N Plummer et al.* [1998]; *Szabo et al.* [1996]).

Anthropogenic organic trace pollutants and nitrate as age indicator

In the nutrition industry the artificial sweeteners became in the last decades an important role as a substitute for sugar. Particularly Acesulfame K is used since the 1990s. Barely degraded in the human organism, Acesulfame K is also rather stable in waste water treatment processes. Due to its high solubility in water it can be used as a chemical marker for waste water input in fresh water resources. A second chemical marker for human intake and therefore occurring in domestic waste water is the widely used pain mitigating drug Naproxen. Since the 1980s, it is applied for medication. Based on its only partial elimination in treatment process, Naproxen occurs in natural waters and effluents of sewage plants [*Arany et al.*, 2013]. In addition to the urban indicators, pesticide traces in the groundwater were used to identify agricultural contributions to the fresh water resources. The herbicide Simazine was available and used since the 1950s to avoid broad-laved weeds and annual grasses. Simazine is adsorbed in soil and can be eliminated via bacterial degradation. Water solubility is low, comparable to Naproxen. Simazine was phased out in Israel in 2012-2014 [*Berman et al.*, 2014]. In arid environments, leaching of the soil zone occurs differently in comparison to humid environments and there is faster leaching due to thin soil zone with less humic matter. Nitrate in groundwater can originate from nitrified ammonium in treatment process of domestic waste water and from fertilizer application in agriculture either as KNO_3 or liquid manure from animal production.

4.3.2 Application of lumped parameter models

Lumped parameter models (LPM) are useful tools to interpret the composition of environmental tracers in groundwater samples as age distributions. LPMs use one of several pre-defined analytical solutions of simplified flow systems and describe the tracer output mathematically with a convolution integral that combines the tracer input history weighed with the age distribution valid for the flow system in question [*A Suckow*, 2012]. The LPM code "Lumpy" [*A Suckow*, 2012] used here implements the convolution integral for flow systems that can be described by e.g. the piston flow model (PM), the exponential model (including Partial Exponential Model - PEM) and the dispersion model (DM). The mean residence time (MRT) is the main fit parameter, for some models additional parameters are necessary as discussed below. Input data are the regional atmospheric tracer input curves and selected hydrogeological characteristics (e.g. delay in the unsaturated zone, infiltration temperature and height etc.).

Atmospheric input

The Tritium input function we use is the data series of Vienna (1960-2014), Austria [*IAEA/WMO*, 2017] and adjusted to the longitudinal an latitudinal difference by a factor of 0.4 to match the much shorter data set of the precipitation station Bet Dagan (1960-2001), Israel [*IAEA/WMO*, 2017]. For time series output the decay correction is to the sampling time, for the synoptic tracer plots the decay correction is to October 31, 2013. The pre-bomb input background value for Tritium was set to 3 TU. Input data for SF_6 and CFC`s refer to *L Plummer et al.* [2006] for the time span 1953 to 2006. Due the gas solubility dependency on temperature and air pressure during infiltration, for the gaseous tracers like CFC`s and SF_6, the infiltration temperature was set to 15°C, based on the average of the regional air temperature in the winter (rain) season, the altitude to 700 m AMSL which is the average altitude of the infiltration area, and the salinity to 0 due to low mineralised rain water. ^{36}Cl input versus time was obtained from Iceland ice core measurements from *Synal et al.* [1990] and observed a latitudinal correction with a factor of 3 based on the latitudinal distribution model by *Heikkilä et al.* [2009]. Background value of $^{36}Cl/Cl$ ratio was assumed to be 10-14 before the input time series starts. This is based on the recent $^{36}Cl/Cl$ ratio in rainwater, which was measured on samples from December 2014/ January 2015 with a weighted value of $8x10^{-15}$.

Unsaturated Zone

To avoid over estimation of travel times (*P G Cook et al.* [1995], *L Plummer et al.* [2006]), the time lag in thick unsaturated zones is quantified as the relative time lag between gas and water bound tracers via a dual approach of applying both water bound tracers (^{3}H, ^{36}Cl) and gas tracers (CFCs, SF6). The thickness of the unsaturated zone in the studied area ranges between 100 to 300 m for the upper and lower aquifer (Table 6, Appendix A.8).

Particularly the wells Samia 2 and Herodion 1 of the Upper Cenomanian were selected to consider wells close to the recharge area and a shallow unsaturated zone. The unsaturated zone (depth to water table) of the wells Herodion 1 and Ein Samia 2 vary between 230 to 250 m. They are located on the eastern mountain part of the groundwater recharge zone and cover the lithology from Bina

to Weradim/ Kefar Shaul formation (Upper Cenomanian), which consist of well-shaped vertical fissures in the limestone and partly karst occurrences. Since this geological setting supports fast and possibly unhindered flow to the groundwater table, the unsaturated zone was approached and modelled by a piston flow model (infiltration temperature of 15°C, (recharge) altitude of 700 m AMSL).

Selected model approach

Piston flow model (PM)

The piston flow model describes the movement of a water parcel along a defined flow path from the aquifer surface towards the spring or well filter, neglecting any mixing, dispersion or diffusion.

Dispersion model (DM)

The dispersion model characterizes transport influenced by dispersion and advective flow. The relative magnitude of both is expressed as the Peclet number Pe (Pe= l ·v/D where l is the length of the considered system, v is the velocity and D is the dispersion constant) [*Huysmans and Dassargues*, 2005].

The model includes only dispersion as mixing process of groundwater with different ages and its age distribution is defined by the following equation [*Maloszewski and Zuber*, 2002; *Małoszewski and Zuber*, 1982]:

$$g(t\text{-}t') = \sqrt{\frac{Pe\cdot\tau}{4\pi(t-t')}}\cdot\frac{1}{t-t'}\cdot\exp\left(-\left(1-\frac{t-t'}{\tau}\right)^2\frac{Pe\cdot\tau}{4(t-t')}\right)$$

Equation 10

Here $\boldsymbol{\tau}$ is the mean residence time (MRT) and t-t' is the age of a water parcel. In our model approach best fits were obtained by applying a Peclet number of 30, which characterizes dominantly advective transport.

Partial exponential model (PEM)

The partial exponential model is related to the exponential model (EM). Based on homogenous infiltration into a homogeneous aquifer, the PEM covers all possible mixing processes of flow lines from infiltration ending in one filter. If the special case that the filter screen extends over the whole depth of the aquifer the PEM is actually an exponential model (EM), with only the MRT as fit parameter. In the case that the filter catches only the lower part of the aquifer, the PEM is equivalent to the exponential piston flow model (EPM) which needs an additional parameter describing the ratio of screened to unscreened part. In case the screen does not cover the complete aquifer and is not situated at the bottom of the aquifer situated for example in the middle of the aquifer, the PEM has three parameters. In Lumpy the PEM is constrained using specific parameters of the well like aquifer bottom, filter bottom, filter top and groundwater surface. Parameters of aquifer depth, screen top, screen bottom and groundwater surface of the investigated wells are given in table 6:

Table 6 Summary of PEM parameters for the wells Samia 2, Herodion 1 and the spring Arugot

	Samia 2	Herodion 1	Arugot
Surface level [mNN]	420	570	-175
Groundwater level [mNN]	220	330	
Filter top [mNN]	245	316	
Filter bottom [mNN]	174	237	
Aquifer bottom [mNN]	150	220	-250
Lumpy parameters (PEM)			
Screen Top - Z1[m]	0	14	0
Screen Bottom - Z2 [m]	46	93	74*
Aquifer Depth - L [m]	70	110	75

4.3.3 Results of dating tracer distribution

From the recharge area in the mountain ridge to the Lower Jordan valley, the subsurface flow direction is influenced by geological structures. Pointing on the main feature, the layer dip of the Cretaceous limestone layers is directed to the valley almost parallel, with only ~5°-10° deviation to the morphologic incidence of ~30°. This results into a main groundwater flow from west to east, interrupted by faults, morphologic valley structures like the Wadi Qilt and Wadi Arugot and geological folds in the subsurface (see cross sections in Figure 41).

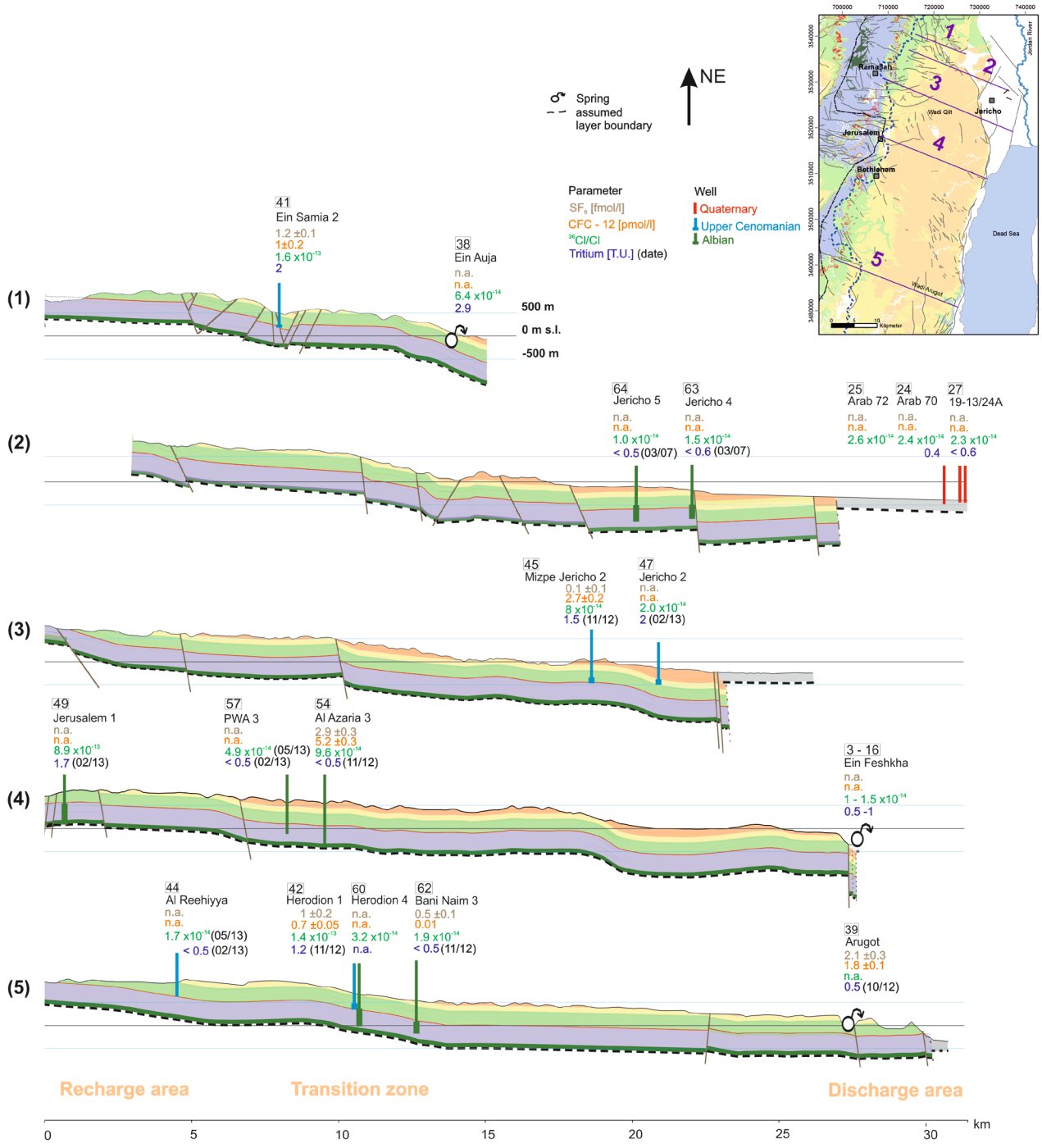

Figure 41 Geological cross sections (parallel oriented and located from recharge to discharge area) including sampling points (wells and springs) with measured concentrations of Tritium, $^{36}Cl/Cl$, CFC - 12 and SF_6 (stratigraphic legend corresponds to figure 2)

The applied parameters $^{36}Cl/Cl$, SF_6, CFCs and partly Tritium allow a regional differentiation.

Recharge area

Rainwater samples from December 2014 and January 2015 contain $^{36}Cl/Cl$ ratios of $1.3*10^{-14}$ to $5.5*10^{-14}$. These values are supported by rain water samples from 1982 by *B. Herut et al.* [1992], (Figure 42) and Tritium concentrations are in the range ~4-6 TU [*IAEA/WMO*, 2017]. Groundwater samples in the recharge area show higher $^{36}Cl/Cl$ ratios of $5*10^{-13}$ to $9*10^{-13}$ and a total chloride content of 22 -65 mg/l (Figure 42) that together indicates an input of bomb peak water. The group of wells in the Upper Cenomanian aquifer represented by Samia 2 and Herodion 1 show $^{36}Cl/Cl$ ratios of $1.41*10^{-13}$ to $1.57*10^{-13}$ and 1 to 2 TU (Figure 40, Figure 41). The lower aquifer (Albian) in the recharge area contains the highest ^{36}Cl values with a $^{36}Cl/Cl$ ratio of $8.9 *10^{-13}$ and 1.7 TU (e.g. well Jerusalem 1 situated in the south of Jerusalem). Gas tracer measurements provided SF6 concentrations of 1.2 fmol/l and CFC-12 concentrations of 1 pmol/l in Samia 2 and equivalent concentrations in Herodion 1 (Figure 41). This implies that the upper Cenomanian aquifer in the recharge area still contains atmospheric input from the last decades since 1960.

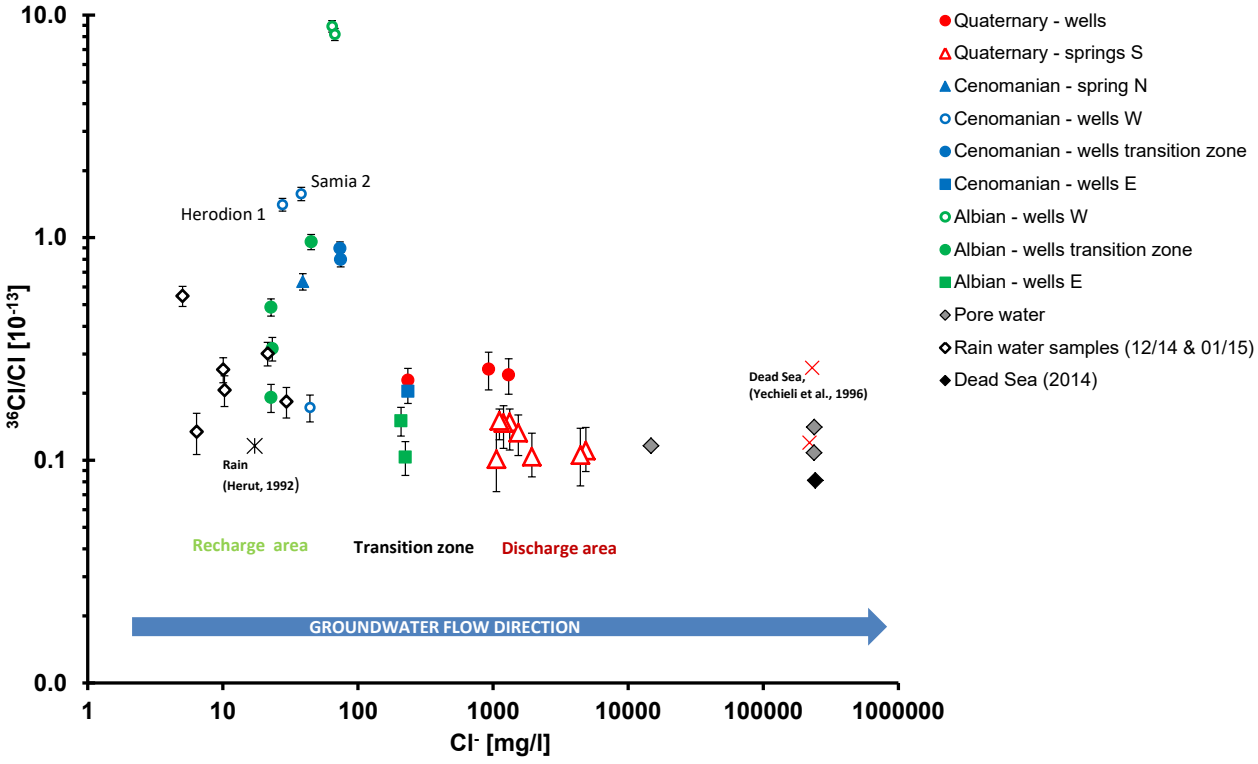

Figure 42 Groundwater data of $^{36}Cl/Cl$ and total chloride content (both logarithmic) from recharge to discharge area

The well Al Reehiyya located in the southern part of the mountain area is an exception in the Upper Cenomanian aquifer due to low $^{36}Cl/Cl$ ratio ($1.73*10^{-14}$) and tritium values of less than 0.5 TU. This indicates either unmixed pre-bomb water or mixing of recent rainwater with much older water to dilute the bomb signals of tritium and $^{36}Cl/Cl$. Besides the lower aquifer group (Albian) being directly connected to the recharge area with thick unsaturated zones, groundwater samples in the mountain area (e.g. PWA 3, Herodion 4 and Bani Naim 3) contain lower concentrations of anthropogenic gases and Tritium ratios <0.5 TU indicating no fresh water input from the last decades. Here, the $^{36}Cl/Cl$ ratios range between $4.87*10^{-14}$ and $1.91*10^{-14}$, i.e. travel times appear

to be longer than 70 years. From the north to the south in the mountain range, the wells PWA 3, Herodion 4 and Bani Naim 3 of the lower aquifer have similar chloride contents and decreasing $^{36}Cl/Cl$ ratios similar to rain water. However, the Tritium content is below 1 TU and indicates mainly pre-bomb water. The well Azaria 3 located in the Albian aquifer and also close to the recharge area (Figure 41) shows $^{36}Cl/Cl$ ratios above those of recent rain and 0.5 TU which may indicate water from between the bomb spikes for tritium and ^{36}Cl. Unfortunately, the anthropogenic gases CFC`s and SF_6 in these wells are well above concentrations possible in equilibrium with the atmosphere and indicate a local surface contamination.

Transition zone

Indicative of the transition zone between recharge and discharge area (fault and graben zone) is the Ein Auja spring emerging from the Upper Cenomanian aquifer (Figure 41). The Tritium content is high (2.9 TU) and mineralisation low, and the spring water has a $^{36}Cl/Cl$ ratio ($6*10^{-14}$) similar to recent rain water (maximum $5.5*10^{-14}$) (Figure 41, Figure 42), reflecting short residence times. In the transition zone, Mizpe Jericho 2 and Jericho 2 show higher $^{36}Cl/Cl$ ratios of $2*10^{-14}$ to $8*10^{-14}$ and Tritium 1.4 to 2 TU in combination with CFC contaminations and higher concentrations than possible in equilibrium with the atmosphere. Here, the hydrogeological knowledge indicates groundwater flow originating from the upper aquifer. The $^{36}Cl/Cl$ signatures are higher than the recent rainwater concentrations, leading to earlier recharge times than the groundwater in Jerusalem 1, Herodion 1 and Samia 2. The Tritium concentration indicates contributions of recent rainwater rapidly infiltrating via faults connected to the Turonian layers.

Discharge area

The heterogeneity of karst formations clearly dominates groundwater flow but may also influence tracer results of the Cretaceous aquifer. High SF_6 and CFC-12 concentrations (2.1 fmol/l and 1.8 pmol/l, respectively) with low Tritium of 0.5 TU in the Arugot spring located in the discharge area point to recent gas exchange processes in karst voids, renewing the gas tracers during groundwater flow by contact with air (Figure 41). Geologically this spring is in the discharge area of the upper Cretaceous aquifer and particularly unaffected by graben structures. In the lower aquifer (Albian) close to the graben fault the groundwater shows low Tritium concentration (≤ 0.5 TU) and $^{36}Cl/Cl$ according to the admixture of geogenic chlorine sources in wells Jericho 4 and 5. With increasing chloride content towards the fault zone and graben area the $^{36}Cl/Cl$ is dissolved to a value between 1 – 2*10-14 close to background in the agricultural wells Arab 72, 70 and 19-13/24A in the graben area (Figure 42). Spring water of Ein Feshkha and groundwater in Lower Jordan Valley sediments can be differentiated by a higher $^{36}Cl/Cl$ ratio of the groundwater of the Quaternary section in comparison to increasing chloride and lower $^{36}Cl/Cl$ ratio in the Ein Feshkha spring water and the Dead Sea. The shallow wells in the Quaternary section draw groundwater of the upper aquifer, flushing from Cretaceous layers via the graben fault into the sediment body but also contain water infiltrated from agricultural irrigation as confirmed by nitrate concentration and pesticide traces of Simazine. The Ein Feshkha springs show tritium values around < 1 TU and $^{36}Cl/Cl$ ratios between $1*10^{-14}$ to $1.5*10^{-14}$, both indicating background and no admixture of water younger than 1950. In general the following general patterns can be extracted: (i) spring water of the upper Cretaceous (Ein Auja) contains groundwater infiltrated after the bomb test demonstrated by Tritium and $^{36}Cl/Cl$ comparable with recent rain water; (ii) along the flow path

and in the lower aquifer $^{36}Cl/Cl$ is shifted to lower ratios due to admixture of saline water, the endmember being brine similar to the Dead Sea and pore water; (iii) the lower aquifer shows detectable admixtures of young water, demonstrated by bomb peak tritium and $^{36}Cl/Cl$ tracer values, only in the vicinity of Jerusalem and Bethlehem (cross sections 4 and 5 in Figure 41); (iv) springs in the south (Ein Feshkha & Arugot) are free of tritium and show background $^{36}Cl/Cl$ ratios indicating no recent recharge although recent gas exchange in karst structures may reset the SF_6 and CFC "clocks".

4.3.4 Infiltration times from anthropogenic organic trace pollutants and nitrate

Simazine, Naproxen und Acesulfame K are detectable in low concentrations in mostly all wells of the Upper Cenomanian and Albian aquifer indicating a water input younger than 40 years. The combination of those tracing molecules with nitrate concentrations results into regional patterns: the highest nitrate concentration combined with Simazine (2 and 10ng/l) and Acesulfame K (3 and 22ng/l, higher concentrations in June 2013) occur in the transition zone, particularly in Mizpe Jericho (~43mg/l), see figure 43. Here, water components from adjacent agriculture fields (irrigation) and untreated water running in the wadis pass the karst layers of the upper Cretaceous layers (Turonian) with low degradation.

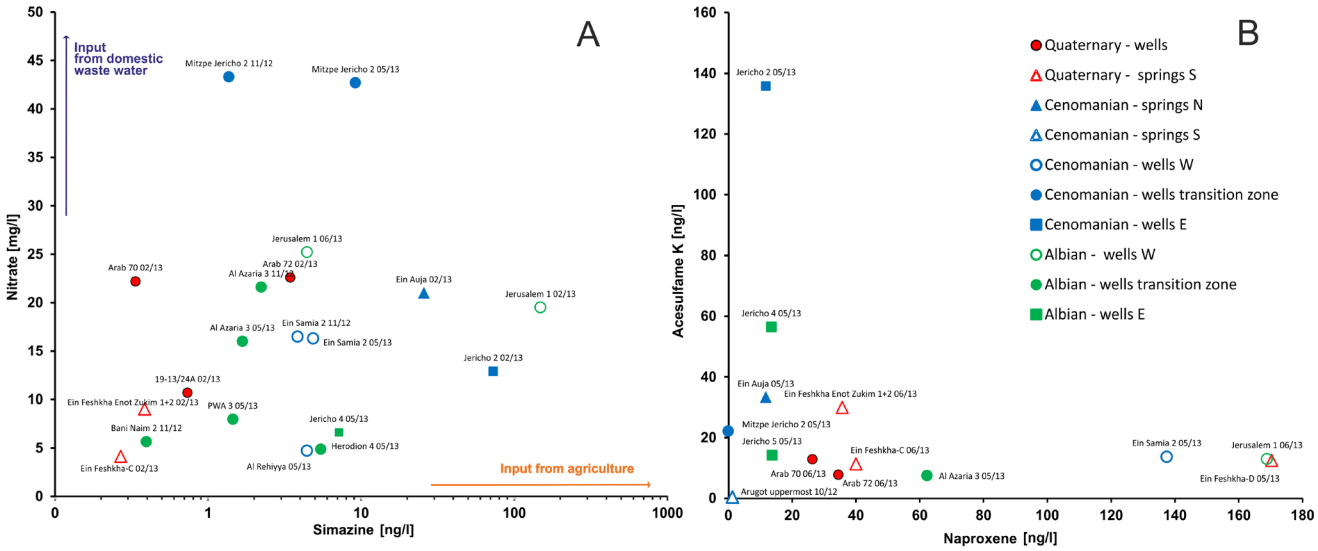

Figure 43 Groundwater results of A: Nitrate and Simazine indicating agricultural contributions and B: Urban input of Acesulfame K and Naproxen

During the sampling campaign in June 2013, the Acesulfame K concentrations tend to increase from recharge to discharge area in combination with a decrease of Naproxen. This type of distribution can be related to irregular input of pollutants to the groundwater in the recharge area. Based on the strong hydrophilic properties of Acesulfame K, it is possible to trace its transport from the recharge area in Jerusalem (mountain area) towards the graben zone, where the highest concentrations of Acesulfame K occur in the wells Jericho 4 (56 ng/l) and Jericho 2 (136 ng/l) close to the graben fault. An increase of Naproxen concentration in Jerusalem 1 (170ng/l) and in Samia 2 (140ng/l) indicates a possible contribution from (processed) domestic waste water

of the populated parts in the recharge area. Decreasing Naproxen concentrations with longer flow path or residence time are related to absorption or degradation due to lower solubility activity in water. Further decentralised inputs of processed waste water can be assumed in the springs of Ein Feshkha (e.g. in Feshkha Big Swimming pool) for example.

4.3.5 Lumped parameter model - evaluation of infiltration times

The application of lumped parameter models gives the option to extract age ranges from combinations of gas and water tracers. Based on the measured tracer distribution in the study area, there is a clear separation of upper and lower aquifer. The lower aquifer contains a very low amount of tracer concentrations and indicates therefore groundwater fractions recharged before 1950. For the upper aquifer an age estimation is discussed via lumped modelling for the recharge and discharge area.

Recharge area

As mentioned in section above, the transport of water and gas tracers in thick unsaturated karst zones is different. In this approach, the mean residence time in the unsaturated zone of the recharge area was estimated in three model scenarios: piston flow model, dispersion model, and partial exponential model. In principle, every model was fitted to a specific MRT for the water tracers of the wells Samia 2 and Herodion 1 (Figure 44). In figure 44 and figure 45, piston flow models with MRTs from 1 to 50 are displayed for tritium (Figure 44 A and B) and for $^{36}Cl/Cl$ (Figure 45 A and B).

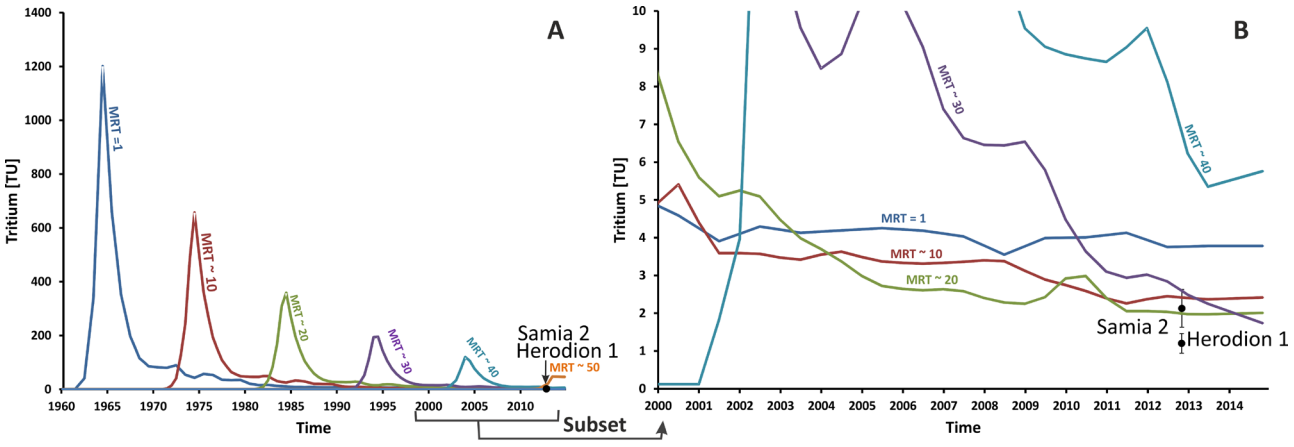

Figure 44 Approach of fitted piston flow models for Samia 2 and Herodion 1 in a tritium v s. time plot (B subset of A)

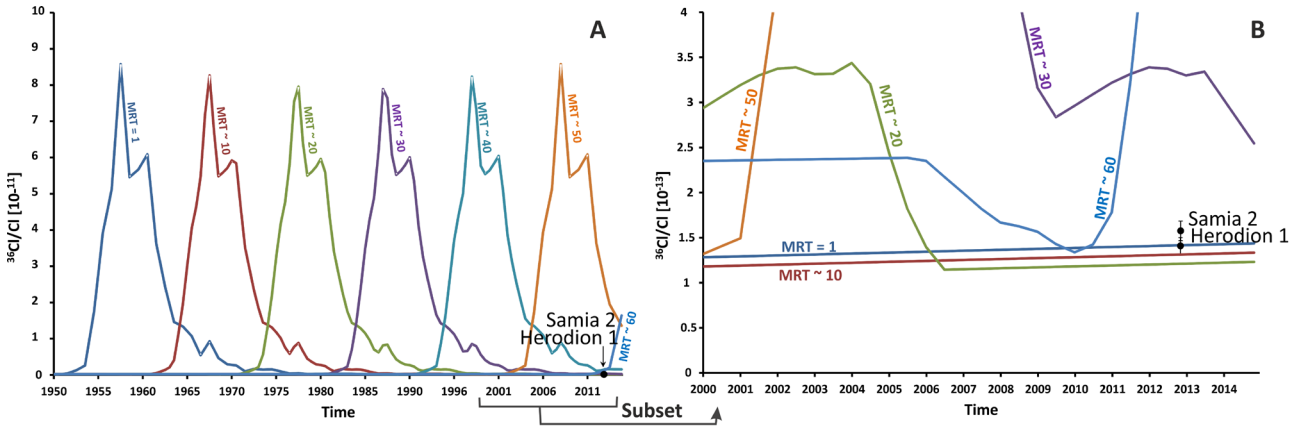

Figure 45 Approach of fitted piston flow models for Samia 2 and Herodion 1 in a ^{36}Cl/Cl vs. time plot (B subset of A)

Comparison of the fit for tritium and ^{36}Cl for both wells indicates a most appropriate fit of a 10 yr MRT piston flow model. The dispersion model fits to 20 yr MRT and for the partial exponential model 20 yr and 16 yr MRT are estimated (Table 7). The infiltrating precipitation passes the unsaturated zone directly after entering the subsurface and can reach the aquifer top after a few hours (Figure 41). In the unsaturated zone the water and gas tracers separate due to the change of pressure and temperature in the underground. While the water phase moves fast along the cracks, fissures and particularly karst tubes to the groundwater surface, the gas phase equilibrates in the open pores and moves via diffusion. Given by the fast transfer velocity of the water phase in the karst holes, a delay of the water- bounded tracers can be neglected. The gas tracer equilibrates with gaseous pore space and is restrained resulting into a travel delay in comparison to the water-bounded tracers. For every applied model (piston flow model, partial exponential model and dispersion model) the gas delay was approached via estimation of similar mean residence times for the water tracers. By using the estimated MRTs of the water tracers, the delay for the gas tracers was fitted to the measurements of the CFCs and SF_6 of the upper aquifer wells Samia 2 and Herodion 1 (Figure 46 and Table 7).

Table 7 Summary of gas delay [yr] for the different models; applied MRT`s [yr] of groundwater in the saturated zone; Peclet number used in the dispersion model. For the parameters of the PEM see table 6

	PM		DM		PEM	
	Samia 2	**Herodion 1**	**Samia 2**	**Herodion 1**	**Samia 2**	**Herodion 1**
Delay [yr]						
CFC-11	24	28	14	18	20	25
CFC-12	17	30	14	20	20	28
CFC-113	23	22	9	14	17	22
SF_6	8	8	0	0	7	6
^{3}H	0	0	0	0	0	0
^{36}Cl/Cl	0	0	0	0	0	0
MRT GW saturated zone	10	10	20	20	30	16
Peclet number			30	30		

There is a variation of gas delay for the different tracers in the two wells (Table 7). Ideally the movements of gas tracers are similar with comparable delays, for example in homogeneous unsaturated zones. However, the lower delay of SF_6 in comparison to the CFC`s can be reasoned in biological degradation processes of the CFC`s in the upper part of the unsaturated karst zone.

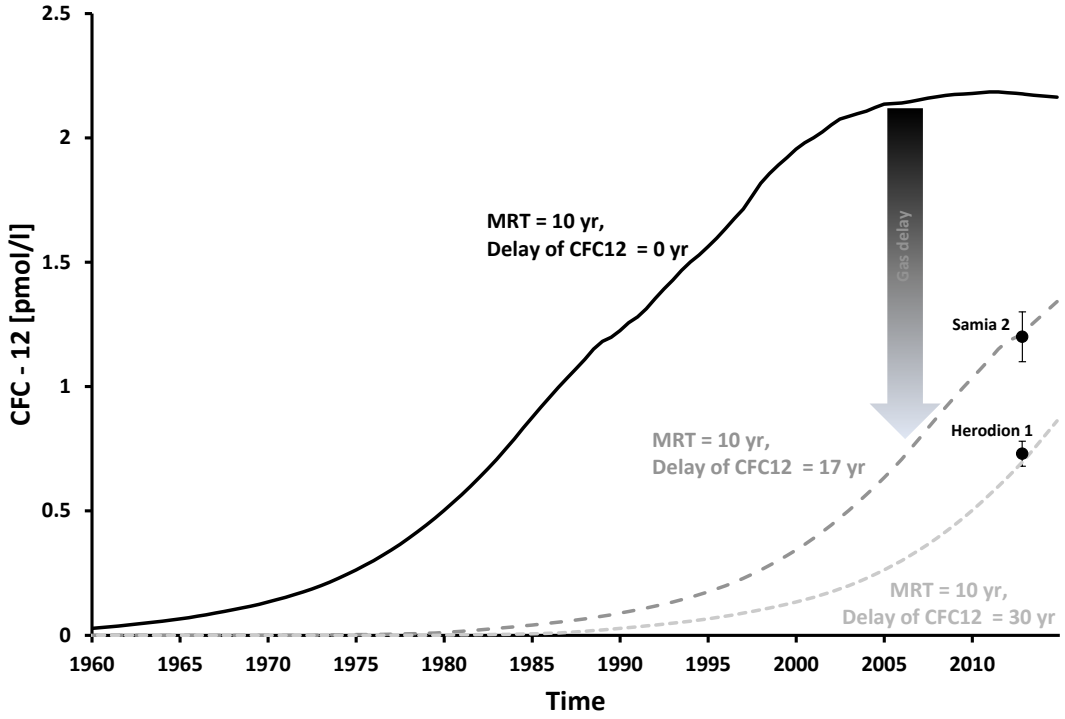

Figure 46 Fit of piston flow model (MRT 10 yr of water tracer, table 7) for estimation of gas delay, exemplary for CFC - 12 vs. time plot

The results for the wells Ein Samia and Herodion 1 include the dispersion model, piston flow model and partial exponential model considering the estimated gas delay in the unsaturated zone and without the gas delay (Figure 46, Figure 47). For Ein Samia, a combination of the gas tracers with the water tracer in different lumped parameter model fit in the time range of 10 to 15 years MRT for the PM, 17 to 28 years MRT for the DM and 26 to 46 years for the PEM. Water movement in the aquifer is exposed to different types of porosity given by e.g. the karst space, structural fractures and pores in the limestone. Those geological characteristics can provide different time transport velocities of water parcels.

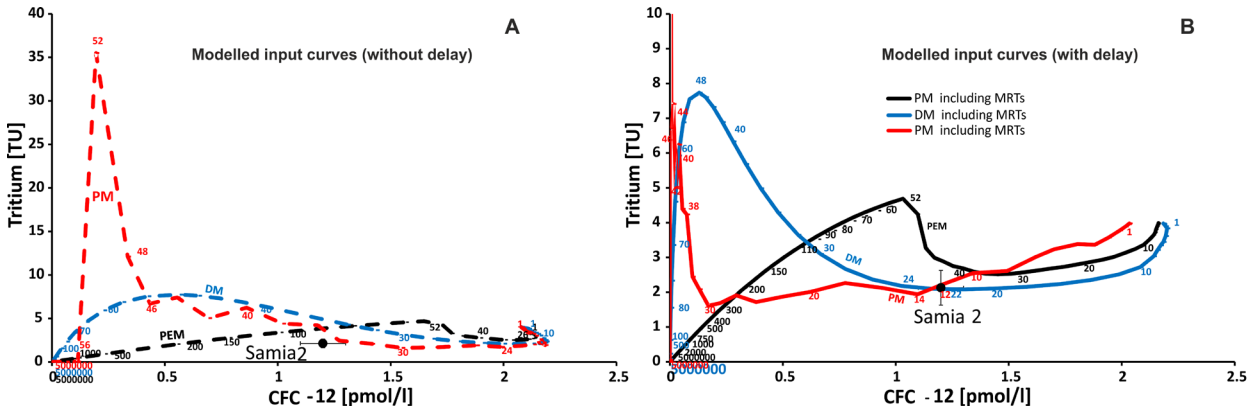

Figure 47 Combined tracer plot for Samia 2 – Tritium versus CFC - 12 with calculated PM (red), PEM (black), DM (blue) without delay (A) and with delay (B)

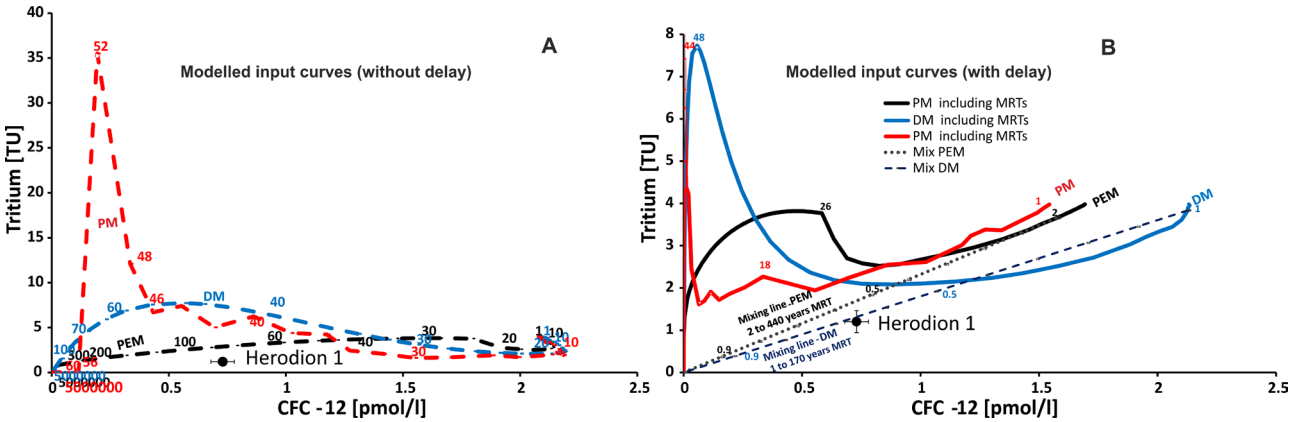

Figure 48 Combined tracer plot for Herodion 1 - Tritium versus CFC-12 with calculated PM (red), PEM (black), DM (blue) without delay (A) and with delay (B)

That means, the results of the applied models consider three different ways of water flow in the aquifer: e.g. it can be based on the diffusion in the pore system (DM) or on a straight flow along a karst tube without any mixing (PM) or includes also the mixing in the filter (PEM). The estimation of MRTs from each model calculation expresses groundwater recharged in the last 10 to 50 years validated by the tracer combinations (Table 8, Samia 2).

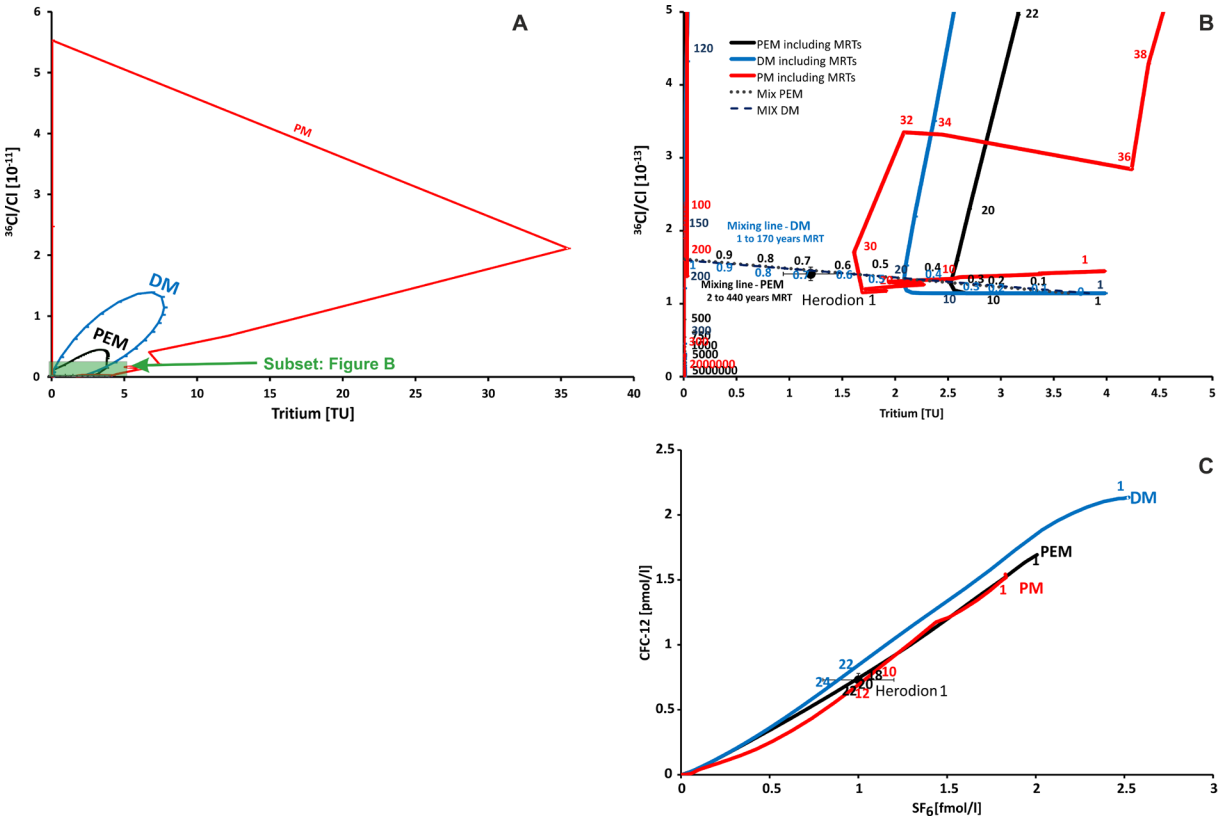

Figure 49 Combined tracer plot for Herodion 1 – CFC - 12 versus SF_6 (C) and $^{36}Cl/Cl$ versus Tritium (A and B) with calculated PM (red), PEM (black), DM (blue)

Table 8 Summary of model results – specific MRT`s of Samia 2 and Herodion 1 for tracer combinations, *estimated fit

	Samia 2			Herodion 1		
	PEM	**DM**	**PM**	**PEM**	**DM**	**PM**
CFC11 vs CFC113	31 - 44	20 - 23	10 - 14	17 - 22	no fit	11 - 13
CFC11 vs. SF_6	31 - 44	21 - 25	9 - 13	21 - 23	17 - 22	10 - 12
CFC12 vs. SF_6	38 - 46	21 - 23	10 - 13	18 - 20	22 - 24	10 - 11
$^{36}Cl/Cl$ vs. SF_6	36 - 37	20 - 22	9 – 15*	17 - 18	19 - 20	9 - 15
$^{36}Cl/Cl$ vs. CFC113	36 - 38	21 - 22	11 – 15*	16 - 28	no fit	9 - 18
$^{36}Cl/Cl$ vs. CFC12	36 - 38	21 - 23	11 – 14*	17 - 18	20 - 21	11 - 12
$^{36}Cl/Cl$ vs. Tritium	36 – 38*	20 - 22	9 - 29		Mixing ratios of 30:70 to 40:60 (1 year MRT and 170 years MRT)	
Tritium vs. SF_6	26 - 44	18 - 23	10 - 15		Mixing ratios of 30:70 to 40:60 (1 year MRT and 170 years MRT)	
Tritium vs. CFC12	38 – 45*	21 - 23	10 - 14		Mixing ratios of 30:70 to 40:60 (1 year MRT and 170 years MRT)	

The Herodion 1 well is situated in the recharge and in a lower part of the upper aquifer (Amminadav Fm.). Model calculations without considering a time lag (delay) of gas tracer do not match the tracer measurements (Figure 48, A). When considering the time lag (Table 7), all tracer combinations for a DM with tritium are possible to fit with mixing lines (endmember 1 yr MRT and 170 yr MRT) in a mixing ratio of 30:70 or 40:60. This caused by to the low Tritium concentration in Herodion 1 (Figure 47and Figure 48). In every further tracer combination, the modelled input curves match Herodion 1 (e.g. Figure 48) and is summarized with an age distribution of 9 - 18 yr MRT with PMs, 17 to 24 yr MRT with DMs and 16 to 28 yr MRT with PEMs (Table 8).

Transition zone/ Discharge area

Wells of the lower aquifer in the recharge area are not interpreted by using this approach due to contaminations in CFC`s (like Al Azaria 3), very low concentrations of the anthropogenic gases (like Bani Naim 3), or are located in confined conditions. Wells of the upper aquifer in the transition zone do not contain enough reliable tracer measurements for application of detailed LPM since the anthropogenic gases are also contaminated (Mizpe Jericho 2, Figure 41). The tritium concentrations of 1.5 and 2 TU in Mizpe Jericho 2 and Jericho 2 indicate a reasonable fraction of recent rain input.

Due to the continuous outflow of the springs along the coastline and its chemical mixing patterns, it is assumed that there is also a connection to the water resources of the Lower Cretaceous aquifer, which could provide water with longer residence times. All springs in the discharge area (e.g. Ein Feskha) have less than 0.5TU and $^{36}Cl/Cl < 2 \times 10^{-14}$. Therefore, two possible calculations i) Figure 6 shows that <0.5TU and $<2 \times 10^{-14}$ is only possible if water is older than 50-60y. Or: ii) recent rain has 4TU therefore 0.5TU is less than 12%. But this is detection limit and therefore expressed as "no recent water detectable". The organic tracers Acsulfame K, Simazine and Naproxen are detectable also in the discharge springs. However, their input function cannot be quantified.

Therefore, we do not know the fraction of recent water that this concentration represents. From tritium it is evident that the fraction is smaller than 12% but enough for the Acsulfame K, Simazine and Naproxen to be detectable. More precise quantification of the young water in these springs is only possible with either a lower detection limit for tritium (e.g. determination of ^{3}H via ingrowth with detection limit 0.005TU) or a precise quantification of the input of Acesulfame K, Simazine, Naproxen. Both are beyond the scope of the present study. However, gas tracers show much smaller MRT in the range of less than two decades as it is shown for the spring Arugot in the discharge area (Figure 50).

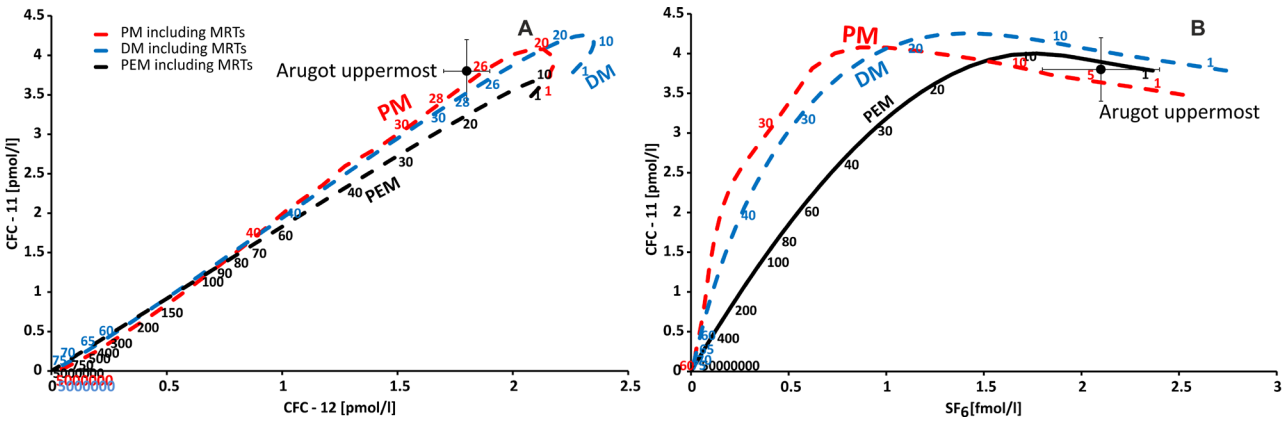

Figure 50 Combined tracer plot for Arugot – CFC - 11 versus CFC - 12 (A) and CFC - 11 versus SF_6 (B) with calculated PM (red), PEM (black), DM (blue)

Their concentration is higher than could be explained by an admixture of 12% modern water in old water. Our explanation is that the GW, while being old (^{3}H and ^{36}Cl free) observes partial re-equilibration in the karst aquifer system before discharging into the springs.

4.3.6 Conclusions of groundwater dating

The present tracer combination allows us to derive details of groundwater flow patterns, mixing end-members and transport times in the upper and lower Cretaceous aquifers between the recharge area around the central mountain ridge and the discharge zones close to the lower Jordan Valley and the Dead Sea. This was possible despite a very rather low number of measurements and a complicated karst hydrogeological setting by the powerful combination of multiple lines of evidence from hydrogeology, hydrochemistry, anthropogenic organic trace substances like sweeteners, fertilizers, pesticides and medical substances and classical environmental age-dating tracers like tritium, CFCs, SF_6 and ^{36}Cl.

The lower Cretaceous aquifer is basically free of tritium and other anthropogenic environmental tracers like CFCs, SF_6 and bomb-derived ^{36}Cl and therefore has groundwater transport times larger than 50 years, which could not be further quantified with the methods presented here. Groundwater in the upper Cretaceous aquifer in most parts contains anthropogenic trace substances, therefore circulates on time scales of several decades maximum and shows clear indications of preferential flow paths as expected for karstified groundwater systems.

In two springs the combination of several environmental tracers (^3H, CFC-11, CFC-12, CFC-113, SF_6, bomb-^{36}Cl) allowed estimates of the age distribution in the saturated zone, gas transfer delays in the unsaturated zone and mixing ratios with older groundwater. These estimates were confirmed by anthropogenic substances from agriculture (nitrate and pesticides like Simazine), pain killers (Naproxen) and sweeteners (Acesulfame K). The multi- tracer methodology presented here to quantify parameters of the flow system is applicable in other data sparse areas with complex hydrogeology (karst or fractured) under anthropogenic influence.

5 Summary and outlook

The Dead Sea region is one of the most extreme areas on the world. Here are combined extreme morphological and climate conditions in short distances - Dead Sea is considered as deepest place on earth. Based on the semi- arid to arid climate conditions the high saline lake drops incredible fast with ~1m per year. It builds the lowest potential for inflow of groundwater from the connected groundwater aquifers of the Cretaceous and Quaternary layers. Motivated to support sustainable management strategies for this region, the present study is focused on the freshwater resources in the Cretaceous layers and its connection to the Quaternary deposits on the western side of the mobile Dead Sea aquifer system.

The main objectives cover mainly the identification of groundwater origins, mixing between aquifers, permeability of the main graben fault between Cretaceous and Quaternary layers, origins of north- western Dead Sea springs (Ein Feshkha) and a further insight to age ranges of groundwater. For this purpose, an exceptional tracer combination consisting of major and trace pattern, REE+Y, stable isotopes, radioactive isotopes and anthropogenic components was applied. To detect the groundwater evolvement from recharge to discharge area, wells and springs were sampled along the flow path towards the main discharge area at the Dead Sea coast “Ein Feshkha” as wells as rock samples from the outcropping formations.

Via this approach, step wise each parameter contributes useful parts to understand the character of the aquifers system. However, the combination of each tracer resulted into the following aspects and interpretations:

The first aspect of investigation was to evaluate the meteoric input to characterize water types of the Cretaceous aquifers and to differentiate between the two main karstified, carbonate Cretaceous aquifers (Upper Cenomanian and Albian). For meteoric groundwater origin in the recharge area, the specific composition of stable isotopes of water isotope like $\delta^{18}O$ and $\delta^{2}H$ as wells as $\delta^{13}CDIC$ give indication of recent meteoric according to the signatures of the meteoric water line and local $\delta^{13}CDIC$ rainwater signatures (<4 years). Groundwater evolvement from rain water and runoff to discharging springs in Ein Feshkha and Dead Sea obtained from the major ions like Na, Cl, Ca, Sr and Mg reveal distinct groundwater groups of Turonian and Upper Cenomanian springs as wells Ein Fehkha springs and Dead Sea.

A further detailed separation of Upper Cenomanian aquifer and Albian aquifer is given by application of $^{87}Sr/^{86}Sr$. By application of a mixing model, it is proved that water rock interaction with rain water lead to lower $^{87}Sr/^{86}Sr$ ratios in the groundwater approaching Cretaceous rock ratio. Along the flow path, two ways of water development can be shown: on way goes in direction of water interfering with the saline input from the Quaternary sediments and the other way leads to longer water interaction according to longer flow path

without input from the Quaternary sediments or brine and therefore more mature water (e.g. Arugot spring). Aquifer rock composition of calcite and dolomite plays a dominant role for dissolved groundwater components of Mg, Ca and Sr in the Cretaceous aquifers. In combination with the REE+Y, the groundwater of the calcite-rich Turonian layers shows a specific REE+Y pattern

with a negative Ce anomaly. Given by that fact, admixtures from the Turonian layers to the Upper Cenomanian and Albian aquifers are back traced.

Groundwater chemistry of the wells along the fault zone gives clear indication of an existing permeability of the fault zone. Groundwater flow conditions are influenced by water extraction from wells. That means, the occurring groundwater depression cone created by water extractions from wells along the graben fault extends to groundwater resources in the Quaternary. Mixture processes are validated by major and trace elements as wells as by the isotope patterns. A clear picture to that can be obtained by combination of $\delta^{34}S$ and $^{87}Sr/^{86}Sr$. Distinct groups of every groundwater are attributable the aquifer layers including the endmembers of the Dead Sea and pore water in the Quaternary sediments. Here from valuable information brings insights to the origin of the two main spring groups at the Ein Feskha site.

The freshwater/brackish spring “Enot Zukim” contains clear patterns of the endmembers lower aquifer and the pore water, whereas the higher saline spring “Summer spring” (emerging only during summer season) covers $\delta^{34}S$ ratios of the upper Cretaceous aquifer and the Dead Sea. Based on that fact, it can be extracted that the upper aquifer almost empties during summer time and gets recharged during winter time. Transfer times and mean residence time frames of the Cretaceous aquifer were analysed with a combination of water- bounded and gas tracers. Describing their patterns with lumped parameter modelling allows the conclusion that the applied gas tracers CFCs and SF_6 stay longer in the unsaturated zone than the applied water-bound tracers tritium and ^{36}Cl. Using CFC`s, SF_6, tritium, $^{36}Cl/Cl$ and organic trace components allows identifying a groundwater component younger than 50 years. A unique determination of an age distribution is, however, not possible with the limited amount of tracer data within this very heterogeneous karst system.

Given that the lower aquifer is nearly free of anthropogenic tracers it is not possible to quantify a young component. Also, the tracers for longer time scales like ^{14}C and helium give no unique result due to their geochemical alteration and uncertain source function. Ideal tracers for centuries or millennia are needed, e.g. ^{39}Ar or ^{81}Kr, to further quantify the age of groundwater in the lower aquifer system. Further detailed information about age ranges could be obtained by layer-wise sampling of groundwater in the well filter. This research could form a basis for future groundwater modelling in the region and provides the necessary information about the connection of the main Cretaceous aquifer system with discharge area.

In addition, the temporarily resolution in four sampling steps could provide a calibration of groundwater models in transient mode. Age information from the Cretaceous aquifer system is most important to support future prediction models of the development of the groundwater system by including the extraction rates. In this context, hydrochemical data set could base also groundwater quantification models. The specific tracer combination provides a detailed scanning of the investigated aquifer system, which in turn bases a successfully transferability in similar climatic, geological and anthropogenic conditions or include also the potential appearing limitations.

References

Akhmadaliev, S., R. Heller, D. Hanf, G. Rugel, and S. Merchel (2013), The new 6MV AMS-facility DREAMS at Dresden, *Nuclear Instruments and Methods in Physics Research Section B: Beam Interactions with Materials and Atoms*, *294*(0), 5-10.

Alemayehu, T., A. Leis, A. Eisenhauer, and M. Dietzel (2011), Multi-proxy approach ($^{2}H/H$, $^{18}O/^{16}O$, $^{13}C/^{12}C$ and $^{87}Sr/^{86}Sr$) for the evolution of carbonate-rich groundwater in basalt dominated aquifer of Axum area, northern Ethiopia, *Chemie der Erde - Geochemistry*, *71*(2), 177-187.

Alvarado, J. C., R. Purtschert, K. Hinsby, L. Troldborg, M. Hofer, R. Kipfer, W. Aeschbach-Hertig, and H. Arno-Synal (2005), ^{36}Cl in modern groundwater dated by a multi-tracer approach ($^{3}H/^{3}He$, SF_6, CFC-12 and ^{85}Kr): A case study in quaternary sand aquifers in the Odense Pilot River Basin, Denmark, *Applied Geochemistry*, *20*(3), 599-609.

Anders, E., and N. Grevesse (1989), Abundances of the elements: Meteoritic and solar, *Geochimica et Cosmochimica Acta*, *53*(1), 197-214.

Arany, E., R. K. Szabó, L. Apáti, T. Alapi, I. Ilisz, P. Mazellier, A. Dombi, and K. Gajda-Schrantz (2013), Degradation of naproxen by UV, VUV photolysis and their combination, *Journal of Hazardous Materials*, *262*, 151-157.

Baker, P. A., J. M. Gieskes, and H. Elderfield (1982), Diagenesis of Carbonates in Deep-Sea Sediments--Evidence From SR/CA Ratios and Interstitial Dissolved SR2+ Data, *Journal of Sedimentary Research*, *52*(1).

Begin (1974), Geological map of Israel, Jericho, Sheet 9-III, 1: 50,000, with Explanatory Notes, *Geological Survey of Israel, Jerusalem*.

Begin (1975), The geology of the Jericho sheet (geological map series 1:50,000), *Geological Survey of Israel Bulletin*, *67*, 1-35.

Bentley, H. W., F. M. Phillips, and S. N. Davis (1986), Chlorine-36 in the terrestrial environment, in *Handbook of Environmental Isotope Geochemistry*, edited by P. Fritz and J.-C. Fontes, pp. 427-480, Elsevier, Amsterdam.

Berman, T., K. Isabella, and R. Shay (2014), Environmental Health in Israel 2014, *Jerusalem: Ministry of Health*.

Bruland, K. W. (1983), In Chemical Oceanography, edited, Riley, J. P., Chester, R., Eds.; Academic Press: London, London.

Bullister, J., and R. Weiss (1988), Determination of CCl_3F and CCl_2F_2 in seawater and air, *Deep Sea Research Part A. Oceanographic Research Papers*, *35*(5), 839-853.

Busenberg, E., and L. N. Plummer (1992), Use of chlorofluorocarbons (CCl_3F and CCl_2F_2) as hydrologic tracers and age-dating tools: The alluvium and terrace system of central Oklahoma, *Water Resour. Res.*, *28*(9), 2257-2283.

Busenberg, E., and L. N. Plummer (2000), Dating young groundwater with sulfur hexafluoride: Natural and anthropogenic sources of sulfur hexafluoride, *Water Resour. Res.*, *36*(10), 3011-3030.

Busenberg, E., and L. N. Plummer (2008), Dating groundwater with trifluoromethyl sulfurpentafluoride (SF_5CF_3), sulfur hexafluoride (SF_6), CF_3Cl (CFC-13), and CF_2Cl_2 (CFC-12), *Water Resour. Res.*, *44*(2), W02431.

Busenberg, E., and L. N. Plummer (2010), A rapid method for the measurement of sulfur hexafluoride (SF_6), trifluoromethyl sulfur pentafluoride (SF_5CF_3), and Halon 1211 (CF_2ClBr) in hydrologic tracer studies, *Geochem. Geophys. Geosyst.*, *11*(11), Q11001.

Clark, I. D., and P. Fritz (1997), *Environmental isotopes in hydrogeology*, CRC press.

Cook, P., and D. K. Solomon (1997), Recent advances in dating young groundwater: chlorofluorocarbons, $^3H^3He$ and ^{85} Kr, *Journal of Hydrology*, *191*(1), 245-265.

Cook, P. G., D. K. Solomon, L. N. Plummer, E. Busenberg, and S. L. Schiff (1995), Chlorofluorocarbons as Tracers of Groundwater Transport Processes in a Shallow, Silty Sand Aquifer, *Water Resour. Res.*, *31*(3), 425-434.

Coppola, E., M. Poulton, E. Charles, J. Dustman, and F. Szidarovszky (2003), Application of artificial neural networks to complex groundwater management problems, *Natural Resources Research*, *12*(4), 303-320.

Cornett, R. J., H. R. Andrews, L. A. Chant, W. G. Davies, B. F. Greiner, Y. Imahori, V. T. Koslowsky, T. Kotzer, J. C. D. Milton, and G. M. Milton (1997), Is ^{36}Cl from weapons' test fallout still cycling in the atmosphere?, *Nuclear Instruments and Methods in Physics Research Section B: Beam Interactions with Materials and Atoms*, *123*(1–4), 378-381.

Danin, A. (1988), Flora and vegetation of Israel and adjacent areas, *The zoogeography of Israel*, *30*, 251-276.

Dansgaard, W. (1964), Stable isotopes in precipitation, *Tellus A*, *16*(4), 436-468.

Davis, S. N., H. W. Bentley, F. M. Phillips, and D. Elmore (1983), Use of cosmic-ray produced radionuclides in hydrogeology, *EOS*, *64*, 283.

DIN38402-62 (2014), German standard methods for the examination of water, waste water and sludge - General information (group A) - Part 62: Plausibility check of analytical data by performing an ion balance (A 62), edited.

Dogramaci, S. S., and A. L. Herczeg (2002), Strontium and carbon isotope constraints on carbonate-solution interactions and inter-aquifer mixing in groundwaters of the semi-arid Murray Basin, Australia, *Journal of Hydrology*, *262*(1–4), 50-67.

Dunkle, S. A., L. N. Plummer, E. Busenberg, P. J. Phillips, J. M. Denver, P. A. Hamilton, R. L. Michel, and T. B. Coplen (1993), Chlorofluorocarbons (CCl_3F and CCl_2F_2) as dating tools and hydrologic tracers in shallow groundwater of the Delmarva Peninsula, Atlantic Coastal Plain, United States, *Water Resour. Res.*, *29*(12), 3837-3860.

Elmore, D., L. E. Tubbs, D. Newman, X. Z. Ma, R. Finkel, K. Nishiizumi, J. Beer, H. Oeschger, and M. Andree (1982), ^{36}Cl bomb pulse measured in a shallow ice core from Dye 3, Greenland, *Nature*, *300*(5894), 735-737.

Flexer, A., and A. Honigstein (1984), The senonian succession in israel—Lithostratigraphy, biostratigraphy and sea level changes, *Cretaceous Research*, *5*(4), 303-312.

Flexer, A., J. Hall, and F. Hirsch (2005), Geological framework of the Levant, volume II: the Levantine Basin and Israel, Part IV, Israel Introduction, *Historical Productions, Jerusalem*.

Friedman, I., L. Machta, and R. Soller (1962), Water-vapor exchange between a water droplet and its environment, *Journal of Geophysical Research*, *67*(7), 2761-2766.

Gat, J. R., and I. Carmi (1970), Evolution of the isotopic composition of atmospheric waters in the Mediterranean Sea area, *Journal of Geophysical Research*, *75*(15), 3039-3048.

Gat, J. R., and W. Dansgaard (1972), Stable isotope survey of the fresh water occurrences in Israel and the Northern Jordan Rift Valley, *Journal of Hydrology*, *16*(3), 177-211.

Gavrieli, I., A. Starinsky, A. Vengosh, and A. Ayalon (1997), Boron, sulfur, strontium, oxygen, and hydrogen isotopes in freshwater of a carbonate aquifer: Judea Mountain, Israel*Rep.*, Geological Survey of Israel, Israel.

Gertman, I., and A. Hecht (2002), The Dead Sea hydrography from 1992 to 2000, *Journal of Marine Systems*, *35*(3), 169-181.

Gräbe, A., T. Rödiger, K. Rink, T. Fischer, F. Sun, W. Wang, C. Siebert, and O. Kolditz (2013), Numerical analysis of the groundwater regime in the western Dead Sea escarpment, Israel+ West Bank, *Environmental Earth Sciences*, *69*(2), 571-585.

Hasan, J. A. (2009), Nature and the Origin of Ein Feshcha Springs (NW Dead Sea), Karlsruhe, Univ., Diss., 2009.

Heikkilä, U., J. Beer, J. Feichter, V. Alfimov, H.-A. Synal, U. Schotterer, A. Eichler, M. Schwikowski, and L. Thompson (2009), 36 Cl bomb peak: comparison of modeled and measured data, *Atmospheric Chemistry and Physics*, *9*(12), 4145-4156.

Herczeg, A., S. Dogramaci, and F. Leaney (2001), Origin of dissolved salts in a large, semi-arid groundwater system: Murray Basin, Australia, *Marine and Freshwater Research*, *52*(1), 41-52.

Herut, B., A. Starinsky, and A. Katz (1993), Strontium in rainwater from Israel: Sources, isotopes and chemistry, *Earth and Planetary Science Letters*, *120*(1–2), 77-84.

Herut, B., B. Spiro, A. Starinsky, and A. Katz (1995), Sources of sulfur in rainwater as indicated by isotopic $\delta^{34}S$ data and chemical composition, Israel, *Atmospheric Environment*, *29*(7), 851-857.

Herut, B., A. Starinsky, A. Katz, M. Paul, E. Boaretto, and D. Berkovits (1992), ^{36}Cl in chloride-rich rainwater, Israel, *Earth and Planetary Science Letters*, *109*(1–2), 179-183.

Hirsch, F. (1983), Geological map of Israel, Bet Guvrin, Sheet 11-III, 1: 50,000, *Geological Survey of Israel, Jerusalem (prel. ed.)*.

Hirsch, F., A. Flexer, A. Rosenfeld, and A. Yellin-Dror (1995), Palinspastic and crustal setting of the eastern Mediterranean, *Journal of Petroleum Geology*, *18*(2), 149-170.

Hodge, V. F., K. J. Stetzenbach, and K. H. Johannesson (1998), Similarities in the Chemical Composition of Carbonate Groundwaters and Seawater, *Environmental Science & Technology*, *32*(17), 2481-2486.

Hoefs, J. (1987), *Stable Isotope Geochemistry*, Springer-Verlag, Berlin.

Hogan, J. F., F. M. Phillips, S. K. Mills, J. M. Hendrickx, J. Ruiz, J. T. Chesley, and Y. Asmerom (2007), Geologic origins of salinization in a semi-arid river: The role of sedimentary basin brines, *Geology*, *35*(12), 1063-1066.

Horowitz, A. (2001), *The Jordan rift valley*, CRC Press.

Huysmans, M., and A. Dassargues (2005), Review of the use of Péclet numbers to determine the relative importance of advection and diffusion in low permeability environments, *Hydrogeology Journal*, *13*(5), 895-904.

IAEA/WMO (2017), Global Network of Isotopes in Precipitation. The GNIP Database.Accessible at: http://www.iaea.org/water.

Johannesson, K. H., K. J. Stetzenbach, and V. F. Hodge (1997), Rare earth elements as geochemical tracers of regional groundwater mixing, *Geochimica et Cosmochimica Acta*, *61*(17), 3605-3618.

Johnston, V. E., and F. McDermott (2008), The distribution of meteoric Cl-36 in precipitation across Europe in spring 2007, *Earth and Planetary Science Letters*, *275*(1–2), 154-164.

Katz, A., and A. Starinsky (2009), Geochemical History of the Dead Sea, *Aquatic Geochemistry*, *15*(1-2), 159-194.

Katz, A., E. Sass, A. Starinsky, and H. D. Holland (1972), Strontium behavior in the aragonite-calcite transformation: An experimental study at 40–98°C, *Geochimica et Cosmochimica Acta*, *36*(4), 481-496.

KIT, K. I. o. T. (2018), The Virtual Institute DEad SEa Research VEnue, edited, Helmholtz Association.

Klein-BenDavid, O., E. Sass, and A. Katz (2004), The evolution of marine evaporitic brines in inland basins: The Jordan-Dead Sea Rift valley, *Geochimica et Cosmochimica Acta*, *68*(8), 1763-1775.

Krauskopf, K. B. (1956), Factors controlling the concentrations of thirteen rare metals in sea-water, *Geochimica et Cosmochimica Acta*, *9*(1-2), 1-B32.

Kroitoru, L. (1987), The characterization of flow systems in carbonatic rocks defined by the ground water parameters: Central Israel, PhD thesis, Weizmann Institute of Science, Feinberg Graduate School, Rehovot.

Krouse, H. R., and B. Mayer (2000), Sulphur and oxygen isotopes in sulphate, in *Environmental tracers in subsurface hydrology*, edited, pp. 195-231, Springer.

Lance, G. N., and W. T. Williams (1967), A general theory of classificatory sorting strategies: II. Clustering systems, *The computer journal*, *10*(3), 271-277.

Lange, T. (2012), Tracing Flow and Salinization Processes at selected Locations of Israel and the West Bank - the Judea Group Aquifer and the Shallow Aquifer of Jericho, PhD thesis, Technische Universtät Freiberg, Freiberg Online Geosciences 31.

Laronne Ben-Itzhak, L., and H. Gvirtzman (2005), Groundwater flow along and across structural folding: an example from the Judean Desert, Israel, *Journal of Hydrology*, *312*(1-4), 51-69.

Lavastre, V., et al. (2010), Establishing constraints on groundwater ages with ^{36}Cl, ^{14}C, ^{3}H, and noble gases: A case study in the eastern Paris basin, France, *Applied Geochemistry*, *25*(1), 123-142.

Lin, R., and K. Wei (2006), Tritium profiles of pore water in the Chinese loess unsaturated zone: implications for estimation of groundwater recharge, *Journal of Hydrology*, *328*(1), 192-199.

Lohninger, H. (08.10.2012), Grundlagen der Statisktik, in *Clusteranalyse, Hauptkomponentenanalyse (PCA), Skalierung von Daten*, edited, Epina Bookshelf.

Love, A., A. L. Herczeg, L. Sampson, R. G. Cresswell, and L. K. Fifield (2000), Sources of chloride and implications for 36Cl dating of old groundwater, southwestern Great Artesian Basin, Australia, *Water Resources Research*, *36*(6), 1561-1574.

Lubberts, R. K., and Z. Ben-Avraham (2002), Tectonic evolution of the Qumran Basin from high-resolution 3.5-kHz seismic profiles and its implication for the evolution of the northern Dead Sea Basin, *Tectonophysics*, *346*(1–2), 91-113.

Lucas, L. L., and M. P. Unterweger (2000), Comprehensive review and critical evaluation of the half-life of Tritium, *Journal of research-National institute of standards and technology*, *105*(4), 541-550.

Lyons, W., S. Tyler, H. Gaudette, and D. Long (1995), The use of strontium isotopes in determining groundwater mixing and brine fingering in a playa spring zone, Lake Tyrrell, Australia, *Journal of Hydrology*, *167*(1-4), 225-239.

Mahara, Y., T. Ohta, T. Kubota, K. Miyakawa, T. Hasegawa, M. Habermehl, and L. Fifield (2012), New dating method: Groundwater residence time estimated from the 4He accumulation rate calibrated by using cosmogenic and subsurface-produced 36Cl, paper presented at EPJ Web of Conferences, EDP Sciences.

Mallast, U., F. Schwonke, R. Gloaguen, S. Geyer, M. Sauter, and C. Siebert (2013), Airborne thermal data identifies groundwater discharge at the north-western coast of the Dead Sea, *Remote Sensing*, *5*(12), 6361-6381.

Maloszewski, P., and A. Zuber (2002), Manual on lumped parameter models used for the interpretation of environmental tracer data in groundwaters*Rep.*

Małoszewski, P., and A. Zuber (1982), Determining the turnover time of groundwater systems with the aid of environmental tracers: 1. Models and their applicability, *Journal of Hydrology*, *57*(3-4), 207-231.

Margaritz, M. (1974), The carbon and oxygen isotopic composition of some carbonate rocks in Israel, *Seminar of the Geological Survey of Israel; Israel;1972*.

Matthess, G. (2005), *Die Beschaffenheit des Grundwassers*, Schweizerbart Science Publishers, Gebrüder Borntraeger, Berlin, Stuttgart.

Mazor, E., and M. Molcho (1972), Geochemical studies on the Feshcha Springs, Dead Sea basin, *Journal of Hydrology*, *15*(1), 37-47.

Mekaiten, Y. (2006), Salinization of groundwater in the southern part of the Yarkon-Taninim aquifer, Master thesis, The Hebrew University of Jerusalem, Department of Geology, Institute of Earthe Sciences, Faculty of Mathematics and Natural Sciences, Jerusalem.

Merchel, S., et al. (2011), Ultra-trace analysis of ^{36}Cl by accelerator mass spectrometry: an interlaboratory study, *Analytical and Bioanalytical Chemistry*, *400*(9), 3125-3132.

Merkel, B. J., B. Planer-Friedrich, and D. K. Nordstrom (2005), Groundwater geochemistry, *A Practical Guide to Modeling of Natural and Contaminated Aquatic Systems*, *1*, 20.

Möller, P., and U. Giese (1997), Determination of easily accessible metal fractions in rocks by batch leaching with acid cation-exchange resin, *Chemical Geology*, *137*(1-2), 41-55.

Möller, P., E. Rosenthal, P. Dulski, S. Geyer, and Y. Guttman (2003), Rare earths and yttrium hydrostratigraphy along the Lake Kinneret–Dead Sea–Arava transform fault, Israel and adjoining territories, *Applied Geochemistry*, *18*(10), 1613-1628.

Möller, P., E. Rosenthal, S. Geyer, J. Guttman, P. Dulski, M. Rybakov, M. Zilberbrand, C. Jahnke, and A. Flexer (2007), Hydrochemical processes in the lower Jordan valley and in the Dead Sea area, *Chemical Geology*, *239*(1-2), 27-49.

Mor, U., and A. Burg (2000), Geological map of Israel, Mizpe Shalem, Sheet 12-III ,1: 50,000 *Geological Survey of Israel, Jerusalem*.

Moser, H., and W. Rauert (1980), *Lehrbuch der Hydrogeologie* Gebrüder Borntraeger, Schweizerbart Science Publishers, Berlin, Stuttgart.

Müller, T., K. Osenbrück, G. Strauch, S. Pavetich, K. S. Al-Mashaikhi, C. Herb, S. Merchel, G. Rugel, W. Aeschbach, and W. Sanford (2016), Use of multiple age tracers to estimate groundwater residence times and long-term recharge rates in arid southern Oman, *Applied Geochemistry*, *74*, 67-83.

Négrel, P., and E. Petelet-Giraud (2005), Strontium isotopes as tracers of groundwater-induced floods: the Somme case study (France), *Journal of Hydrology*, *305*(1–4), 99-119.

Oster, H., C. Sonntag, and K. O. Münnich (1996), Groundwater age dating with chlorofluorocarbons, *Water Resources Research*, *32*(10), 2989-3001.

Paul, M., A. Kaufman, M. Magaritz, D. Fink, W. Henning, R. Kaim, W. Kutschera, and O. Meirav (1986), A new ^{36}Cl hydrological model and ^{36}Cl systematics in the Jordan River/Dead Sea system, *Nature*, *321*(6069), 511-515.

Pavetich, S., et al. (2014), Interlaboratory study of the ion source memory effect in ^{36}Cl accelerator mass spectrometry, *Nuclear Instruments and Methods in Physics Research Section B: Beam Interactions with Materials and Atoms*, *329*(0), 22-29.

Plummer, L., E. Busenberg, and P. Cook (2006), Principles of chlorofluorocarbon dating, in *Use of chlorofluorocarbons in hydrology: A guidebook*, edited.

Plummer, L. N., E. Busenberg, S. Drenkard, P. Schlosser, B. Ekwurzel, R. Weppernig, J. B. McConnell, and R. L. Michel (1998), Flow of river water into a karstic limestone aquifer—2. Dating the young fraction in groundwater mixtures in the Upper Floridan aquifer near Valdosta, Georgia, *Applied Geochemistry*, *13*(8), 1017-1043.

Prokoph, A., G. A. Shields, and J. Veizer (2008), Compilation and time-series analysis of a marine carbonate δ^{18}O, δ^{13}C, ^{87}Sr/^{86}Sr and δ^{34}S database through Earth history, *Earth-Science Reviews*, *87*(3–4), 113-133.

Rao, S. M., and P. Mamatha (2004), Water quality in sustainable water management, *Current science*, 942-947.

Rauch, M. (2005), Geochemie von Rudistenschalen–Beiträge zur Meerwasserchemie (Sr/Ca, Mg/Ca, δ^{13}C) und Paläoklima der Kreide.

Raz, E. (1986), Geological map of Israel, En-Gedi, Sheet 16-I ,1: 50.000 *Geological Survey of Israel, Jerusalem*.

Rebeix, R., C. Le Gal La Salle, A. Mayer, R. Finkel, C. Claude, J. Sültenfuß, and R. Simler (2014), ^{36}Cl deposition rate reconstruction from bomb pulse until present: A study based on groundwater records, *Applied Geochemistry*, *50*, 199-208.

Rofe, and Raffety (1963), Geological and Hydrological Report, Jerusalem District Water Supply*Rep.*, Central Water Authority, Jordan.

Rosenfeld, A., and F. Hirsch (2005), The Cretaceous of Israel, *Geological Framework of the Levant*, *2*, 393-436.

Rosenthal, E., A. Flexer, and P. Möller (2009), The hydrochemical history of the Rift in *The water of the Jordan Valley: scarcity and deterioration of groundwater and its impact on the regional development*, edited, pp. 75-82, Springer Berlin, Heidelberg.

Roth, I. (1973), Geological Map of Israel, Wadi el Qilt, Sheet 12-I, 1: 50,000, with Explanatory Notes, *Geol Surv Israel, Jerusalem*.

Rozanski, K., R. Gonfiantini, and L. Araguas-Araguas (1991), Tritium in the global atmosphere: Distribution patterns and recent trends, *Journal of Physics G: Nuclear and Particle Physics*, *17*(S), S523.

Rozanski, K., L. Araguás-Araguás, and R. Gonfiantini (1993), Isotopic patterns in modern global precipitation, *Climate change in continental isotopic records*, 1-36.

Rugel, G., S. Pavetich, S. Akhmadaliev, S. M. Enamorado Baez, A. Scharf, R. Ziegenrücker, and S. Merchel (2016), The first four years of the AMS-facility DREAMS: Status and developments for more accurate radionuclide data, *Nuclear Instruments and Methods in Physics Research Section B: Beam Interactions with Materials and Atoms*, *370*, 94-100.

Schlosser, P., M. Stute, H. Dörr, C. Sonntag, and K. O. Münnich (1988), Tritium/^{3}He dating of shallow groundwater, *Earth and Planetary Science Letters*, *89*(3), 353-362.

Schönwiese, C.-D. (2006), Praktische Statistik fuer Meteorologen und Geowissenschaftler, edited, Gebrüder Bornträger,Schweizerbart Science Publishers, Stuttgart, Germany.

Shachnai, E. (2000), Geological map of Israel, Ramallah, Sheet 8-IV ,1: 50,000 *The Israel Geological Survey, Jerusalem*.

Shand, P., D. Darbyshire, A. Love, and W. Edmunds (2009), Sr isotopes in natural waters: applications to source characterisation and water–rock interaction in contrasting landscapes, *Applied Geochemistry*, *24*(4), 574-586.

Shiklomanov, I. (1993), in *Water in crisis: a guide to the worlds fresh water resources*, edited by P. H. Gleick, Oxford University Press, New York.

Siebert, C. (27.06.2018), SMART - Sustainable Management of Available Water Resources with Innovative Technologies, in *UFZ research inside SMART*, edited, Helmholtz Centre for Environmental Research GmbH - UFZ , http://www2.ufz.de/index.php?de=15689

Siebert, C., et al. (2014), Challenges to estimate surface- and groundwater flow in arid regions: The Dead Sea catchment, *Science of The Total Environment*, *485–486*(0), 828-841.

Sneh, A., and Y. Avni (2011), Geological map of Israel, Jerusalem, Sheet 11-II, 1:50,000, *Geological Survey of Israel, Jerusalem*.

Sneh, A., and Y. Roth (2012), Geological map of Israel, Hevron, Sheet 11-IV ,1: 50,000 *Geological Survey of Israel, Jerusalem*.

Solomon, D. K., R. Poreda, S. Schiff, and J. Cherry (1992), Tritium and helium: 3 as groundwater age tracers in the Borden aquifer, *Water Resources Research*, *28*(3), 741-755.

Stanley, S. M., and L. A. Hardie (1998), Secular oscillations in the carbonate mineralogy of reef-building and sediment-producing organisms driven by tectonically forced shifts in seawater chemistry, *Palaeogeography, Palaeoclimatology, Palaeoecology*, *144*(1–2), 3-19.

Starinsky, and Katz (2014), The Story of Saline Water in the Dead Sea Rift – The Role of Runoff and Relative Humidity, in *Dead Sea Transform Fault System: Reviews*, edited by Z. Garfunkel, Z. Ben-Avraham and E. Kagan, pp. 317-353, Springer Netherlands.

Starinsky, A., M. Bielski, B. Lazar, E. Wakshal, and G. Steinitz (1980), Marine^{87}Sr/^{86}Sr ratios from the Jurassic to Pleistocene: evidence from groundwaters in Israel, *Earth and Planetary Science Letters*, *47*(1), 75-80.

Starinsky, A., M. Bielski, B. Lazar, G. Steinitz, and M. Raab (1983), Strontium isotope evidence on the history of oilfield brines, Mediterranean Coastal Plain, Israel, *Geochimica et Cosmochimica Acta*, *47*(4), 687-695.

Stein, M., A. Starinsky, A. Katz, S. L. Goldstein, M. Machlus, and A. Schramm (1997), Strontium isotopic, chemical, and sedimentological evidence for the evolution of Lake Lisan and the Dead Sea, *Geochimica et Cosmochimica Acta*, *61*(18), 3975-3992.

Steinhausen, D., and K. Langer (1977), *Clusteranalyse: Einführung in Methoden und Verfahren der automatischen Klassifikation; mit zahlreichen Algorithmen, FORTRAN-Programmen, Anwendungsbeispielen und einer Kurzdarstellung der multivariaten statistischen Verfahren*, Walter de Gruyter.

Steuber, T., and J. Veizer (2002), Phanerozoic record of plate tectonic control of seawater chemistry and carbonate sedimentation, *Geology*, *30*, 1123.

Steuber, T., and M. Rauch (2005), Evolution of the Mg/Ca ratio of Cretaceous seawater: Implications from the composition of biological low-Mg calcite, *Marine Geology*, *217*(3–4), 199-213.

Stosch, H. (2000), Geochemie der Seltenen Erden, *Vorlesungsskript Universität Köln*.

Suckow, A. (2012), Lumpy–an interactive lumped parameter modeling code based on MS access and MS excel, paper presented at Proceedings of European Geosciences Union Congress.

Suckow, A., C. Sonntag, M. Gröning, and U. Thorweihe (1993), Groundwater recharge in the Umm Kedada Basin, NW-Sudan, derived from environmental isotopes of soil moisture in samples collected from deep dug wells, in *Geoscientific Research in Northeast Africa*, edited by U. Thorweihe and H. Schandelmeier, pp. 677-685, Balkema, Rotterdam.

Sültenfuß, J., and G. Massmann (2004), Dating with the ^{3}He-tritium-method: an example of bank filtration in the Oderbruch region, *Grundwasser*, *9*(4), 221-234.

SUSMAQ (2001), Data Review on the West Bank Aquifers, Sustainable Management for the West Bank and Gaza Aquifers*Rep. SUSMAQ-MOD #02V0.2*, Palestine.

Synal, H. A., J. Beer, G. Bonani, M. Suter, and W. Wölfli (1990), Atmospheric transport of bomb-produced ^{36}Cl, *Nuclear Instruments and Methods in Physics Research Section B: Beam Interactions with Materials and Atoms*, *52*(3–4), 483-488.

Szabo, Z., D. E. Rice, L. N. Plummer, E. Busenberg, S. Drenkard, and P. Schlosser (1996), Age Dating of Shallow Groundwater with Chlorofluorocarbons, Tritium/Helium: 3, and Flow Path Analysis, Southern New Jersey Coastal Plain, *Water Resour. Res.*, *32*(4), 1023-1038.

Thornthwaite, C. W., and J. R. Mather (1955), The water balance, edited, Drexel Institute of Technology, Laboratory of Climatology, Centerton, NJ (EUA).

TIBCOSoftwareInc. (Copyright 1984-2017), Statistica, in *Version 13*, edited.

Tichomirowa, M., C. Heidel, M. Junghans, F. Haubrich, and J. Matschullat (2010), Sulfate and strontium water source identification by O, S and Sr isotopes and their temporal changes (1997–2008) in the region of Freiberg, central-eastern Germany, *Chemical Geology*, *276*(1–2), 104-118.

Toll, M. (2008), Investigating Unconsolidated Aquifers in an Arid Environment–A Case Study from the Lower Jordan Valley/Jordan, in *Climatic Changes and Water Resources in the Middle East and North Africa*, edited, pp. 289-324, Springer.

Torfstein, A. (2008), Brine Freshwater Interplay and Effects on the Evolution of Saline Lakes: Dead Sea Rift Terminal Lakes, PhD thesis, Hebrew University of Jerusalem, Jerusalem.

Torfstein, A., I. Gavrieli, and M. Stein (2005), The sources and evolution of sulfur in the hypersaline Lake Lisan (paleo-Dead Sea), *Earth and Planetary Science Letters*, *236*(1–2), 61-77.

Tosaki, Y., G. Massmann, N. Tase, K. Sasa, T. Takahashi, Y. Matsushi, M. Tamari, Y. Nagashima, K. Bessho, and H. Matsumura (2010), Distribution of $^{36}Cl/Cl$ in a river-recharged aquifer: Implications for the fallout rate of bomb-produced 36Cl, *Nuclear Instruments and Methods in Physics Research Section B: Beam Interactions with Materials and Atoms*, *268*(7–8), 1261-1264.

Tosaki, Y., et al. (2007), Application of ^{36}Cl as a dating tool for modern groundwater, *Nuclear Instruments and Methods in Physics Research Section B: Beam Interactions with Materials and Atoms*, *259*(1), 479-485.

Trettin, R., K. Knöller, H. Loosli, and P. Kowski (2002), Evaluation of the sulfate dynamics in groundwater by means of environmental isotopes, *Isotopes in Environmental and Health Studies*, *38*(2), 103-119.

Veizer, J. (1989), Strontium isotopes in seawater through time, *Annual Review of Earth and Planetary Sciences*, *17*, 141.

Veizer, J., et al. (1997), Strontium isotope stratigraphy: potential resolution and event correlation, *Palaeogeography, Palaeoclimatology, Palaeoecology*, *132*(1–4), 65-77.

Veizer, J., et al. (1999), $^{87}Sr/^{86}Sr$, $\delta^{13}C$ and $\delta^{18}O$ evolution of Phanerozoic seawater, *Chemical Geology*, *161*(1–3), 59-88.

Vengosh, A., A. J. Spivack, Y. Artzi, and A. Ayalon (1999), Geochemical and boron, strontium, and oxygen isotopic constraints on the origin of the salinity in groundwater from the Mediterranean coast of Israel, *Water Resources Research*, *35*(6), 1877-1894.

Wigley, T. M. L., and L. N. Plummer (1976), Mixing of carbonate waters, *Geochimica et Cosmochimica Acta*, *40*(9), 989-995.

Yechieli, Y., D. Ronen, and A. Kaufman (1996), The source and age of groundwater brines in the Dead Sea area, as deduced from ^{36}Cl and ^{14}C, *Geochimica et Cosmochimica Acta*, *60*(11), 1909-1916.

Yechieli, Y., D. Ronen, I. Carmi, and A. Kaufman (1994), New tritium data in waters of the Dead Sea area, *Israel Journal of Earth Sciences*, *43*, 213-220.

Yellin-Dror, A., J. Guttman, A. Flexer, H. Hötzl, W. Ali, and J. Bensabat (2009), 3-D Hydrogeological model of the Marsaba-Feshkha region, in *The Water of the Jordan Valley*, edited by H. Hötzl, P. Möller and E. Rosenthal, pp. 287-312, Springer Berlin Heidelberg.

Zak, I. (1967), The geology of Mount Sedom PhD thesis, Hebrew University Jerusalem.

Zilberman, T., I. Gavrieli, Y. Yechieli, I. Gertman, and A. Katz (2017), Constraints on evaporation and dilution of terminal, hypersaline lakes under negative water balance: The Dead Sea, Israel, *Geochimica et Cosmochimica Acta*, *217*, 384-398.

Appendix A